Iowa Research Online
The University of Iowa's Institutional Repository

University of Iowa
Iowa Research Online

Theses and Dissertations

2014

# Drug transporters in the nasal epithelia and their contribution in drug delivery

Manar I. Al-Ghabeish
*University of Iowa*

Copyright 2014 Manar I. Al-Ghabeish

This dissertation is available at Iowa Research Online: http://ir.uiowa.edu/etd/1529

Recommended Citation
Al-Ghabeish, Manar I.. "Drug transporters in the nasal epithelia and their contribution in drug delivery." PhD (Doctor of Philosophy) thesis, University of Iowa, 2014.
http://ir.uiowa.edu/etd/1529.

Follow this and additional works at: http://ir.uiowa.edu/etd

Part of the Pharmacy and Pharmaceutical Sciences Commons

# DRUG TRANSPORTERS IN THE NASAL EPITHELIA AND THEIR CONTRIBUTION IN DRUG DELIVERY

by

Manar Ibrahim Moh'd Al-Ghabeish

A thesis submitted in partial fulfillment
of the requirements for the Doctor of
Philosophy degree in Pharmacy
in the Graduate College of
The University of Iowa

May 2014

Thesis Supervisor: Professor Maureen Donovan

Copyright by

MANAR IBRAHIM MOH'D AL-GHABEISH

2014

All Rights Reserved

Graduate College
The University of Iowa
Iowa City, Iowa

CERTIFICATE OF APPROVAL

PH.D. THESIS

This is to certify that the Ph.D. thesis of

Manar Ibrahim Moh'd Al-Ghabeish

has been approved by the Examining Committee
for the thesis requirement for the Doctor of Philosophy
degree in Pharmacy at the May 2014 graduation.

Thesis Committee:

Maureen Donovan, Thesis Supervisor

Douglas Flanagan

Aliasger Salem

Mahfoud Assem

Todd Scheetz

To my parents, Ibrahim and Islam

"A little knowledge that acts is worth infinitely more than much knowledge that is idle."
Khalil Gibran

ACKNOWLEDGMENTS

I would like to express my sincere gratitude and appreciation to my advisor Dr. Maureen Donovan for her guidance and help throughout my graduate education at the University of Iowa. Without her persistent support and supervision, I would not have become the scientist I am today.

I acknowledge the guidance and critical evaluation of my work provided by the members of my dissertation committee, Dr. Douglas Flanagan, Dr. Aliasger Salem, Dr. Mahfoud Assem, and Dr. Todd Scheetz. I would also like to thank Dr. Assem for his technical assistance and Dr. Scheetz for help in data analysis.

I would like to thank Dr. Vijay Kumar, member of my comprehensive exam committee, for his valuable feedback and his encouragement.

I would like to express my appreciation for the assistance provided by Kathy Wlaters and the stuff of the Central Microscopy Research Facility (CMRF) at the University of Iowa.

I would like to thank all my past and present lab mates and colleges in the college of pharmacy for their help and discussion and above all friendship. I especially thanks: Hefei Zhang, Chin Ming Lee, Varsha Dhamankar, Maya George, Ana Ferreira, Amal Ayyoub, Mai Tu, and Supreet Agarwal.

I sincerely appreciate all the help and support from my family and friends in Jordan and Egypt and the ones I met in Iowa.

Finally, my parents, my brother Ziad and sister Haneen, I would like to thank them all for their love and never ending support.

ABSTRACT

The nasal route has primarily been used to deliver drugs for the treatment of local diseases such as nasal infections, nasal congestion and allergies. The nasal route can also be used as a non-invasive alternative route to deliver drugs systemically when a rapid onset of action and/or avoidance of hepatic metabolism are desired. Moreover, there is a growing interest in the use of this route for direct transport of drugs from the nose to the brain. Most of the drugs that have been studied for nasal delivery are either small molecules which are lipophilic enough to passively diffuse through the nasal epithelia or macromolecules where bioavailabilities less than 1% are clinically effective and acceptable. This study focused on identifying carrier proteins or transporters in the nasal mucosa that could improve the absorption of specific drug substrates across the nasal respiratory and olfactory epithelia.

The presence of drug transporters in the nasal mucosa of humans and commonly used animal models were investigated. DNA microarray results for nasal samples from humans and two commonly used models, mice and rats, were obtained from GenBank and were analyzed in collaboration with the University of Iowa Center for Bioinformatics and Computational Biology. While cow tissues are frequently used in *in-vitro* nasal permeability analyses, there is limited information available in GenBank for this species. Both DNA microarray analysis and RT-PCR were performed on bovine nasal explants to determine transporter expression. Good agreement between the microarray and RT-PCR results was observed.

While human and three animal species commonly used as models in nasal drug delivery research (mouse, rat, and cow) show similar patterns of expression for several transporters, interspecies differences in the level of expression were observed. Therefore, the

expression level of transporters remains a factor to consider when translating results obtained using animal models to humans.

The nucleoside transporter family was selected for further evaluation of the potential to improve the nasal absorption of substrates. Nucleoside transporters are integral proteins responsible for mediating and facilitating the flux of nucleosides across cellular membranes; they are also known to be responsible for the uptake of nucleoside analog drugs such as anti-cancer and anti-viral agents. RT-PCR and Western blotting were used to verify the presence of two transporter subtypes, ENT1 and CNT3, in the bovine nasal respiratory and olfactory mucosa. The expression level of both transporters in the respiratory mucosa was comparable to that in the olfactory mucosa. Using immunohistochemistry, ENT1 and CNT3 were found to be localized primarily at the apical surface of the nasal epithelial cells. This indicates that the nasal epithelium likely absorbs exogenous nucleosides for intracellular uses such as nucleic acid synthesis and regulating other cellular activities.

The contribution of the nucleoside transporters to the permeation of a nucleoside analogue drug, alovudine, across the nasal epithelia was also studied. The transport of alovudine showed a non-linear increase with increasing donor concentration over the range of 50 to 3000 μM which suggests that nucleoside transporters play a role in its uptake. Polarized transport was not observed suggesting that the facilitative nature of ENT1 plays a major role in alovudine transport. S-(4-nitrobenzyl)-6-thioinosine (NBMPR), an ENT1 inhibitor, incompletely decreased alovudine permeability across the nasal mucosa. This demonstrates that at least one transporter, ENT, plays a significant role in the uptake of this nucleoside drug across the nasal mucosa.

TABLE OF CONTENTS

LIST OF TABLES ..... ix

LIST OF FIGURES ..... xii

CHAPTER 1:INTRODUCTION ..... 1
1.1 .The nasal anatomy ..... 1
1.2. Transport mechanisms across the nasal epithelium ..... 8
1.3. Nasal drug delivery ..... 9
1.4. Nose-brain transport ..... 13
1.5. Models used for nasal transport ..... 18
1.6. Transporter expression in the nasal mucosa ..... 21

CHAPTER 2:OBJECTIVES ..... 24

CHAPTER 3:IDENTIFICATION OF DRUG TRANSPORTERS IN THE NASAL MUCOSA ..... 26
3.1. Introduction ..... 26
3.2. Materials and methods ..... 31
3.2.1. Reagents and materials ..... 31
3.2.2. Methods ..... 32
3.3. Results and discussion ..... 43

CHAPTER 4:IDENTIFICATION AND LOCALIZATION OF ENT1 AND CNT3 IN THE NASAL MUCOSA ..... 59
4.1. Introduction ..... 59
4.2. Materials and methods ..... 65
4.2.1. Reagents and materials ..... 65
4.2.2. Methods ..... 66
4.3. Results and discussion ..... 74
4.3.1. RNA extraction and cDNA production ..... 74
4.3.2. RT-PCR ..... 76
4.3.3. Protein extraction and BCA assay ..... 79
4.3.4. Western blot and immunoblotting ..... 80
4.3.5. Bright field imaging ..... 81
4.3.6. Immunohistochemistry and confocal imaging ..... 84

CHAPTER 5:PERMEATION OF ALOVUDINE THROUGH THE NASAL MUCOSA ..... 91
5.1. Introduction ..... 91
5.2. Materials and methods ..... 95
5.2.1. Reagents and materials ..... 95
5.2.2. Methods ..... 97
5.3. Results and discussion ..... 102

CHAPTER 6:SUMMARY ..... 116

APPENDIX A:GEL IMAGES FOR RCR PRODUCTS ..... 119

APPENDIX B:CONDITIONS SET FOR PRIMER DESIGN ..... 128

APPENDIX C:PARAFFIN PROCESSING FOR BRIGHT FIELD IMAGING.....129

APPENDIX D:DNA SEQUENCING.....133

APPENDIX E:AMINO ACID ALIGNMENTS OF HUMAN ENT1AND CNT3 AGAINST COWS.....134

APPENDIX F:TEER VALUES FOR BOVINE NASAL MUCOSA.....136

APPENDIX G:TRANSPORT STUDIES DATA.....139

REFERENCES.....160

LIST OF TABLES

Table 1.1**:** Nasal cavity characteristics of human and various animal species. ..... 7

Table 1.2**:** Nasal epithelium characteristics..... 9

Table 1.3: Examples of commercially available nasal products. ..... 11

Table 1.4**:** Production rates and volumes of CSF in different species. ..... 20

Table 3.1**:** Major human drug transporters: classification, chromosome locus and example substrates**.** ..... 28

Table 3.2**:** RNA concentration (ng/μL), absorbance at 260 nm and 280 nm, and 260/280 and 260/230 ratios determined from RNA samples extracted from bovine nasal respiratory (Resp) and olfactory (Olf) tissues of three cows for microarray analysis. ..... 33

Table 3.3**:** RNA concentration (ng/μL), 260/280 and 260/230 ratios, rRNA ratio 28s/18s and RIN determined by Agilent 2100 Bioanalyzer for RNA samples extracted from bovine nasal respiratory and olfactory tissues and treated with DNAse for microarray analysis. ..... 35

Table 3.4**:** Conditions for selecting primers by Primer-BLAST. ..... 38

Table 3.5**:** List of primers designed using Primer-BLAST. ..... 39

Table 3.6**:** Materials used to prepare the cDNA production mixture. ..... 42

Table 3.7: Materials used for PCR. ..... 42

Table 3.8**:** PCR conditions. ..... 42

Table3. 9: Expression levels of gene transcripts for known efflux transporter expression determined from analysis of microarray data obtained from NCBI's Gene Expression Omnibus (human, mouse and rat) and from Afftmetrix microarray analysis and RT-PCR (cow).. ..... 48

Table 3.10: Expression levels of gene transcripts for known peptide and monocarboxylate transporter expression determined from analysis of microarray data obtained from NCBI's Gene Expression Omnibus (human, mouse and rat) and from Afftmetrix microarray analysis and RT-PCR (cow). ..... 49

Table 3.11: Expression levels of gene transcripts for known nucleoside transporter expression determined from analysis of microarray data obtained from NCBI's Gene Expression Omnibus (human, mouse and rat) and from Afftmetrix microarray analysis and RT-PCR (cow). ..... 50

Table 3.12: Expression levels of gene transcripts for known organic cation transporter expression determined from analysis of microarray data obtained from NCBI's Gene Expression Omnibus (Human, Mouse and Rat) and from Afftmetrix microarray analysis and RT-PCR(cow).. ..... 51

Table 3.13: Expression levels of gene transcripts for known organic anionic transporter expression determined from analysis of microarray data obtained from NCBI's Gene Expression Omnibus (Human, Mouse and Rat) and from Afftmetrix microarray analysis and RT-PCR(cow).. ....52

Table 3.14: Expression levels of gene transcripts for known heterodimeric amino acid transporter expression determined from analysis of microarray data obtained from NCBI's Gene Expression Omnibus (Human, Mouse and Rat) and from Afftmetrix microarray analysis and RT-PCR(cow).. ....53

Table 3.15: Drug transporter expression reported in the nasal mucosa of humans, mice and rats and the method used for determination. ....55

Table 4.1**:** Classifications and characterization of human nucleoside transporter subtypes. ....64

Table 4.2: Primers designed for bovine ENT1 and CNT3 using Primer 3 ....68

Table 4.3**:** Mixture used for PCR. ....68

Table4. 4**:** PCR conditions for determination of ENT1 and CNT3 from bovine samples. ....69

Table 4.5: Lysis buffer component ....70

Table 4.6**:** BCA protein assay reagents. ....70

Table 4.7**:** Running buffer components ....72

Table 4.8: Transfer buffer component ....72

Table 5.1**:** Krebs-Ringer buffer ....96

Table 5.2**:** Flux values (mean and standard deviation, n=3) of alovudine in the mucosal to submucosal (M-S) and submucosal to mucosal (S-M) directions across the bovine respiratory and olfactory mucosa at different alovudine concentrations in the donor compartment. ....112

Table A.1: RT-PCR performed at annealing temperature of 62℃. ....120

Table A.2 : RT-PCR (trial 1 1) performed at annealing temperature of 55℃. ....121

Table A..3: RT-PCR (trial 2) performed at annealing temperature of 55℃. ....122

Table A.4: RT-PCR performed at annealing temperature of 58℃. ....123

Table A.5: RT-PCR performed at annealing temperatures of 55 and 58℃. ....124

Table A.6: RT-PCR performed at annealing temperature of 55 C. ....125

Table A.7: RT-PCR performed at annealing temperature of 55 ℃. ....126

Table A.8: RT-PCR performed at annealing temperature of 55 ℃. ....127

Table B.1: Conditions set for primer design using Primer3-web 0.4.0 software for *Bos taurus* sequences of ENT1 (SLC29A1) and CNT3 (SLC28A3).....128

Table C.1: Paraffin processing procedure .....129

Table C.2: Station components.....130

Table C.3: Solutions used for staining .....131

Table C.4: Staining procedure.....132

Table F.1: TEER values for bovine respiratory and olfactory nasal mucosa tissues after the exposure to alovudine in KRB at 15 min (start of experiment) and 2 hours (end of experiment).....136

Table F.2: TEER values for bovine respiratory and olfactory nasal mucosa tissues after the exposure to alovudine in KRB containing DMSO at 15 min (start of experiment) and 2 hours (end of experiment).....138

LIST OF FIGURES

Figure 1.1**:** Human nasal cavity structure. ..... 2

Figure 1.2**:** Bright field images of the different types of surface epithelia that line the rat nasal airways..... 4

Figure 1.3**:** Illustration of the lateral wall and turbinates in the nasal passage of a mouse..... 6

Figure 1.4**:** Distribution of peroxidase label in rat main olfactory bulb and olfactory mucosa..... 13

Figure 1.5**:** Pathways of drug distribution in the nasal cavity and central nervous system.. ..... 16

Figure 1.6**:** Autoradiographic images showing signal distribution in different brain regions following intranasal administration of [$^{125}$I]-IGF-I.. ..... 17

Figure 1.7**:** Diagrammatic representation of the lateral wall and turbinates in the nasal airway of the human, monkey, dog, rabbit, and rat. ..... 19

Figure 3.1: Heat map representation of microarray data of drug transporters expression in the nasal mucosa in humans, mice, rats and cows. ..... 54

Figure 4.1: Chemical structures of endogenous nucleosides. ..... 60

Figure 4.2: Predicted transmembrane topologies of mammalian members of the ENT and CNT families. ..... 61

Figure 4.3**:** Mammalian nucleoside transport systems of the equilibrative nucleoside transporter (ENT) and concentrative nucleoside transporter (CNT) protein families. And the chemical structure of nitrobenzylmercatopurine ribonucleoside (NBMPR). ..... 63

Figure 4.4: Bovine nasal tissue sectioned using conventional cryostat and CryoJane® ..... 74

Figure 4.5**:** Example of RNA gel image showing the two characteristic bands of 18S and 28S rRNA subunits for one of the bovine olfactory (O) and respiratory (R) samples. ..... 75

Figure 4.6**:** Gel image of the RT-PCR products indicating the expression of ENT1, CNT3, and GAPDH genes in bovine respiratory and olfactory samples. ..... 76

Figure 4.7: Gel image for the RT-PCR showing the presence of 2 bands for CNT3 samples. Lane 1: 100 bp ladder; Lanes (2,4,6,8):respiratory Samples (R); Lanes (3,5,7,9):olfactory Samples (O)..... 77

Figure 4.8**:** The DNA sequence of the amplified region of CNT3 as expected according to GeneBank (CNT3: NM_001192167.1) and the sequence of the PCR products of the bovine nasal samples..... 78

Figure 4.9: Gel images for the RT-PCR conducted over a number of different cycles..... 79

Figure 4.10**:** Calibration curve for BSA in PBS using the Micro BCA Protein Assay kit. Absorbance was measured at 562 nm. ..... 80

Figure 4. 11: Western blotting showing a band for ENT1 in the bovine respiratory and olfactory samples. ..... 82

Figure 4.12: Bright field images for H&E stained bovine respiratory and olfactory mucosa ..... 83

Figure 4. 13: ENT1 expression in the respiratory mucosa. ..... 87

Figure 4.14ENT1 expression in the olfactory mucosa.. ..... 88

Figure 4.15**:** CNT3 expression . in the respiratory mucosa .. ..... 89

Figure 4.16**:** CNT3 expression in the olfactory mucosa.. ..... 90

Figure 5.1**:** Chemical structure and estimated physical properties of alovudine (3'-fluorodeoxythymidine). ..... 91

Figure 5.2**:** Concentration-dependent influx of $^{3}$H-alovudine (FLT) in oocytes producing human nucleoside transporter proteins and the kinetic parameters of [$^{3}$H] FLT influx. ..... 94

Figure 5.3**:** Diffusion chambers used in transport studies. Each chamber consists of two pieces between which the tissue explants can be mounted. Electrodes for TEER measurement are shown in the back chamber. ..... 95

Figure 5.4: Diagrammatic representation of the cross-section of the bovine nasal cavity showing the respiratory region and the olfactory region. ..... 97

Figure 5.5: HPLC chromatograph of alovudine (7.5 min) in Kreb's Ringer buffer. Mobile phase: 0.05 M ammonium phosphate buffer (pH=6) containing 20% methanol; Column: Zorbax C18 4.6 x 250 mm, 5 μm; Flow rate: 1 mL/min; Wavelength: 254 nm. ..... 100

Figure 5.6**:** Calibration curve for alovudine in Kreb's Ringer buffer. ..... 101

Figure 5.7**:** Representative plot of cumulative amount of drug (alovudine) appearing in the receiver chamber as a function of time during steady state period. ..... 104

Figure 5.8: Flux of alovudine in the mucosal to submucosal (M-S) and submucosal to mucosal (S-M) directions across the bovine respiratory mucosa as a function of the alovudine concentration in the donor compartment (n=3). ..... 110

Figure 5.9: Flux of alovudine in the mucosal to submucosal (M-S) and submucosal to mucosal (S-M)) directions across the bovine olfactory mucosa as a function of the alovudine concentration in the donor compartment (n=3 ..... 111

Figure 5.10**:** Alovudine transport in the mucosal to submucosal (M-S) and submucosal to mucosal (S-M) directions across the bovine respiratory and olfactory mucosa. ..... 113

Figure 5.11: Comparative plot for alovudine flux through bovine respiratory and olfactory mucosa in the mucosal to submucosal (M-S) and submucosal to

mucosal (S-M) directions after normalization of the flux to tissue thickness value of 1 cm (n=3). ....114

Figure 5.12**:** Mean flux value (n=3) for alovudine through bovine respiratory and olfactory tissue at a500μM donor concentration in the presence and absence of 200 nM NBMPR, an ENT1 inhibitor. ....115

Figure E.1: Amino acid alignments of human ENT1 (NP_004946.1) against cows ENT1 (NP_001029570.2) showing 87% identical amino acid sequences. ....134

Figure E.2: Amino acid alignments of human CNT3 (NP_001186562.1) against cows CNT3 (NP_001179096.1) showing 79% identical amino acid sequences. ....135

# CHAPTER 1

# INTRODUCTION

The oral route is the most common and convenient route for drug administration, however, drugs can be subject to acid or enzymatic degradation and hepatic metabolism before reaching the systemic circulation following administration by this route. Therefore, alternative delivery routes could offer an advantage over the oral route in terms of stability as well as for improved local treatments and drug targeting. The nasal mucosa is an interesting application site for the purpose of systemic delivery as well as central nervous system (**CNS**) targeting. In this chapter, a brief review of the nasal anatomy and cellular morphology, as well as the advantages and limitations of nasal route for drug delivery, are described.

## 1.1 .The nasal anatomy

The human nasal cavity is divided longitudinally into symmetrical halves by the nasal septum. Each half opens to the environment through the nares and extends posteriorly to the nasopharynx. Both halves consist of four regions (**Figure 1.1**): (1) the vestibule, (2) the atrium, (3) the olfactory region, and (4) the respiratory region [1, 2]. The vestibule is the most anterior region of the nasal cavity and presents a surface area of about 0.6 $cm^2$. It leads to the atrium via the internal ostium, a narrow inlet, and then to the main chamber of the nasal cavity [2, 3]. The olfactory region is located in the roof of the nasal cavity and covers about 20 $cm^2$ of the nasal surface area[4]. The respiratory region represents the greatest fraction of the surface of the nasal cavity and in human the region contains three turbinates, the superior, the middle and the inferior which project from the lateral wall of each half of the nasal cavity [1, 2, 5, 6]. The main chamber of an adult human nasal cavity is about 5 to 8 cm long with a total surface area of 150-200 $cm^2$ [7].

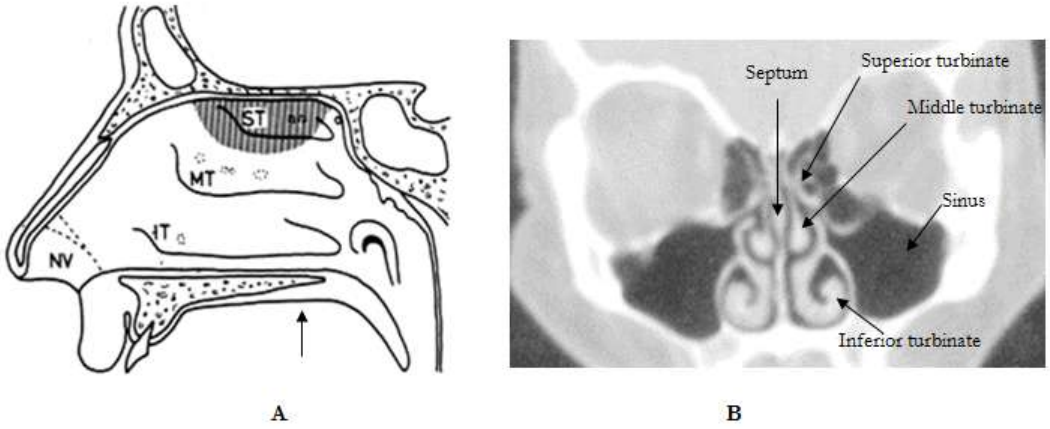


Figure 1.1**:** Human nasal cavity structure. (**A**) Lateral wall and turbinates of the nasal cavity. NV: nasal vestibule; IT: inferior turbinate with the orifice of the nasolacrimal duct; MT: middle turbinate with orifices of the frontal sinus, anterior ethmoidal sinuses and maxillary sinus; ST: superior turbinate with orifices of posterior ethmoidal sinuses. Hatched area in A: olfactory region. (**B**) Cross-section through the middle of the nasal cavity showing the slit-like nature of the nasal airways and the relation to turbinates structures and the paranasal sinuses [1].

Along with providing an open airway and the sensory function of olfaction, the nasal cavity plays an important protective function by filtering, warming, and humidifying inhaled air before it reaches the lower airways. Inhaled particles and pathogens are entrapped by the hairs projecting from the surface of the vestibule or on the mucus layer that covers the respiratory and olfactory epithelium. The mucus layer is cleared by cilia in a process called mucociliary clearance and the entrapped particulates are cleared into the gastrointestinal tract through the nasopharynx [2, 5]. A significant population of enzymes, such as cytochrome P450 isoforms (CYP1A, CYP2A and CYP2E) and carboxylesterases, are found in the nasal cavity[8]. Those enzymes help in metabolizing exogenous compounds to convert them into less toxic forms that are readily eliminated.

Examining the histology of the nasal cavity, various types of cells are present in specific regions of the nasal cavity (**Figure 1.2**). The exterior region of the cavity (the

vestibule) is covered with squamous epithelium that changes into a translational epithelium post the nasal valve/atrium region [1, 2, 6]. The respiratory epithelium consists of four major cell types: ciliated and non-ciliated pseudostratified columnar cells, goblet cells, and basal cells. The ciliated cells facilitate the transport of mucus into the nasopharynx. Many of the columnar cells are covered with microvilli which enhance the respiratory surface area and aid in the exchange of substances, including water, into and from the cells. Goblet cells are secretory cells that produce the mucin that forms the mucus layer. Basal cells are progenitors of other cell-types; they do not extend to the apical epithelial surface and, instead, lie on a thickened layer of collagen called the basement membrane. Beneath the basement membrane, the lamina propria is richly supplied with blood vessels and it also contains nerves, glands, and lymphatics [1, 2].

In the upper region of the nasal cavity, the olfactory region is covered with the olfactory epithelium. It is similar to the respiratory epithelium but contains specialized olfactory cells (olfactory receptor cells) which are important for odorant perception. The remaining cells are ciliated, pseudostratified columnar cells called sustentacular cells; the region also contains basal cells. The lamina propria in this region contains blood vessels, olfactory axon bundles and other nerve fascicles. Bowman's glands secrete mucus onto the epithelial surface that acts as a "solvent" for odorous substances [2, 6].

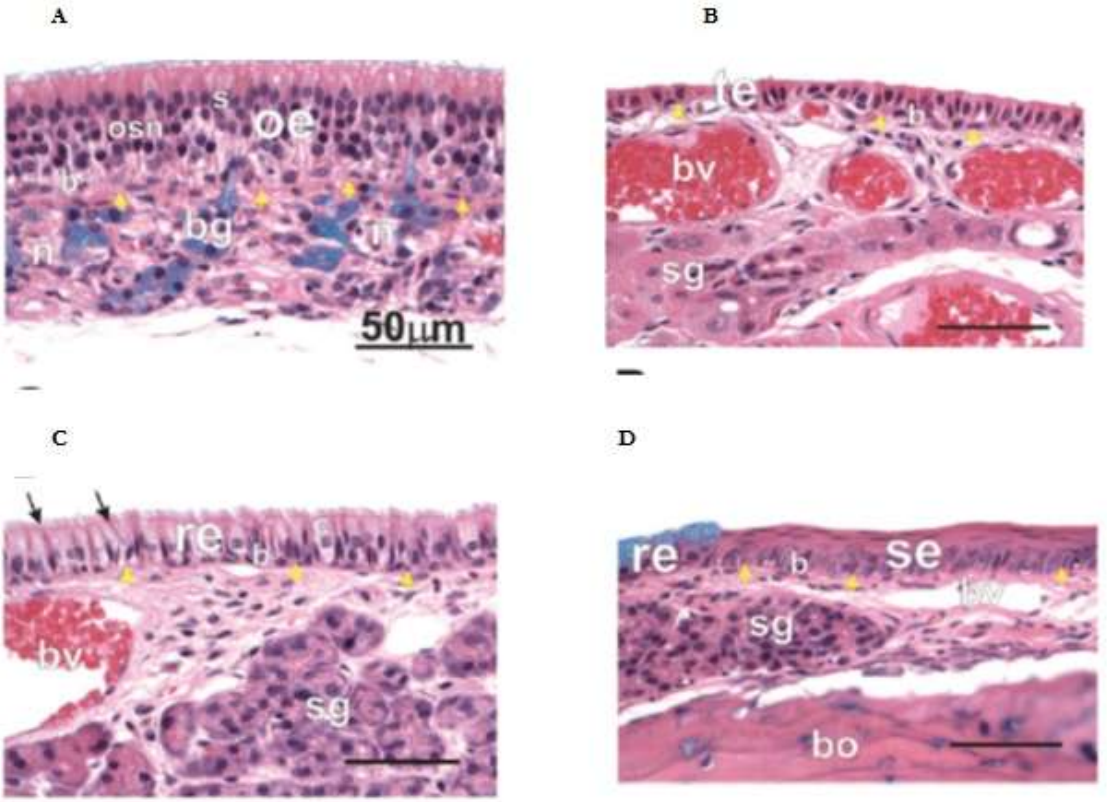


Figure 1.2**:** Bright field images of the different types of surface epithelia that line the rat nasal airways. Humans, mice and cows, the species relevant to this work, contain similar cell types. Tissue sections are stained with hematoxylin and eosin for routine cellular and acellular morphology, and alcian blue (AB; pH 2.4) to identify epithelial cells with acidic mucosubstances (i.e., mucous cells). (**A**) Olfactory epithelium (oe) lining the dorsal septum and containing a prominent apical row of nuclei and cytoplasm of sustentacular cells (s), several middle layers of nuclei in the cell bodies of olfactory sensory neurons (OSN), and basal cells (b) lining the basal lamina. The luminal surface contains numerous cilia from OSNs and microvilli projecting from the apical surface of sustentacular cells. Bowman's glands (bg), with large amounts of intracellular AB-stained mucosubstances, and nerve bundles (n) are present in the lamina propria. Yellow arrowheads identify the basal lamina separating the surface epithelium from the underlying lamina propria. (**B**) Transitional epithelium (te) lining the proximal lateral meatus and composed of nonciliated, cuboidal to low columnar apical cells, and basal cells (b). Blood vessels (bv) and subepithelial glands (sg) are present in the lamina propria. (**C**) Respiratory epithelium lining the midseptum and containing ciliated cells (c), basal cells (b), and narrow, nonciliated serous cells (arrows), interspersed among the ciliated cells, that normally contain no or scant amounts of acidic mucosubstances; (**D**) Stratified squamous epithelium (se) lining the floor of the ventral meatus. There is a sharp transition from respiratory epithelium (re) containing numerous AB-staining mucous cells to se. A thin lamina propria containing some subepithelial glands (sg) and blood vessels (bv) lies between the surface epithelium and bone (bo) [7].

Although there are some general similarities between the nasal structures in humans and other mammalian species, there are some striking interspecies differences in the gross architecture of the nose. Humans and higher animals have relatively simple noses with a primary function of conditioning air for breathing; these species are classified as microsmatic. In comparison, rodents and dogs, commonly used laboratory animals, have more complex noses with olfaction as a primary function, thus they are classified as macrosmatic [3, 7]. Therefore, while the human nose has three turbinates, the turbinates in the laboratory animals have more complex folding and branching pattern [7]. **Figure 1.3** illustrates the complex structure of the turbinates in mice. The morphology of the cell types in the nose has been found to be similar in many animals, including humans, but there are notable differences in the distribution of epithelial cell populations. The major difference is seen in the overall percentage of the olfactory epithelium within the nasal cavity. **Table 1.1** compares the anatomical features of human nose to those of other laboratory animals.

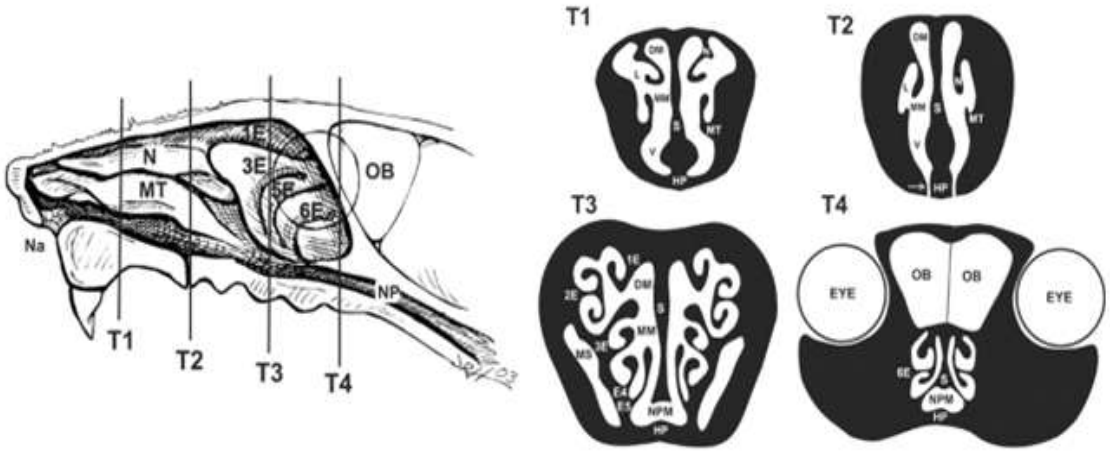


Figure 1.3**:** Illustration of the lateral wall and turbinates in the nasal passage of a mouse. Vertical lines indicate the location of the anterior faces of 4 tissue blocks routinely sampled for light microscopic examination (T1–T4). N: nasoturbinate; MT: maxilloturbinate; 1E–6E: 6 ethmoturbinates; Na: naris; NP: nasopharynx; HP: hard palate; OB: olfactory bulb of the brain; S: septum; V: ventral meatus; MM: middle meatus; L: lateral meatus; DM: dorsomedial meatus; arrow in T2: nasopalatine duct; MS: maxillary sinus; NPM: nasopharygeal meatus[7].

Table 1.1**:** Nasal cavity characteristics of human and various animal species [3,4].

| **Species** | **Surface area ($cm^2$)** | **Surface area/ kg body weight** | **Volume ($cm^3$)** | **Length (cm)** | **Turbinate complexity** | **Olfactory region ($cm^2$)** |
|---|---|---|---|---|---|---|
| Human | 181.0 | 2.5 | 19.0 | 8.0 | Simple scroll | 20.0 |
| Monkey | 61.6 | 7.7 | 8.0 | 5.3 | Simple scroll | 8.0 |
| Dog | 220.7 | 22.0 | 20.0 | 10.0 | Very complex | 169.5 |
| Sheep | 327.0 | 8.2 | 114.0 | 18.0 | Double scroll | - |
| Rabbit | 61.0 | 20.3 | 6.0 | 5.2 | Complex scroll | 9.3 |
| Guinea pig | 27.0 | 45.0 | 0.9 | 3.4 | Complex scroll | - |
| Rat | 10.4 | 41.6 | 0.4 | 2.3 | Complex scroll | 20.0 |

## 1.2. Transport mechanisms across the nasal epithelium

When a compound is administered to the nasal cavity, it can be deposited at one or more of the anatomical regions including the vestibule, atrium, respiratory or olfactory region. The keratinized squamous and translational epithelia that line the vestibule and atrium have no or few cilia. Therefore, compounds deposited in this region will remain stationary, or will be slowly transferred to the nasopharynx by sniffing, or will drip from the nose or be wiped off. Because the respiratory epithelium covers the largest portion of the nasal cavity and it is highly vascularized, compounds deposited in the respiratory region can gain access to the systemic circulation. This region is considered to be the main site in the nasal cavity for systemic absorption. Finally, compounds deposited on the olfactory epithelium, which is innervated with olfactory sensory neurons, could lead to transport of the compounds to CNS (discussed later) [2, 8]. **Table 1.2** summarizes the characteristics of the primary regions of the nasal cavity.

Compounds may cross the epithelial mucosa by paracellular or transcellualr pathways; the paracellular pathway is primarily involved in the transport of small polar drugs and it takes place through the intercellular spaces between adjacent cells. Tight junctions that exist between cells have a size between 3.6 -8.4Å, thus large molecules cannot pass using this pathway and the paracellular transport of molecules is dependent on their size [2].

Compounds can also cross the epithelium by crossing the epithelial cells (transcellular pathway). This pathway involves passive diffusion across the cell membranes and particularly involves the transport of lipophilic molecules. Large molecules, typically with molecular weights greater than 1,000 Da, including peptides and proteins, typically rely on endocytosis to cross the epithelium [2]. Furthermore, transcellular transport can be mediated by carrier proteins or transporters which exist in the cellular membrane and are

responsible for the trafficking of endogenous mediators and for the elimination products of cellular metabolism.

Table 1.2**:** Nasal epithelium characteristics [2].

| **Nasal sections** | **Epithelial characteristics cells/functions** | **Surface area in humans** | **Vascularization** | **Permeability** |
|---|---|---|---|---|
| **Vestibule** | Stratified squamous and keratinized epithelial cells with nasal hairs/Support and protection | ≈ 0.6 $cm^2$ | Low | Poor |
| **Atrium** | Stratified squamous cells/Support<br>Pseudostratified epithelial cells/Support | Not reported | Low | Moderate |
| **Respiratory region** | Columnar non-ciliated cells/Support<br>Columnar ciliated cells/Support and mucociliary clearance<br>Goblet cells/Mucus secretion<br>Basal cells/Progenitors of other cell types | ≈ 130 $cm^2$ | Very high | Good |
| **Olfactory region** | Sustentacular cells/Support<br>Olfactory receptor cells/Olfaction perception<br>Basal cells/Progenitors of other cell types | ≈ 15 $cm^2$ | High | Potential site for nose-brain transport |

## 1.3. Nasal drug delivery

The nasal route has primarily been used to deliver drugs for the treatment of local diseases such as nasal infections, nasal congestion and allergies. The nasal route can also be used as an alternative to the oral and parental routes for systemic drug administration. As a systemic delivery route, the nasal mucosa offers many advantages such as providing rapid

drug absorption with a quick onset of action, enhancing oral bioavailability by avoiding gastrointestinal and hepatic first-pass metabolism, and being painless and non-invasive [2, 5, 9]. **Table 1.3** shows examples of commercially available nasal formulations, including peptides and proteins.

The nasal route has some limitations that must be considered when formulating a drug product, however. One limitation is the mucous layer and associated mucociliary clearance. The half-life for clearance for liquid and powder formulations is on the order of 15- 20 min [5]. The size of the nasal airway also restricts the volume of formulation administered to no more than 100-150 μL [2]. Moreover, the permeabilities of polar compounds and high molecular weight molecules are reduced, yet they are still greater than the permeabilities for those molecules in the gastrointestinal tract. Molecules can be metabolized in the lumen of the nasal cavity or during passage across the nasal epithelia by various enzymes present.

Table 1.3: Examples of commercially available nasal products [2, 10, 11].

| Drug | Brand | Supplier | Dosage Form | Main Indication |
|---|---|---|---|---|
| **Local Delivery** | | | | |
| Azelastine | Astelin (Available in US) | Meda Pharmaceuticals | Spray solution | Management/treatment of symptoms of seasonal and perennial rhinosinusitis |
| Beclomethasone | Beconase (Available in US) | GlaxoSmithKline | Spray suspension | |
| Budesonide | Rhinocort (Available in US) | AstraZeneca | Spray suspension | |
| Mometasone | Nasonex (Available in US) | Schering-Plough | Spray suspension | |
| Olapatadine | Patanase (Available in US) | Alcon Laboratories | Spray solution | |
| Sodium cromoglicate | Nasalcrom | Sanofi Aventis | Spray solution | |
| Triamcinolone acetninde | Nasacort (Available in US) | Sanofi Aventis | Spray suspension | |
| Mupirocin | Bactroban (Available in US) | GlaxoSmithKline | Ointment | Eradication of nasal staphylococci |

Table 1.3 continued

| **Systemic Delivery** | | | | |
|---|---|---|---|---|
| Nicotine | Nicotrol NS (Available in US) | Pfizer | Spray solution | Smoking cessation |
| Cyanocobalamin | Nascobal (Available in US) | Strativa pharmaceuticals | Spray solution | Vitamin B12 deficiency |
| Salmon Calcitonin | Miacalcin (Available in US) | Novartis | Spray solution | Treatment of postmenopausal osteoporosis |
| Buserelin | Suprefact | Sanofi-Aventis | Spray solution | Treatment of prostate cancer |
| Nafarelin | Synarel (Available in US) | Roche Laboratories | Spray solution | Management of endometriosis |
| Zolmitriptan | Zomig Nasal | AstraZeneca | Spray solution | Treatment of migraine and cluster headaches |
| Sumatriptan | Imigran | GlaxoSmithKline | Spray solution | |
| Fentanyl | Instanyl | Nycomed Pharma | Spray solution | Pain management |
| Butorphanol | Stadol NS | Bristol-Myers Squibb | Spray solution | |
| Live attenuated influenza vaccine | FluMist (Available in US ) | MedImmune, Inc. | Spray suspension | Flu prevention |

## 1.4. Nose-brain transport

In the beginning of the last century, viruses such as vesicular stomatitis and poliomyletis were observed to enter the brain via the nasal cavity. Those viruses likely were transmitted along the olfactory nerves to the olfactory bulb and then on to other parts of the brain [6, 12]. Studies have also reported that tracer materials such as potassium ferrocynaide, colloidal gold and horseradish peroxidase can also be transported across the olfactory epithelium to the brain [6]. In fact, Thorne et al. showed that the tracer material, wheat germ agglutinin-horseradish peroxidase (**WGA-HRP**), was transported from the nasal olfactory epithelium to the olfactory bulb (**Figure 1.4**) [13].

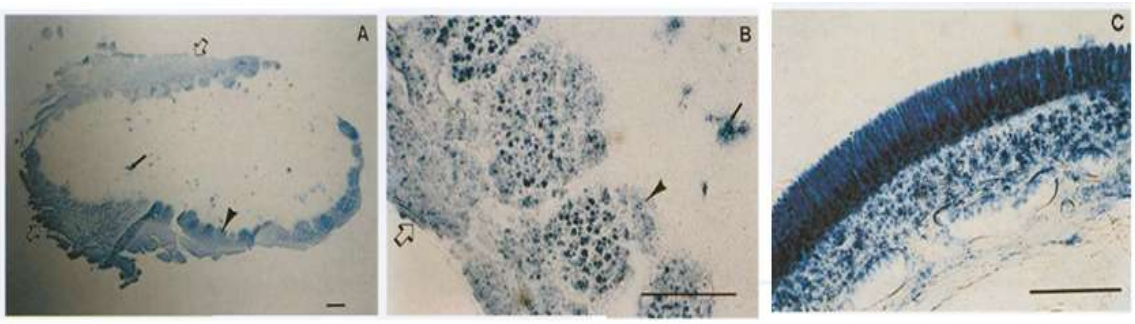


Figure 1.4**:** Distribution of peroxidase label in rat main olfactory bulb and olfactory mucosa. (**A**) 3,3',5,5'-Tetramethylbenzidine (TMB) stained coronal section of bulb following intranasal administration of 1.0% wheat germ agglutinin-horseradish peroxidase (WGA-HRP) showing dense labeling of the olfactory nerve layer (onl) and glomerular layer (gl). (**B**) Higher power magnification image of the gl and onl in rats following intranasal administration of 1.0% WGA-HRP. (**C**) TMB stained section through the olfactory mucosa rat given 1.0% WGA-HRP intranasal. showing dense labeling of the olfactory epithelium and more diffuse labeling in the underlying lamina propria. Open arrows indicate the onl, arrowheads indicate individual glomeruli in the gl and small arrows indicate artifactual labeling associated with blood cells. Bars= 100 μm [13].

There is a growing interest in the use of the nasal route for the direct transport of drugs from the nose to the brain. Several studies have shown that low molecular weight compounds reached the brain in greater amounts after intranasal administration in rats. Compounds including methotrexate [14, 15], hydroxyzine [16], melatonin [17], remoxipride [18], tacrine[19] and 5-flurouracil [20] were shown to have improved CNS bioavailability following nasal administration. In these reports, the amounts of drug in the brain or the concentrations in the cerebrospinal fluid (**CSF**) were measured after intranasal administration along with their concentrations in the plasma. Because the concentrations ratio following nasal administration was higher than obtained following intravenous administration, direct transport to the brain was suggested.

Direct transport of some therapeutics from the nasal cavity to the CNS has also been shown to occur in humans. For example, Born et al. showed that the insulin concentration in CSF was increased in healthy humans 30 min after its intranasal administration compared to placebo [21]. Moreover, administration of intranasal insulin to healthy humans improved memory (delayed word recall) without changing insulin or glucose blood levels [22, 23]. Thus, intranasal insulin appears to be a promising approach in the treatment of cognitive impairments such as Alzheimer's disease [24, 25]. Other examples of direct protein delivery to the brain include melanocortin and cholecystokinin[21 ,26].

There are several proposed mechanisms and pathways by which molecules can access the brain from the nasal cavity (**Figure 1.5**). The olfactory nerve pathways suggested are the major pathways for direct nose-brain delivery. Molecules may be taken up by the olfactory receptor neurons and then the molecules travel through the axons to the olfactory bulb in the brain. This form of transport is usually slow, taking several hours to days, and most molecules that are transported by this pathway are small and highly lipophillic.

Molecules could be also transported by faster extracellular mechanisms, taking 30 or fewer minutes, using the perineuronal channels that are created by olfactory ensheathing cells which envelope the axons of the olfactory neurons and play an important role in neuron regeneration [6, 27].

It has also been shown that molecules can also be transported via the trigeminal nerves that innervate the respiratory and the olfactory epithelia. Thorne and Pronk investigated the brain delivery of radio-labeled insulin-like growth factor-I ($^{125}$I-IGF-I) in rats and showed that the tissue distribution of $^{125}$I-IGF-I following intranasal administration resulted in its rapid entry into the CNS through two routes: one associated with the olfactory pathway connecting the nasal cavity and the olfactory bulb and rostral brain regions (e.g., anterior olfactory nucleus and frontal cortex) and the another pathway associated with the trigmential system connecting the brainstem and the spinal cord (**Figure 1.6**) [28]. Numerous subsequent reports also suggested multiple nose-brain pathways including through the lymphatic channels directly connecting the brain and CSF [27, 28].

Finally, another possible pathway to reach the brain from the nasal cavity is the vascular route [27]. Drugs can enter the venous blood supply in the nasal passages and instead of going into the systemic circulation they could rapidly transfer to the carotid arterial blood supply feeding the brain and spinal cord, a process known as counter-current transfer [29-31]. There is increasing evidence also suggesting mechanisms involving the perivascular spaces that are associated with the outermost layer of the cerebral blood vessels and the basement membrane of the brain resulting in the nose to brain pathways [28, 32, 33].

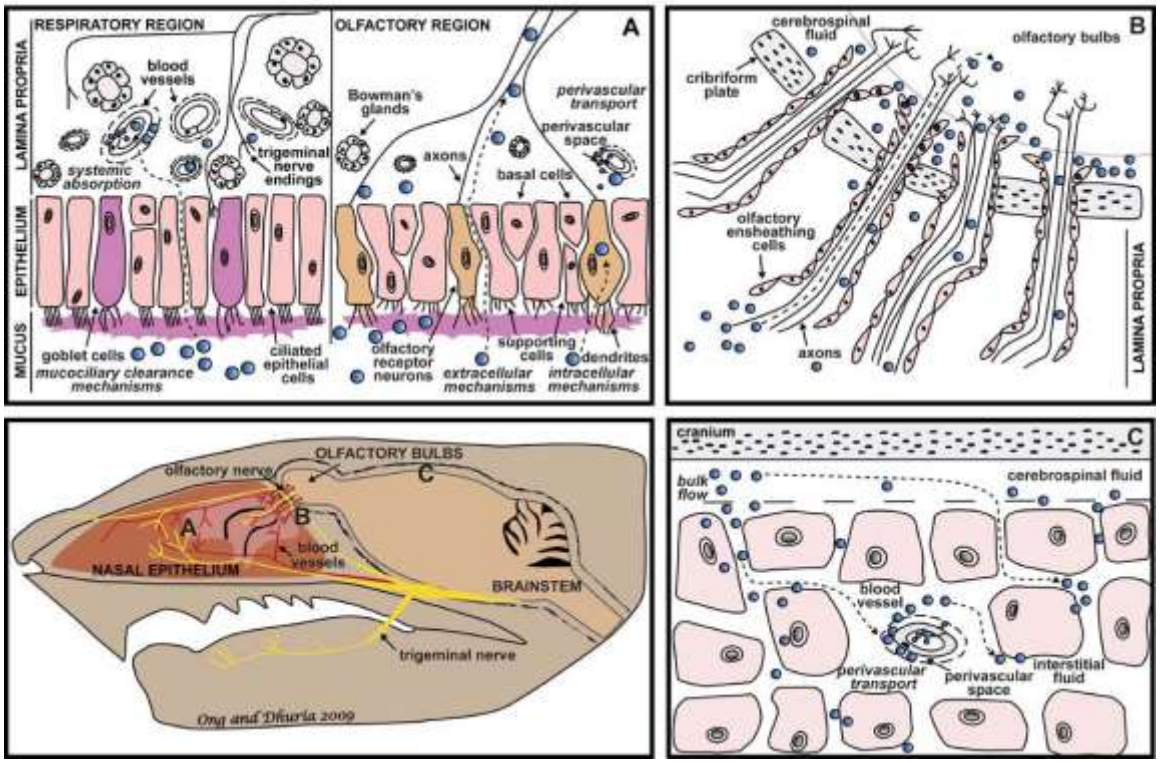


Figure 1.5**:** Pathways of drug distribution in the nasal cavity and central nervous system. Following intranasal administration, drugs (blue circles) come into contact with the nasal mucosa. (**A**) Drugs can be transported through the nasal mucosa to the CNS by entering perivascular channels (dashed lines surrounding blood vessels) in the lamina propria or via extracellular or intracellular mechanisms involving olfactory and trigeminal nerves (dashed arrows). The blood supply to the respiratory epithelium is relatively greater compared to the olfactory epithelium, making it an ideal site for systemic absorption of nasally applied drugs. (**B**) After reaching the lamina propria, drugs can enter channels created by olfactory ensheathing cells surrounding the olfactory nerves, where they can access the CSF and olfactory bulbs (dashed arrows). (**C**) From the CSF, drugs can be distributed via bulk flow mechanisms and mix with brain interstitial fluid throughout the brain (dashed arrows)[27].

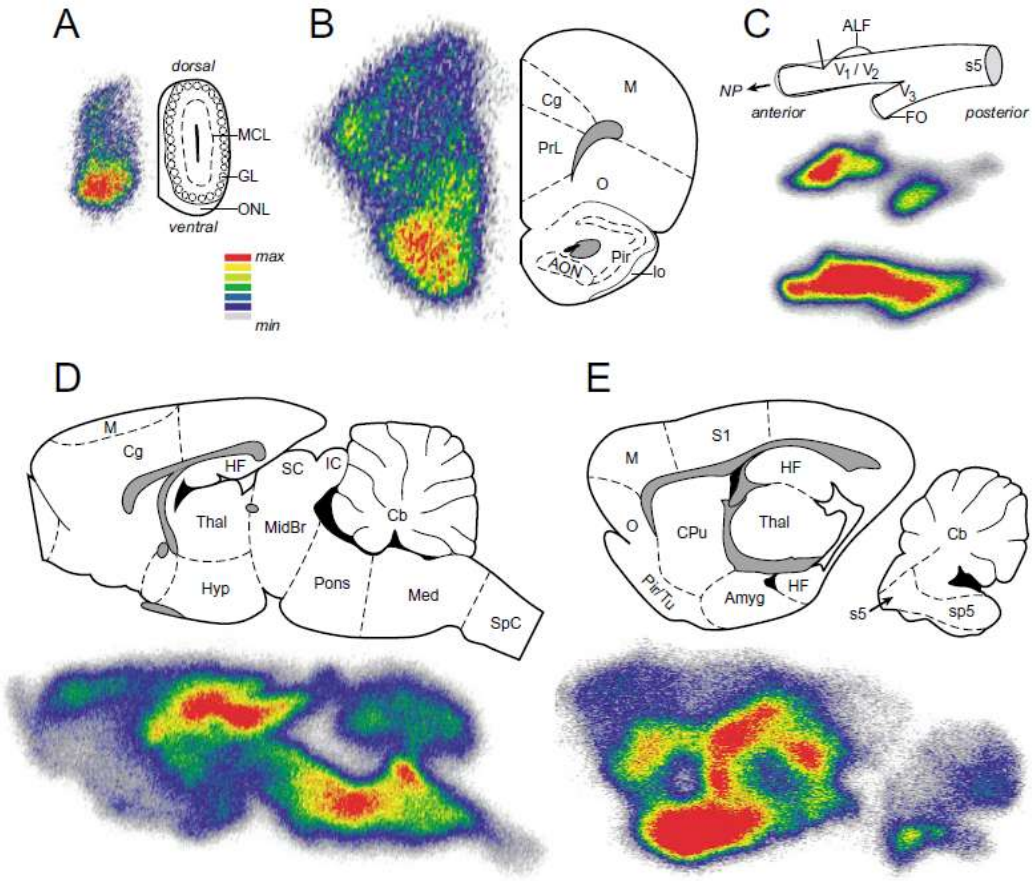


Figure 1.6**:** Autoradiographic images showing signal distribution in different brain regions following intranasal administration of [$^{125}$I]-IGF-I. (**A**) Coronal section (150 µm) through the olfactory bulb. Signal is highest in the ventral olfactory bulb. (**B**) Coronal brain section (150 µm) approximately 3.9 mm anterior to bregma. Signal intensity is highest ventrally. (**C**) Transverse sections (150 µm) through the trigeminal nerve. Highest signal is observed anteriorly. (**D**) Sagittal brain section (150 µm) approximately 0.3 mm lateral to the midline. (**E**) Sagittal brain section (150 µm) approximately 3.8 mm lateral to the midline. (MCL: mitral cell layer of olfactory bulb, GL: glomerular layer of olfactory bulb, ONL: olfactory nerve layer of olfactory bulb, M:primary and secondary motor cortices, O:orbital cortex, PrL: prelimbic cortex, Cg: cingulate cortex, AON: anterior olfactory nucleus, lo: lateral olfactory tract, Pir: piriform cortex, NP: nasal passage, ALF: anterior lacerated foramen, FO: foramen ovale, s5: sensory root of trigeminal nerve, HF: hippocampal formation, Thal: thalamus, Hyp: hypothalamus, SC: superior colliculus, IC: inferior colliculus, MidBr: midbrain, Cb: cerebellum, Med: medulla, S1: primary somatosensory cortex, CPu: caudoputamen, Amyg: amygdale, Tu: olfactory tubercle, sp5: spinal trigeminal nucleus[28].

## 1.5. Models used for nasal transport

Advances in nasal drug delivery research and its application to humans depends, to a great extent, on the use of preclinical animal models. Commonly used animals for *in vivo* studies include monkeys, dogs, rabbits, and rodents [6, 74]. However, it is important when evaluating the results obtained from animals, to consider the differences between humans and the animal model used. For example, the olfactory regions in dogs and rodents covers a larger surface area of the nasal cavity than in humans, while the relative surface area ratio is closer in humans and monkeys (**Figure 1.7**) [7]. Thus, what should be noted that the delivery of a compound from the nasal cavity of rats to the brain, for instance, could be an overestimation of what may happen in humans [7]. Another example of interspecies differences is the volume and the production rate of CSF among the species (**Table 1.4**). The CSF is rapidly transferred into the general circulation, thus, the absorption rate to the peripheral bloodstream is almost equal to the production rate of CSF [34]. For example, based on the total volume and rate of production of CSF in humans and rats, it will take 5 hours for the entire CSF to be replaced in humans while it only requires 1 hour in rats [6]. That makes the CSF turnover differences between humans and animal species important in the determination of distribution of the drugs in the CNS and their clearance.

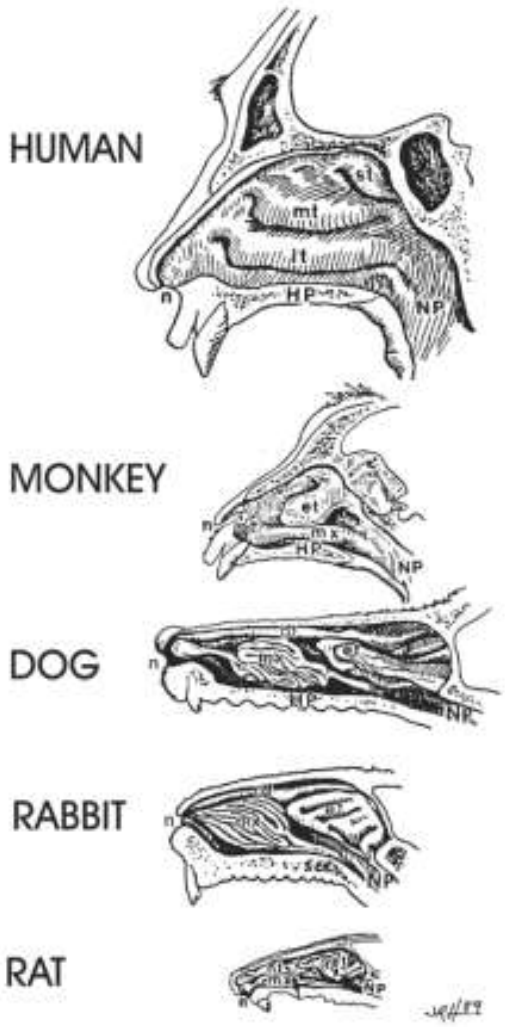


Figure 1.7**:** Diagrammatic representation of the lateral wall and turbinates in the nasal airway of the human, monkey, dog, rabbit, and rat. HP: hard palate; n: naris; NP: nasopharynx; et: ethmoturbinates; nt: nasoturbinate; mx: maxilloturbinate; mt: middle turbinate; it: inferior turbinate; st: superior turbinate [7].

Table 1.4**:** Production rates and volumes of CSF in different species [6].

| **Species** | **Production rate (mL/hr)** | **Volume in brain (mL)** |
|---|---|---|
| Mouse | 0.018 | 0.035 |
| Rat | 0.18 | 0.15 |
| Rabbit | 0.6 | 2.3 |
| Monkey | 2.5 | -- |
| Sheep | 7.1 | 14.2 |
| Human | 21.0 | 100.0 |

The utilization of excised nasal tissues and cell culture systems provides a rapid method to evaluate the permeability properties of drug molecules and to evaluate cellular mechanisms of absorption. These systems offer additional advantages such as separating of permeation from subsequent absorption and limiting the number of required animal experiments [35, 36]. Cell culture of human nasal cells provides one type of *in vitro* model. Primary human cell cultures of the nasal epithelia were obtained from traumatic samplings, such as surgical biopsies, or nasal swabbing. The difficulties of obtaining human cells, as well as the short life-span of the primary cell cultures and the need for standardization between cultures represent major limitations to the use of these primary cell cultures as a nasal model. There have been several approaches to immortalize the nasal epithelial cells; the only cell line that is currently available commercially is RPMI 2650, which was derived from an anaplastic squamous cell carcinoma of the human nasal septum and is closely related to the human nasal epithelium regarding karyotype. Its cytokeratin polypeptide pattern and the presence of mucus on the cell surface suggest the similarity to the normal epithelium [36]. On the other hand, RPMI 2650 shows histological differences from the nasal epithelia such as

multilayered cell growth and the absence of ciliary function. Moreover, studies are ongoing to optimize the growth conditions and validate their use in drug transport studies [36, 37].

In the absence of a standard cell culture model, tissues from rabbits, cows, pigs and sheep have been used in permeability studies and in the characterization of potential drug absorption [35, 38]. In our group the bovine nasal mucosa was selected as model membrane mainly because of its availability, its reproducible quality, the ability to separate respiratory and olfactory mucosa, and the ability to obtain large quantities of tissue. Schmidt et al. first reported the use of excised bovine mucosa as an *in vitro* model to study drug transport and metabolism in nasal epithelium[39]. These tissues retained their viability for in vitro studies for up to 3 hours which was demonstrated by positive viability staining, constant transepithelial electrical resistance, a constant rate of metabolic turnover, along with a linear permeation profile for a therapeutic peptide and mannitol[39].

### 1.6. Transporter expression in the nasal mucosa

The presence of transporters in the nasal mucosa helps in explaining and/or predicting the permeation of specific substrates across the nasal mucosa. The major focus of nasal drug delivery studies is on the applicability of this route for different therapeutic compounds and identifying methods to enhance nasal permeability. Fewer studies have been pursued to understand the mechanisms of nasal permeability, especially transporters may be involved [9, 40-42]. Chemutruri and Donovan investigated the role of the organic cation transporters (**OCT**s) in the transport of dopamine across the nasal mucosa[42]. Dopamine flux across the bovine nasal mucosal explants increased in a non-linear manner with increasing dopamine donor concentration. The saturable transport observed suggests that at least one transporter was involved in dopamine uptake. Moreover, the flux of dopamine decreased in the presence of amantidine, an OCT 1-2 inhibitor, and guanidine, an OCT2 inhibitor,

indicating that OCTs mediate dopamine uptake by the bovine nasal mucosa. Finally, OCT2 was shown to be expressed in the nasal mucosa using Western blotting [42].

Lee et al. looked for the relative contribution of the direct pathway to the brain permeation of 17 model drugs after the nasal administration in rats [43]. The model drugs under study possessed a variety of different physiochemical properties including molecular weights, log P/D, and PAMPA permeability values. All model drugs were systemically absorbed after nasal administration, but only 5 of 15 showed direct transport to the brain as indicated by the amount in the brain after nasal administration compared to the amount after intravenous administration. There was no correlation between the fraction transferred to the brain directly and the chemical properties and/or PAMPA permeability values of the model drugs. However, the five compounds directly transported to the brain were found to be substrates of the transporters OAT3 and/or OCT2. Those transporters have been reported to be expressed in the rat olfactory nasal mucosa [43]. These findings indicate the potential involvement of transporters in nasal permeation and direct brain transport.

Other studies have examined efflux transporters and their potential role in limiting substrate transport across the nasal mucosa [44-46]. To understand the lack of CSF distribution of chlorpheniranmine and chlorcyclizine following intranasal administration compared to other antihistamines, e.g. hydroxizine, that readily reach the CNS through the nasal route, Kandimalla and Donovan studied the permeation of chlorpheniranmine and chlorcyclizine across the nasal mucosa[46]. The flux of these two compounds in the mucosal to submucosal direction was lower than in the submucosal to mucosal direction suggesting that both compounds were pumped out from the nasal mucosa by transporters. One of the efflux transporters that was found to be expressed on the apical side of the nasal mucosa was P-glycoprotein (**P-gp**). In the presence of verpamil and quinidine, P-gp and multidrug

resistance protein1 (**MRP1**) inhibitors, the flux of chlorpheniranmine and chlorcyclizine in the mucosal to submucosal direction increased[45, 46]. Graff et al. evaluated the P-gp-mediated efflux of $^{3}$H verapamil from brain with the co-administration of rifampin, a P-gp inhibitor, and the influence of delivery route (nasal vs. systemic) on brain uptake. Rifampin was shown to inhibit P-gp and enhance the brain uptake of $^{3}$H verapamil in mice regardless of the route of administration. In addition, complete inhibition was achieved when both the substrate and inhibitor was intranasally administered. P-gp was localized in the olfactory epithelium and olfactory bulb in these mice [44].

Identifying transporters in absorptive mucosae has been pursed extensively, especially in the intestinal mucosa. The gene expression patterns of membrane transporters and channel proteins in the human intestine were identified using microarray [47, 48]. Moreover, the relative abundance of the transporters' mRNA at different regions of the small intestine was measured using quantitative polymerase chain reaction (**q-PCR**) [49-51]. Finally, several studies compared the transporter expressions in human intestine with the human intestinal cell line, Caco-2, and animal models such as rats and mice [49-52]. Compared to the intestinal mucosa, not much is known about transporter expression in the nasal mucosa. Few studies describe efflux and/or uptake transporters in the nasal mucosa, specifically the olfactory mucosa, however; expression of most of the drug transporters has not been yet identified[16, 42, 53-57]. Gene expression analysis of all the transporter genes can allow identification of key transporters with major role in drug transport through nasal route. Subsequent transport studies will establish their clinical significance and could improve the nasal absorption of specific drug substrates.

# CHAPTER 2

## OBJECTIVES

The work described in the following chapters was undertaken in order to: (1) identify transporters in the nasal mucosa that could improve the nasal absorption of specific drug substrates; (2) compare the transporter expression among human and animal models commonly used to evaluate nasal drug absorption; (3) determine the distribution of some transporters, namely nucleoside transporters, in the nasal mucosa; and (4) determine the contribution of these transporters to the overall permeability of drug substrates across the nasal respiratory and olfactory mucosa.

**Specific Aims**

1. Identify and compare the expression of transporters that are involved in the uptake and efflux of drug substrates in human and in animal models commonly used in nasal transport studies (mice, rats, and cows) using DNA microarray.
2. Use reverse transcriptase- polymerase chain reaction (**RT-PCR**) to confirm the gene expression of transporters identified by microarray in the bovine nasal mucosa.
3. Evaluate the distribution of the nucleoside transporters, specifically ENT1 and CNT3, in the nasal mucosa.
4. Investigate the *in vitro* permeability of a nucleoside analog drug compound, alovudine, across the nasal mucosa.
5. Determine the contribution of ENT1 to the total permeability of alovudine across the nasal mucosa by studying alovudine permeation in the presence of an ENT1 inhibitor.

Examining the expression of drug transporters in the nasal mucosa will assist in identifying the transporters with a major role in drug transport across the nasal mucosa. Moreover, determining species similarities and differences in the expression of transporters is useful especially in translating information obtained from animal models to humans. Finally, determining the contribution of transporters in the nasal permeation of drug substrate will help in predicting the absorption behavior of the drug after intranasal administration.

# CHAPTER 3

# IDENTIFICATION OF DRUG TRANSPORTERS IN THE NASAL MUCOSA

## 3.1. Introduction

"Carrier proteins" or "transporters" are proteins that span cellular membranes and are responsible for the intake and the efflux of crucial endogenous substances such as sugars, amino acids, nucleosides and inorganic ions. The specificity of transporters is not limited to their physiological substrates but it also includes the uptake of exogenous compounds and participates in the efflux of toxins, environmental or metabolite, thus protecting the cell. Moreover, drugs with significant structural similarities to the endogenous substrates can also be substrates for these transporters. Thus, transporters can influence the absorption, disposition and the elimination of drug substrates [58].

The transporters of greatest current interest in drug disposition belong to one of two major classes, (1) ATP-binding cassette (**ABC**) or (2) solute carrier (**SLC**) transport families. ABC transporters are a family of transporters that hydrolyze ATP to produce the energy required to transport substrates across membranes. Thus, ABC transporters are primary active transporters [58].In eukaryotes, ABC transporters act as exporters which mean they mediate the efflux of compounds out of cells [59]. ABC transporters, therefore, play an important role in protecting the tissues against the entry of toxins [60]. Furthermore, they export a wide variety of endogenous substances associated with normal physiologic processes such as getting rid of metabolites and the disposition of lipids in membranes [59]. The over expression of ABC transporters has long been known to be related to drug resistance [60-62].

There is 48 known human ABC transporters that are grouped into 7 subfamilies designated A through G [60]. The most studied drug transporters belonging to the ABC family are multidrug resistance protein (**MDR**), multidrug resistance-associated protein (**MRP**), and breast cancer resistance protein (**BCRP**) [58]. MDR or P-glycoprotein (**P-gp**) forms a small gene family of the subfamily ABCB in high mammalians, with 2 isoforms in humans and 3 in rodents. Isoforms 1 and 3 are drug transporters while isoforms 2 exports phosphatidylcholine into the bile [61]. Nine out of 12 members of the ABCC, a subfamily of ABC family, are recognized to be involved in drug efflux in cells and those are the MRPs. There is only one member of the subfamily ABCG that is involved in drug efflux which is ABCG2 or BRCB [60].

The majority of drug uptake transporters belong to the SLC transporter family. In contrast to the ABC transporters, SLC transporters do not directly utilize ATP. Some SLC transporters couple with ion gradients, such as the sodium or proton gradients across the membrane, to transport substrates against their concentration gradient. The ion gradient is created by other primary active transporters. As a result, these transporters are referred to as secondary active transporters. Other SLC transporters transport along the concentration gradient but enable a higher rate of transport than through passive diffusion and are therefore classified as facilitated transporters [58, 63]. SLC transporters currently represent 43 families including about 300 transporter genes in humans [63]. Among the families that have been studied extensively for their role in drug absorption, the organic cation, organic cation/carnitine, organic anion, peptide, monocarboxylate and nucleoside transporters are of particular current interest [58]. **Table 3.1** lists major drug transporter families and the family members of the ABC and SLC transporters.

Table 3.1**:** Major human drug transporters: classification, chromosome locus and example substrates**.**

| Transporter family | Family member (Common names) | Gene name | Human chromosome locus | Examples of substrate |
|---|---|---|---|---|
| **Organic cation transporter (OCT)** | OCT1 | SLC22A1 | 6q26 | metformin, famotidine, and norepinephrine |
| | OCT2 | SLC22A2 | 6q26 | |
| | OCT3 | SLC22A3 | 6q26-q27 | |
| **Organic cation/cartinine transporter (OCTN)** | OCTN1 | SLC22A4 | 5q31.1 | carntine, betaine and verpamil |
| | OCTN2 | SLC22A5 | 5q31 | |
| | OCTN3 | SLC22A21 | 5q31 | |
| | CT2 | SLC22A16 | 6q22.1 | |
| **Organic anion transporter (OAT)** | OAT1 | SLC22A6 | 11q13.1-q13.2 | salicylates, penicillin, methotrexate and acyclovir |
| | OAT2 | SLC22A7 | 6p21.2-p21.1 | |
| | OAT3 | SLC22A8 | 11q11.7 | |
| | OAT4 | SLC22A11 | 11q13.1 | |
| | OAT5 | SLC22A10 | 11q12.3 | |
| | OAT6 | SLC22A20 | Unknown | |
| | URAT1 | SLC22A12 | 11q13.1 | |
| **Organic anion transporter polypeptide (OATP)** | OATP1C1 | SLCO1C1 | 12p12.2 | fexofenadine, atorvastatin, and benzyl penicillin |
| | OATP1B1 | SLCO1B1 | 12p12.2 | |
| | OATP1A2 | SLC01A2 | 12p12 | |
| | OAT1B3 | SLCO1B3 | 12p12 | |
| | OATP2A1 | SLCO2A1 | 3q21 | |
| | OATP2B1 | SLCO2B1 | 11q13 | |
| | OATP3A1 | SLCO3A1 | 15q26 | |
| | OATP4A1 | SLCO4A1 | 20q13.33 | |
| | OATP4C1 | SLCO4C1 | 5q21.2 | |
| | OATP5A1 | SLCO5A1 | 8q13.3 | |
| | OATP6A1 | SLCO6A1 | 5q21.1 | |
| **Peptide transporter (PEPT)** | PEPT1 | SLC15A1 | 13q33-q34 | captopril, alafosfalin and valacylovir |
| | PEPT2 | SLC15A2 | 3q21.1 | |
| | PHT1 | SLC15A4 | 12q24.32 | |
| | PHT2 | SLC15A3 | 11q12.2 | |

Table 3.1 continued

| | | | | |
|---|---|---|---|---|
| **Monocarboxylate transporter (MCT, sMCT)** | MCT1 | SLC16A1 | 1p12 | phenethicillin and valproic acid |
| | MCT2 | SLC16A7 | 12q13 | |
| | MCT3 | SLC16A8 | 22q12.3-q13.2 | |
| | MCT4 | SLC16A3 | 17q25 | |
| | SMCT1 | SLC5A8 | 12q23 | |
| | SMCT2 | SLC5A12 | 11p14 | |
| **Nucleoside transporter (CNT,ENT)** | CNT1 | SLC28A1 | 15q25-26 | gemcitabine, ribavirin and zidovudine |
| | CNT2 | SLC28A2 | 15q15 | |
| | CNT3 | SLC28A3 | 9q22.2 | |
| | ENT1 | SLC29A1 | 6p21.1-p21.2 | |
| | ENT2 | SLC29A2 | 11q13 | |
| | ENT3 | SLC29A3 | 10q22.1 | |
| | ENT4 | SLC29A4 | 7p22.1 | |
| **Multidrug resistance protein (MDR)** | MDR1 or P-gp | ABCB1 | 7q21.1 | vinblastine, doxorubicin, digoxin, and dexamethasone |
| **Multidrug resistance associated protein (MRP)** | MRP1 | ABCC1 | 16p13.1 | doxorubicin , methotrexate and vinblastine |
| | MRP2 | ABCC2 | 10q24 | |
| | MRP3 | ABCC3 | 17q22 | |
| | MRP4 | ABCC4 | 13q32 | |
| | MRP5 | ABCC5 | 3q27 | |
| | MRP6 | ABCC6 | 16p13.1 | |
| | MRP7 | ABCC10 | 6p21.1 | |
| | MRP8 | ABCC11 | 16q12.1 | |
| | MRP9 | ABCC12 | 16q12.1 | |
| **Breast cancer resistance protein (BCRP)** | BCRP1 | ABCG2 | 4q22 | mitoxantrone, etoposide, and anthracycline |

Another SLC transporter family that was previously studied for its role in drug transport is amino acid family. The amino acid transporter family is divided into two subfamilies: the cationic amino acid transporters (**CAT** family, SLC7A1-4) and the glycoprotein- associated amino acid transporters (**gpaAT** family, SLC 7A5-7) also called the light chains or catalytic chains of heterodimeric amino acid transporters (**HAT**) [64]. Large neutral amino acid transporters (LAT 1 and LAT2 ) are HAT transporters that interact with large neutral amino acids and have been suggested to contribute in the transport of several drugs such as L-DOPA, gabapentin, and thyroid hormones [65].

In order to better understand the role of transporters in nasal absorption, the gene expression of drug transporters in nasal mucosa of a variety of used animal models was investigated and compared to the reported gene expression in humans. Knowledge of the presence of drug transporters in the nasal mucosa can assist in the prediction of the absorption properties of drug substrates following nasal administration and in the selection of appropriate animal models for use in preclinical investigations.

Mice and rats are commonly used to investigate nasal drug absorption, yet their small nasal cavities limit the use of their tissues for *in-vitro* investigations. Bovine tissue explants have been used to investigate drug transport through the nasal respiratory and olfactory mucosae, yet limited information is available regarding the similarities and differences among these various animal models compared to humans. Knowing the gene expression profiles in each species can assist in the correct selection of model systems when the drug under investigation is a transporter substrate.

## 3.2. Materials and methods

### 3.2.1. Reagents and materials

TRIzol® reagent and the SuperScript™ II Reverse Transcriptase kit were purchased from Invitrogen (Life Technologies, Carlsbad, CA). The PCR kit, Molecular Markers and Blue Juice (6X) were purchased from New England-Biolabs (Ipswich, MA). Other reagents used were: chloroform (Marcon Chemicals, Avantor Performance Materials, Center Valley, PA), 2-propanol (Sigma-Aldrich, St. Louis, MO), DNase and RNase free water (Gibco Life Technologies, Carlsbad, CA), agarose (Research Products International Corp, Mount Prospect, IL), 10X Tris/Borate/EDTA (**TBE**) buffer and ethidium bromide (10 mg/ml) (Bio-Rad, Life Research Clinical Diagnostics, Hercules, CA), deoxyribonucleotide (**dNTP**) (Applied Biosystem -Roche, Indianapolis, IN).

**Gel preparation:** The 1 or 2 % agarose was prepared by adding 2 or 4 g of agarose, respectively, to 200 ml of 1X TBE buffer (diluted with Nanopure water) and heated by placing in a microwave until the solution was clear followed by cooling for several minutes. To make a small gel (20 wells), 75 ml was used and for the large gel (40 wells) 125 ml was used (both horizontal gel systems from Owl Scientific, Thermo Scientific, Waltham, MA). Ethidium bromide 7.5 µl or 15 µl of 1 mg/ml solution (prepared from stock (10 mg/ml) and protected from light) was added to the small and large gels, respectively. The agarose-containing solution was poured into the respective mold, combs were placed over the gels, and the system was checked to make sure no bubbles were present. The gels were left to solidify.

### 3.2.2. Methods

#### 3.2.2.1. Microarray analysis

##### 3.2.2.1.1. RNA extraction

Respiratory and olfactory nasal tissues were excised from 3 male cows (about 2 years old) and were snap-frozen using liquid nitrogen. The tissues were minced in the presence of 1mL TRIzol® reagent using a scalpel. Chloroform (0.2 mL) was added to each sample, shaken for 15 seconds and centrifuged (Eppendorf centrifuge 5810R, Hauppauge, NY) at 12000 x g for 15 min at 5 ºC. The supernate was carefully withdrawn, and the RNA was precipitated by adding 0.5 mL isopropanol followed by centrifuging at 12000 x g for 10 min at 5 ºC. The RNA was washed by adding 1 mL of 70% ethanol to the pellet followed by centrifuging at 7500 x g for 5 min at 5 ºC. The ethanol layer was withdrawn and the pellet was left to dry and was then reconstituted with 40 μL DNase and RNase free water. An aliquot (35 μL) of the sample was withdrawn into a small tube and the reminder was withdrawn for further quantification.

##### 3.2.2.1.2. RNA quantification

A 2 μL sample was withdrawn and the concentration (ng/μL) of RNA was determined using a Nanodrop spectrophotometer (Thermo Scientific, Waltham, MA). The absorption at 260 nm and at 280 nm was measured and the ratios between absorbance at 260 and 280 nm and between 260 and 230 nm were determined (**Table 3.2**).

##### 3.2.2.1.3. RNA treatment

The samples were treated with DNase (2 units per 10-15 ug of RNA) at 37 ºC for 10 min. The DNase was deactivated by the addition of EDTA (concentration in the total mixture was equal to 0.05 M) along with heating at 75 ºC for 10 min. A sample (10 μL) was

placed on dry ice and transferred to the DNA Core Facility, University of Iowa for microarray analysis.

Table 3.2**:** RNA concentration (ng/μL), absorbance at 260 nm and 280 nm, and 260/280 and 260/230 ratios determined from RNA samples extracted from bovine nasal respiratory (Resp) and olfactory (Olf) tissues of three cows for microarray analysis[1].

| Sample name | RNA concentration (ng/μL) | Absorbance at 260 nm | Absorbance at 280 nm | 260 / 280 ratio | 260/ 230 ratio |
|---|---|---|---|---|---|
| **Resp 1** | 430.70 | 10.78 | 5.69 | 1.89 | 0.91 |
| **Olf 1** | 511.90 | 12.80 | 7.06 | 1.83 | 0.89 |
| **Resp 2** | 381.70 | 9.54 | 4.97 | 1.92 | 1.69 |
| **Olf 2** | 532.00 | 13.30 | 6.91 | 1.92 | 0.89 |
| **Resp 3** | 404.20 | 10.12 | 5.63 | 1.81 | 0.60 |
| **Olf 3** | 397.00 | 9.93 | 5.41 | 1.84 | 0.78 |

3.2.2.1.4. Microarray analysis

For optimal results from the DNA microarray analysis, the RNA that is used to synthesize the required cDNA should meet the following criteria: (1) The RNA concentration should not be below 100 ng/μL and should be treated with DNAase to remove any genomic DNA present. (2) The RNA samples should have minimal protein contamination which is indicated by the ratio between the absorbance at 260 and 280 nm which should be greater than 1.8. The samples should have minimal traces of phenol and other organic contaminants indicated by the lack of an absorbance peak at 270 nm. The DNA Core Facility checks these characteristics in the RNA samples using NanoDrop (Thermo Scientific, Waltham, MA).

[1] According to the Nanodrop manual, RNA concentration (c) is calculated from Beer-Lambert equation [$Abs = abc$] from the 260 nm absorbance (abs) and RNA extinction coefficient (a) of 40 ng-cm/μL and a cell path length (b) of 1 cm.

Moreover, the RNA integrity was checked using an RNA LabChip® with an Agilent 2100 Bioanalyzer (Agilent Technologies, San Clara, CA). The RNA samples were electrophoretically separated on the chips and evaluated via laser induced fluorescence detection by the Agilent 2100 bioanalyzer. An electropherogram was generated and analyzed to display the RNA Integrity Number (**RIN**) along with RNA concentration and the 28s/18s rRNA ratio (**Table 3.3**). The RIN is a measure for RNA integrity which ranges from 1 to 10 with 1 indicating the most degraded RNA profile and 10 being the most intact. In our study, the RIN must be above 6 to be included in the microarray analysis.

Fifty nanograms of total RNA was converted by **SPIA®**(Single Primer Isothermal Amplification) to cDNA using the Ovation RNA Amplification System v2 (NuGEN Technologies, San Carlos, CA) according to the manufacturer's recommended protocol. The amplified SPIA® cDNA product was purified through a QIAGEN QIAquick PCR Purification Column (QIAGEN, Hilden, Germany) according to modifications from NuGEN. A sample (3.75 ug) of this product was fragmented (average fragment size = 85 bases) and biotin labeled using the NuGEN FL-Ovation cDNA Biotin Module v2 (NuGEN Technologies, San Carlos, CA) per the manufacturer's recommended protocol. The resulting biotin-labeled cDNA was mixed with Affymetrix eukaryotic hybridization buffer, placed onto Affymetrix GeneChip Bovine Expression Arrays, and incubated at 45 ºC for 18 h at 60 rpm rotation in an Affymetrix Model 640 Genechip Hybridization Oven (Affymetrix, Inc., Santa Clara, CA). Following hybridization, the arrays were washed, stained with streptavidin-phycoerythrin (Molecular Probes, Inc., Eugene, OR) and the signal was amplified with anti-streptavidin antibody (Vector Laboratories, Inc., Burlingame, CA) using the Affymetrix Model 450 Fluidics Station (Affymetrix, Inc., Santa Clara, CA). Arrays were scanned with an Affymetrix Model 3000 scanner with 7G upgrade (Affymetrix, Inc., Santa Clara, CA) and

data were collected using the GeneChip operating software (**GCOS**) v1.4. Expression value estimates were generated using the Microarray Analysis Suite (**MAS**) v5.0, software.

Table 3.3**:** RNA concentration (ng/μL), 260/280 and 260/230 ratios, rRNA ratio 28s/18s and RIN determined by Agilent 2100 Bioanalyzer for RNA samples extracted from bovine nasal respiratory and olfactory tissues and treated with DNAse for microarray analysis.

| Sample name | RNA concentration (ng/μL) | Ratio 260/280 | Ratio 260/230 | rRNA ratio 28s/18s | RIN |
|---|---|---|---|---|---|
| **Resp 1** | 128 | 2.00 | 0.64 | 1.1 | 8.3 |
| **Olf 1** | 262 | 2.04 | 1.01 | 1.0 | 7.2 |
| **Resp 2** | 259 | 2.10 | 0.84 | 0.7 | 6.2 |
| **Olf 2** | 297 | 2.09 | 0.90 | 1.3 | 7.9 |
| **Resp 3** | 130 | 1.91 | 0.64 | 1.2 | 6.9 |
| **Olf 3** | 203 | 2.02 | 0.97 | 1.0 | 6.7 |

3.2.2.1.5. Microarray data analysis

Microarray expression data for nasal mucosa were identified and collected from NCBI's Gene Expression Omnibus. Only samples from normal (non-diseased, non-treated) tissues were used. A total of 71 samples from humans (GSE11348, GSE2395, GSE8987, GSE9150), 15 samples from mouse (GSE1680, GSE2437, GSE3455, GSE4915, GSE4927), and 34 samples from rat (GSE5019, GSE5349, GSE7002) were analyzed. These samples were all run on 3' IVT arrays from Affymetrix, from which expression present/absent calls were obtained using the MAS5 algorithm provided from Affymetrix. In addition, 6 samples from three cows were evaluated experimentally were described previously - three samples each from olfactory and respiratory epithelia. Expression in these samples was evaluated using the Affymetrix Bovine Genome Array, with normalization and gene-level expression values obtained using Partek® Genomics Suite™ software (Partek, Inc., St. Louis, MI).

Genes expressed above the 50$^{th}$ percentile were defined as highly expressed, while expression values between the 15$^{th}$ and 50$^{th}$ percentile were classified as medium expressed. Orthologs of the genes of interest were identified using Ensembl BioMart resource, a web tool provided by EMBL-EBI and Wellcome Trust Sanger Institute.

3.2.2.2. RT-PCR

3.2.2.2.1. Primer Design

Primers were designed using Primer-BLAST, a web tool for finding specific primers provided by NCBI. It uses Primer 3-web software to design PCR primers and then submits them to BLAST search against a user-selected database. The BLAST results are automatically analyzed to avoid primer pairs that can cause amplification of targets other than the input template. *Bos taurus* mRNA sequences of the drug transporters of interest were found using the NCBI nucleotide search and the sequence (NCBI reference number) then was submitted for primer selection.

The conditions for selecting primers are described in **Table 3.4**. To avoid amplifying genomic DNA that might be present in the samples, the primers were selected to span an exon-exon junction. In addition, primers were selected so that their binding site did not include a known single nucleotide polymorphism (**SNP**). The primers designed are3 listed in **Table 3.5**. Even though the tool performs a BLAST search, the primers pairs were also submitted manually for nucleotide BLAST (provided by NCBI), and all of the primers achieved a good alignment score (40-50), 100% query coverage of the corresponding *Bos taurus* mRNA, and an expect value (**E value**) close to zero. The lower the E-value, or the closer it is to zero, the more "significant" the match between the designed primers and a

certain sequence in the database. In our case, that sequence was part of a transporter gene of interest.

3.2.2.2.2. RNA extraction and cDNA production for PCR

RNA was extracted from at least 2 cows using the method described previously. cDNA was synthesized using SuperScript ™ II Reverse Transcriptase. Each RNA sample (10 μL containing 1-5 μg) was taken and mixed with 1 μL of oligo dT, a short sequence of deoxy-thymine nucleotides (500 μg/mL). The sample was placed in a thermal cycler (Techne Genius, Houston, TX) where it was heated at 70 ºC for 10 min to denature the RNA. Then it was placed on ice for 2 min and 9 μL of the mixture prepared according to **Table 3.6** was added; the sample was placed in the thermal cycler to be heated at 42 ºC for 90 min. The samples were diluted by adding 40 μL of DNase and RNase free water. The prepared cDNA samples were stored at -20 ºC.

3.2.2.2.3. PCR

Mixtures were prepared according to **Table 3.7** and placed in the thermal cycler. PCR was performed using 35 cycles as described in **Table 3.8**. The expression of the glyceraldehyde 3-phosphate dehydrogenase (GAPDH) gene, a "housekeeping gene", was used as an internal control. The PCR products (6 μL) were analyzed using 2% agarose gel electrophoresis and the gel was imaged using an AlphaImager 2200, V5.5 (Alpha Innotech Corporation, San Leandro, CA).The annealing temperatures tried were 62, 58 and 55 °C. While 55 °C annealing temperatures suited the PCR for most of the genes, a higher annealing temperature of 58 °C was used for MRP2, PEPT1, and PEPT2.

Table 3.4**:** Conditions for selecting primers by Primer-BLAST.

| **Parameter** | **Parameter range** |
|---|---|
| PCR product size (bp) | 200-1000 |
| $T_m$ (℃) | Min 57(default)<br>Opt 60 (default)<br>Max 63(default) |
| Max temperature difference between Tm | 3 (default) |
| Primer size (Nt) | Min 20<br>Opt 21<br>Max 25 |
| GC % | Min 40<br>Max 60 |
| Maximum self complementarity | 8 (default) |
| Maximum 3'self complementarity | 3 (default) |

Table 3.5**:** List of primers designed using Primer-BLAST.

| Trans-porter | Gene | NCBI reference number | Primer | Primer sequence | E value |
|---|---|---|---|---|---|
| **ENT1** | SLC29A1 | NM_001034398.1 | Sense | AGCGCCTGGAAGGCCTACTTCA | 0.045 |
| | | | Anti-sense | AGCACAGGCCATGAGCAAGCA | |
| **ENT2** | SLC29A2 | NM_001103269.1 | Sense | TTCCTGTGGCCCGACGAAGACA | 0.045 |
| | | | Anti-sense | ACACCAGCTGCACGGTTGACA | |
| **CNT1** | SLC28A1 | BC108101.1 | Sense | TGTGTGGCCGGGATCCTCTACA | 0.012 |
| | | | Anti-sense | TTCTGTCCCCGCTACGCACAGA | |
| **CNT2** | SLC28A2 | XM_002690906.1 | Sense | TGACGATGCACACCCCCTTCCT | 0.045 |
| | | | Anti-sense | ACCGCGGTAGTGAAACCGCAA | |
| **CNT3** | SLC28A3 | NM_001192167.1 | Sense | TGGTGGCGAACATTGCCGTGA | 0.012 |
| | | | Anti-sense | AGCCATGGAAGTGAGTCCACCGA | |
| **MRP1** | ABCC1 | NM_174223.1 | Sense | CCAAGTCCAGAAAGCAGCCGGT | 0.045 |
| | | | Anti-sense | TGATGAACAGCAGCGCCGTGT | |
| **MRP2** | ABCC2 | XM_002698487.1 | Sense | TCCTCGTTGTTGGATAGCCCGGA | 0.016 |
| | | | Anti-sense | ACACACCATCGCCTGCTGTGT | |
| **MRP3** | ABCC3 | NM_001192756.1 | Sense | TGGTCTTGCTAATCCCGCTCAACG | 0.003 |
| | | | Anti-sense | ACACACTGGTCTGGGCCAGGTT | |
| **MRP4** | ABCC4 | XM_002683737.1 | Sense | TGTGATTGGTGTGGTGGGCGTG | 0.012 |
| | | | Anti-sense | AGACAGGACCAGGCCAACGTGT | |

Table 3.5 continued

| | | | | | |
|---|---|---|---|---|---|
| **MRP5** | ABCC5 | NM_001077907.1 | Sense | ACCAGCAATTCAGGGCAGCACC | 0.047 |
| | | | Anti-sense | CCACTGGGTGCTGGTGTTTGGA | |
| **OCT3** | SLC22A3 | XM_002690372.1 | Sense | TTCCTGCTGCTGTGCCTAACGG | 0.012 |
| | | | Anti-sense | ACACGAGGTCAAACTCGCTGACG | |
| **BCRP** | ABCG2 | NM_001037478.2 | Sense | ACAGAGCCGGGGTGCTCTTCTT | 0.11 |
| | | | Anti-sense | ATGCTGCAAAGCCGCATAGCC | |
| **PEPT1** | SLC15A1 | NM_001099378.1 | Sense | TGCGTGTCTGCATTTGGCGGA | 0.011 |
| | | | Anti-sense | GGATGGCGTTCACCGTCTGCAT | |
| **PEPT2** | SLC15A3 | NM_001079582.1 | Sense | GCCATCTCCGAAAATCTGTGGCT | 0.012 |
| | | | Anti-sense | AGCAATGGCTGCTCCCAGGAT | |
| **MCT1** | SLC16A1 | NM_001037319.1 | Sense | AACTAGGCAGCCGGCAAAGGAC | 0.05 |
| | | | Anti-sense | AAGGCAAGCCCAAGACCTCCA | |
| **MCT2** | SLC16A7 | NM_001076336.2 | Sense | CAGTGCCGGAGACCAGCAGTT | 0.19 |
| | | | Anti-sense | TCACCACTGGCCGGCTACCAT | |
| **MCT3** | SLC16A8 | XM_002687932.1 | Sense | ATGCTTTACGGCACAGGCCC | 0.18 |
| | | | Anti-sense | AGGCGATGCAGAAGGCGACAA | |
| **MCT4** | SLC16A3 | NM_001109980.1 | Sense | CAGCCTCTGTCAGGACGCAGAA | 0.013 |
| | | | Anti-sense | TTGAGCGCCAAACCCAAGCCA | |
| **sMCT1** | SLC5A8 | NM_001164861.1 | Sense | TGCACCAGACCAGCTCATGCC | 0.19 |
| | | | Anti-sense | AAGCCAGTGCAGCCATGCCAA | |

Table 3.5 continued

| | | | | | |
|---|---|---|---|---|---|
| **sMCT2** | SLC5A12 | NM_001101059.1 | Sense | TCATGTCCGCCGTCACTG TCCT | 0.003 |
| | | | Anti-sense | GGCAGCCACGGTGCTCA AAGTT | |
| **MDR1** | ABCB1 | XM_002686731.2 | Sense | TGACCGCCCACAGAAGA AGTGC | 0.052 |
| | | | Anti-sense | AATAGCGAAAGCGAGCC GAGGG | |
| **y+LAT1 Light chain** | SLC7A7 | NM_001075151.1 | Sense | TTCAGGGCTGGGGAAGG GCAAT | 0.052 |
| | | | Anti-sense | CCCACAATCAGGCACACG CCAT | |
| **$b^{0+}$AT Light chain** | SLC7A9 | NM_001035054.1 | Sense | TGCCGCTGCCATCTTGCT CAT | 0.047 |
| | | | Anti-sense | AGCGGCGCCGATGGTTG AAAA | |
| **Asc-1 Light chain** | SLC7A10 | NM_001104989.1 | Sense | TGGCTTGCCTGATGCTCT TGACG | 0.014 |
| | | | Anti-sense | AGCGTGTACGTGTCTCCC ACGA | |
| **xCT Light chain** | SLC7A11 | XM_002694373.1 | Sense | ATGCGTACGCCGGCTGG TTTT | 0.19 |
| | | | Anti-sense | AAGCTGGGATGAACAGC GGCA | |

Table 3.6**:** Materials used to prepare the cDNA production mixture.

| **Material** | **Volume (µL) for one sample** |
|---|---|
| 5X First-strand buffer<br>(250 mM Tris-HCl, pH 8.3 at room temperature; 375 mM KCl; 15 mM $MgCl_2$) | 4 |
| DTT (Dithiothreitol,0.1 M) | 2 |
| dNTP (Deoxynucleotide Triphosphates,10mM) | 1 |
| Reverse Transcriptase(200 U/µL) | 0.25 |
| DNase and RNase water | Up to 20 µL total volume |

Table 3.7: Materials used for PCR.

| **Material** | **Volume (µL) for one sample** |
|---|---|
| cDNA(from olfactory and respiratory samples) | 2 |
| Forward and reverse primer 1:1 mix (ENT1,CNT3 or GAPDH) (10mM) | 1 |
| 10X Standard *Taq* Reaction Buffer<br>(100 mM Tris-HCl, pH 8.3 at room temperature; 500 mM KCl; 15mM $MgCl_2$ ) | 2 |
| dNTP(10mM) | 0.4 |
| Taq polymerase (5000 U/mL) | 0.2 |
| DNase and RNase water | Up to 20 µL total volume |

Table 3.8**:** PCR conditions.

| | | **Temperature (°C)** | **Duration** |
|---|---|---|---|
| **Step 1: Initialization** | | 95 | 5 min |
| **Step 2:** | **Denaturation** | 95 | 30 sec |
| | **Annealing** | 55,58 or 62 | 30 sec |
| | **Elongation** | 72 | 30 sec |
| **Step 3: Final elongation** | | 72 | 10 min |

## 3.3. Results and discussion

Recently, microscale technologies for molecular analysis have caused a revolution in biological investigation. Along with the nucleic acid sequencing techniques that helped in the completion of the human genome project, many methods were developed for high throughput analysis of gene expression and genetic variation. Examples of these methods include Northern blotting, *in situ* hybridization, RT-PCR, and DNA microarray analysis. DNA microarray is among the most widely used methods of expression profiling of genes because it offers the advantage of analyzing a large number of genes in parallel [66].

**Tables 3.9-14** list the results of the microarray analysis for the various transporter family genes in the nasal tissues of humans, mice, rats and cows. The microarrays for the animal models did not contain all of the probes for the genes of interest; thus, the gene expression for these transporters has yet to be determined. The exact nasal region of origin (olfactory or respiratory) for the human samples was not reported, and only olfactory data were reported for both mice and rats.

The nasal mucosa from humans and the animal species showed the expression of a variety of efflux transporters (**Table 3.9**). MRP1and 3 were highly expressed in the nasal mucosa of all the species and MRP 4, 5, and 6 were also moderately to highly expressed in these species. MDR 1 was expressed in humans, rats and mice, and while the microarray results indicated it was not expressed in bovine nasal mucosa, RT-PCR demonstrated its expression in cows. In comparison, MRP 2, 8 and 9 were weakly expressed in humans and mice (no data available for MRP8), and no probe datasets were available for rats or cows. While there were similarities in the levels of expression among species for many transporters, the level of expression for several showed variation between humans and the animal models. For example, MRP7 was more weakly expressed in mice compared to human and cows and

while BCRP was highly expressed in all the animal models but was weakly expressed in humans.

With regard to the uptake transporters, the nucleoside transporters were present in the nasal mucosa of humans and animals (**Table 3.11**). The concentrative nucleoside transporter, CNT3, was shown to be moderately to highly expressed in all species, and equilibrative transporters, ENT 1 and ENT 2, were also expressed in all of species except for ENT2 which was reported to be weakly expressed in mice.

The organic cation transporters (**OCT**s) and organic cation/carnitine transporters (**OCTN**s) are two additional families of drug transporters which were found to be expressed in the nasal mucosa of all the species investigated (**Table 3.12**).OCTN1 and 2 were highly expressed in the human nasal mucosa but microarray data from the animal models were only available for OCTN2; they also showed high expression of the transporter. OCT 1, 2 and 3 were weakly expressed in the human nasal mucosa while their expression varied among the animal models. The organic anion transporters (**OAT**s), on the other hand, were minimally expressed or not expressed in any of the species (**Table 3.13**). Therefore, they appear to have minimal contribution to drug transport at this mucosal surface.

Finally, several peptide, monocarboxylate and amino acid transporters (**Tables 3.10** and **14**) were also observed to be highly expressed in the human nasal mucosa as well as in the other species investigated. These transporters could be of great interest when considering the nasal route to study the permeation of investigational amino acid-like and peptidomimetic drugs and prodrugs.

The microarray data are also presented in a heat map shown in (**Figure 3.1**) which was constructed by uploading the expression percentages for the drug transporters measured in the different species to the website, CIMminer

(http://www.discover.nci.nih.gov/cimminer/,Oct 25 2013 ) , developed the Genomics and Bioinformatics Group, Laboratory of Molecular Pharmacology (**LMP**), Center for Cancer Research (**CCR**) National Cancer Institute (**NCI**). The several open spaces noted in the bovine section, and to a lesser extent in the rat section, indicate unavailable data due to missing probes. The heat map was constructed to cluster genes with low expression near the top and the genes that are more highly expressed at the bottom. Due to the small bovine sample size, the heatmap cannot be used for quantitative comparisons, but it can help in the initial determination of agreement and disagreement of the level of expression of the transporters between the species. For example, ABCC1 (MRP1) and SLC7A6 (y+LAT2) are highly expressed (shades of red) in all species while SLC22A6 (OAT1) and SLC22A7 (OAT2) are weakly expressed (blue). SLC29A2 (ENT2) showed a high variation in expression between the species.

RT-PCR was performed using bovine nasal olfactory and respiratory samples to verify the results obtained from the microarray analysis. While PCR depends on the specific hybridization of pre-determined primers and the defined targeted sequence, DNA microarray depends on the hybridization of targeted nucleotide sequences to probes which are placed on the microarray chip. Since primers used for PCR can be purposely designed, in contrast to the commercially marketed microarrays, one can design more specific primers for PCR, and PCR can be used to evaluate the expression of genes of known sequence that are not present on a commercial microarray. This is of particular importance in the case of bovine gene expression, because the bovine genome is not as well documented as the human, mouse or rat genomes, and the currently available bovine microarray is not as extensively annotated as the microarrays for the other species.

RT-PCR was also performed to verify the microarray results reported (**Tables 3.9-14**). The gel images for the PCR products are compiled in **Appendix A**. Of the 19 transporter genes that were both annotated on the Affymetrix GeneChip Bovine Expression Array and had RT-PCR performed on bovine mucosal samples, six genes showed disagreement between the microarray expression reported and the RT-PCR results these transporters include MRP4, OCT1, MCT1, LAT2, and ENT2 all of which were indicated to be highly expressed by the microarray analysis but could not be identified using RT-PCR, and MDR1 which was not determined to be significantly expressed from the microarray but whose RNA was readily detected by RT-PCR . This disagreement is may be the result of the lack of specific probe combinations for these genes on the Bovine Expression Array which increases the likelihood for false positive identification. While microarray offered a rapid, simultaneous screen for many genes, RT-PCR was used for confirmation and can be used to determine the expression of genes with no probes on the microarray (e.g. CNT1 and CNT2).

The microarray analysis results for each of other the species investigated in this study were compared with other results reported in the literature (**Table 3.15**). Overall, the microarray results agreed well with the gene expression results found by other methods such as RT-PCR. A few species-dependent differences were noted especially for the expression of OCT1 and OCT3 in the human and mice nasal mucosae [55,67,68].

While the presence of the transcribed product (mRNA) of the gene may not necessarily indicate the presence of the encoded protein, examining gene expression is a convenient and acceptable method to determine the likely presence of proteins. **Table 3.15** shows that the gene expression of transporters identified using microarray or RT-PCR techniques agreed well with reports of transporter protein presence detected by Western

blotting or immunohistochemistry in humans, mice and rats. In addition, the presence of OCT2, OCTN2, and MRP1 in the bovine nasal mucosa has been confirmed by Western blotting and immunohistochemistry [42, 45, 69].

In general, there were no differences observed between the gene expression profiles of bovine nasal respiratory and olfactory tissues. This may not necessarily confirm that the drug transporters will always have similar activities in both tissues, however. The nasal respiratory and the olfactory mucosa may have different levels of transporter proteins expressed in these tissues or their locations may differ within the different regions. For instance, OCT2 and OCTN2 proteins were shown to have different levels of expression in the bovine nasal respiratory mucosa (higher in OCTN2) and olfactory mucosa (higher in OCT2), as revealed by ELISA analysis [69]. Moreover, immunohistochemistry showed that OCT2 was expressed on the apical surface of the rat nasal olfactory mucosa as well as in the Bowman glands while it was primarily detected in the sub-epithelial regions of the rat respiratory mucosa. Other transporters have also shown variable immunolocalization in the rat nasal respiratory and olfactory mucosae including ENT1, ENT2, and MRP1 [53].

The presence of a number of well-characterized drug transporter systems in the nasal respiratory and olfactory mucosa suggests that they can play a significant role in the absorption and distribution of substrate compounds following nasal administration. Information regarding the expression of transporters in the nasal mucosa of humans and animal models can assist in the correct selection of model systems when the drug under investigation is a transporter substrate. In addition, knowledge of species differences in transporter expression can help in translating information obtained about drug transporters and the permeation of their substrates from animal models to humans.

Table 3. 9: Expression levels of gene transcripts for known efflux transporter expression determined from analysis of microarray data obtained from NCBI's Gene Expression Omnibus (human, mouse and rat) and from Afftmetrix microarray analysis and RT-PCR (cow). *

| **Transporter family** | **Gene name** | **Family member** | **Human nasal mucosa** | **Mouse olfactory mucosa** | **Rat olfactory mucosa** | **Cow olfactory (Microarray)** | **Cow respiratory (Microarray)** | **Cow olfactory (RT-PCR)** | **Cow respiratory (RT-PCR)** |
|---|---|---|---|---|---|---|---|---|---|
| Multidrug resistance proteins | ABCB1 | MDR1 | Medium | High | Medium | Not/Weak | Not/Weak | Yes | Yes |
| Multidrug resistance-associated proteins | ABCC1 | MRP1 | High | High | High | High | High | Yes | Yes |
| | ABCC2 | MRP2 | Not/Weak | Not/Weak | -- | -- | -- | No | No |
| | ABCC3 | MRP3 | High | High | -- | High | High | Yes | Yes |
| | ABCC4 | MRP4 | High | Medium | -- | High | High | No | No |
| | ABCC5 | MRP5 | High | High | High | Medium | Medium | Yes | Yes |
| | ABCC6 | MRP6 | Medium | Not/Weak | Not/Weak | Not/Weak | Not/Weak | -- | -- |
| | ABCC10 | MRP7 | High | Not/Weak | -- | High | High | -- | -- |
| | ABCC11 | MRP8 | Not/Weak | -- | -- | -- | -- | -- | -- |
| | ABCC12 | MRP9 | Not/Weak | Not/Weak | -- | -- | -- | -- | -- |
| Breast cancer resistance protein | ABCG2 | BCRP1 | Not/Weak | High | High | High | High | Yes | Yes |

* For microarray, genes expression above the 50th percentile was defined as **High**; expression values between the 15th and 50th percentile were classified as **Medium;** and expression levels below the 15th percentile were defined as **Weak/Not**. --: data not available.

Table 3.10: Expression levels of gene transcripts for known peptide and monocarboxylate transporter expression determined from analysis of microarray data obtained from NCBI's Gene Expression Omnibus (human, mouse and rat) and from Afftmetrix microarray analysis and RT-PCR (cow). *

| **Transporter family** | **Gene name** | **Family member** | **Human nasal mucosa** | **Mouse olfactory mucosa** | **Rat olfactory mucosa** | **Cow olfactory (Microarray)** | **Cow respiratory (Microarray)** | **Cow olfactory (RT-PCR)** | **Cow respiratory (RT-PCR)** |
|---|---|---|---|---|---|---|---|---|---|
| Peptide transporters | SLC15A1 | PEPT1 | Medium | Weak | -- | High | High | Yes | Yes |
| | SLC15A2 | PEPT2 | High | High | High | High | High | Yes | Yes |
| Monocarboxylate transporters | SLC16A1 | MCT1 | High | Medium | High | High | High | No | No |
| | SLC16A7 | MCT2 | High | Medium | High | -- | -- | Yes | Yes |
| | SLC16A8 | MCT3 | Not/Weak | Not/Weak | Not/Weak | -- | -- | Yes | Yes |
| | SLC16A3 | MCT4 | High | Weak | High | High | High | Yes | Yes |
| | SLC5A8 | sMCT1 | Not/Weak | Medium | High | -- | -- | Yes | Yes |
| | SLC5A12 | sMCT2 | Medium | Not/Weak | Not/Weak | -- | -- | No | No |

* For microarray, genes expression above the 50th percentile was defined as **High**; expression values between the 15th and 50th percentile were classified as **Medium;** and expression levels below the 15th percentile were defined as **Weak/Not**. --: data not available.

Table 3.11: Expression levels of gene transcripts for known nucleoside transporter expression determined from analysis of microarray data obtained from NCBI's Gene Expression Omnibus (human, mouse and rat) and from Afftmetrix microarray analysis and RT-PCR (cow). *

| **Transporter family** | **Gene name** | **Family member** | **Human nasal mucosa** | **Mouse olfactory mucosa** | **Rat olfactory mucosa** | **Cow olfactory (Microarray)** | **Cow respiratory (Microarray)** | **Cow olfactory (RT-PCR)** | **Cow respiratory (RT-PCR)** |
|---|---|---|---|---|---|---|---|---|---|
| Concentrative nucleoside transporters | SLC28A1 | CNT1 | Not/Weak | -- | Not/Weak | -- | -- | Yes | Yes |
| | SLC28A2 | CNT2 | Not/Weak | Not/Weak | -- | -- | -- | No | No |
| | SLC28A3 | CNT3 | High | Not/Weak | Medium | High | High | Yes | Yes |
| Equilibrative nucleoside transporters | SLC29A1 | ENT1 | High | Medium | High | High | High | Yes | Yes |
| | SLC29A2 | ENT2 | Medium | Not/Weak | High | High | High | No | No |

* For microarray, genes expression above the 50th percentile was defined as **High**; expression values between the 15th and 50th percentile were classified as **Medium;** and expression levels below the 15th percentile were defined as **Weak/Not**. --: data not available.

Table 3.12: Expression levels of gene transcripts for known organic cation transporter expression determined from analysis of microarray data obtained from NCBI's Gene Expression Omnibus (Human, Mouse and Rat) and from Afftmetrix microarray analysis and RT-PCR(cow). *

| **Transporter family** | **Gene name** | **Family member** | **Human nasal mucosa** | **Mouse olfactory mucosa** | **Rat olfactory mucosa** | **Cow olfactory (Microarray)** | **Cow respiratory (Microarray)** | **Cow olfactory (RT-PCR)** | **Cow respiratory (RT-PCR)** |
|---|---|---|---|---|---|---|---|---|---|
| Organic cation transporters | SLC22A1 | OCT1 | Not/Weak | Not/Weak | Not/Weak | High | High | No** | No** |
| | SLC22A2 | OCT2 | Not/Weak | High | Medium | -- | -- | Yes** | Yes** |
| | SLC22A3 | OCT3 | Not/Weak | Not/Weak | Medium/ High | -- | -- | No | No |
| Organic cation/carnitine transporters | SLC22A4 | OCTN1 | High | Not/Weak | -- | -- | -- | Yes** | Yes** |
| | SLC22A5 | OCTN2 | High | High | High | High | High | Yes** | Yes** |

* For microarray, genes expression above the 50th percentile was defined as **High**; expression values between the 15th and 50th percentile were classified as **Medium;** and expression levels below the 15th percentile were defined as **Weak/Not**. --: data not available.

** Performed by Maya George [69] .

Table 3.13: Expression levels of gene transcripts for known organic anionic transporter expression determined from analysis of microarray data obtained from NCBI's Gene Expression Omnibus (Human, Mouse and Rat) and from Afftmetrix microarray analysis and RT-PCR(cow). *

| **Transporter family** | **Gene name** | **Family member** | **Human nasal mucosa** | **Mouse olfactory mucosa** | **Rat olfactory mucosa** | **Cow olfactory (Microarray)** | **Cow respiratory (Microarray)** |
|---|---|---|---|---|---|---|---|
| Organic anion transporters | SLC22A6 | OAT1 | Not/Weak | Not/Weak | Not/Weak | Not/Weak | Not/Weak |
| | SLC22A7 | OAT2 | Not/Weak | Not/Weak | Not/Weak | Not/Weak | Not/Weak |
| | SLC22A8 | OAT3 | Not/Weak | Not/Weak | Not/Weak | Not/Weak | Not/Weak |
| Organic anion transporter polypeptides | SLCO1A2 | OATP1A2 | Medium | -- | Not/Weak | High | High |
| | SLCO1B1 | OATP1B1 | Not/Weak | Not/Weak | Not/Weak | -- | -- |
| | SLCO2A1 | OATP2A1 | High | Medium | Not/Weak | High | High |
| | SLCO2B1 | OATP2B1 | Medium/ High | Medium | High | High | High |
| | SLCO3A1 | OATP3A1 | High | High | High | High | High |
| | SLCO4A1 | OATP4A1 | Medium | Medium | High | High | High |
| | SLCO4C1 | OATP4C1 | High | Medium | -- | High | High |

* For microarray, genes expression above the 50th percentile was defined as **High**; expression values between the 15$^{th}$ and 50$^{th}$ percentile were classified as **Medium;** and expression levels below the 15$^{th}$ percentile were defined as **Weak/Not**. --: data not available.

Table 3.14: Expression levels of gene transcripts for known heterodimeric amino acid transporter expression determined from analysis of microarray data obtained from NCBI's Gene Expression Omnibus (Human, Mouse and Rat) and from Afftmetrix microarray analysis and RT-PCR(cow)*.

| **Transporter family** | **Gene name** | **Family member** | **Human nasal mucosa** | **Mouse olfactory mucosa** | **Rat olfactory mucosa** | **Cow olfactory (Microarray)** | **Cow respiratory (Microarray)** | **Cow olfactory (RT-PCR)** | **Cow respiratory (RT-PCR)** |
|---|---|---|---|---|---|---|---|---|---|
| Heterodimeric amino acid transporters | SLC7A5 | LAT1 | Medium | High | High | High | High | Yes** | Yes** |
| | SLC7A8 | LAT2 | High | Medium | High | High | High | No** | No** |
| | SLC7A7 | y+LAT1 | Medium | Medium | High | High | High | Yes | Yes |
| | SLC7A6 | y+LAT2 | High | High | High | High | High | -- | -- |
| | SLC7A9 | $b^{0+}AT$ | Not/Weak | Medium | Not/Weak | Medium | Medium | Yes | Yes |
| | SLC7A10 | Asc-1 | Not/Weak | Medium | Not/Weak | -- | -- | Yes | Yes |
| | SLC7A11 | xCT | High | Weak | -- | -- | -- | Yes | Yes |

* For microarray, genes expression above the 50th percentile was defined as **High**; expression values between the 15th and 50th percentile were classified as **Medium;** and expression levels below the 15th percentile were defined as **Weak/Not**. --: data not available.

** Performed by Ana Ferreira [70].

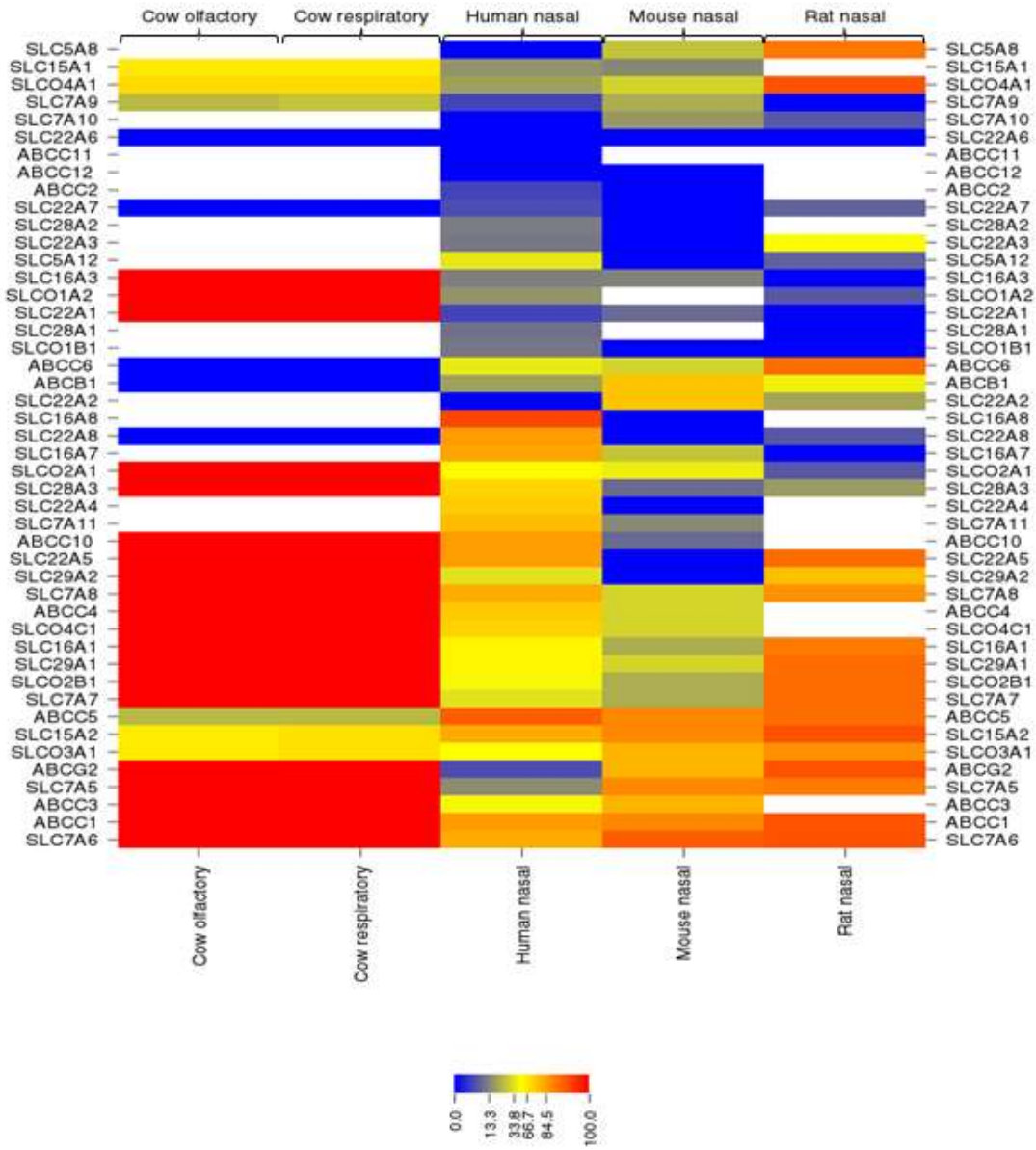


Figure 3.1: Heat map representation of microarray data of drug transporters expression in the nasal mucosa in humans, mice, rats and cows.

Table 3.15: Drug transporter expression reported in the nasal mucosa of humans, mice and rats and the method used for determination.

| Transporter Family | Family Member | Gene Name | Human (nasal primary cell culture) | | Mouse | | Rat | |
|---|---|---|---|---|---|---|---|---|
| Organic cation transporter (OCT) | SLC22A1 | OCT1 | Yes | RT-PCR, Western blotting and immunohistochemistry [67, 68] | Yes | RT-PCR[55] | weak | Branched DNA technology[53] |
| | SLC22A2 | OCT2 | No | RT-PCR ,Western blotting and immunohistochemistry [67, 68] | Yes | RT-PCR[55] | Yes | RT-PCR, branched DNA technology, and immunohistochemistry[43, 53] |
| | SLC22A3 | OCT3 | Yes | RT-PCR ,Western blotting and immunohistochemistry [67, 68] | No | RT-PCR[55] | weak | Branched DNA technology[53] |
| Organic cation/cartinine transporter (OCTN) | SLC22A4 | OCTN1 | Yes | RT-PCR ,Western blotting and immunohistochemistry [67, 68] | Yes | RT-PCR[55] | weak | Branched DNA technology[53] |
| | SLC22A5 | OCTN2 | Yes | RT-PCR ,western blotting and immunohistochemistry [67, 68] | Yes | RT-PCR[55] | -- | |

Table 3.15 continued

| | | | | | | | | |
|---|---|---|---|---|---|---|---|---|
| Organic anion transporter (OAT) | SLC22A6 | OAT1 | -- | | Yes | RT-PCR[55] | -- | |
| | SLC22A7 | OAT2 | -- | | No | RT-PCR[55] | -- | |
| | SLC22A8 | OAT3 | -- | | No | RT-PCR[55] | Yes | RT-PCR[43] |
| Organic anion transporter polypeptide (OATPs) | SLCO1 | OATP1 | -- | | -- | | Yes | RT-PCR[54] |
| | SLCO2 | OATP2 | -- | | -- | | Yes | RT-PCR[54] |
| | SLCO3 | OATP3 | -- | | -- | | Yes | Branched DNA technology and immunohistochemistry[53] |
| Monocarboxylate transporters (MCTs) | SLC16A1 | MCT1 | -- | | -- | | Yes | RT-PCR , Western blotting and immunohistochemistry[65] |
| | SLC16A7 | MCT2 | -- | | -- | | Yes | RT-PCR , western blotting and immunohistochemistry[65] |

Table 3.15 continued

| | | | | | | | | |
|---|---|---|---|---|---|---|---|---|
| Nucleoside transporters (CNT,ENT) | SLC28A1 | CNT1 | No | RT-PCR[40] | -- | | -- | |
| | SLC28A2 | CNT2 | Yes | RT-PCR[40] | -- | | -- | |
| | SLC28A3 | CNT3 | Yes | RT-PCR[40] | -- | | -- | |
| | SLC29A1 | ENT1 | -- | | -- | | Yes | Branched DNA technology and immunohistochemistry[53] |
| | SLC29A2 | ENT2 | -- | | -- | | Yes | Branched DNA technology[53] |
| Multidrug resistance protein (MDR) | ABCB1 | MDR1 | -- | | -- | | Yes | RT-PCR, Western blotting and immunohistochemistry[54] |

Table 3.15 continued

| | | | | | | | | |
|---|---|---|---|---|---|---|---|---|
| Multidrug resistance associated protein (MRP) | ABCC1 | MRP1 | -- | | -- | | Yes | RT-CR, branched DNA technology, and immunohistochemistry [53, 54, 71] |
| | ABCC2 | MRP2 | -- | | -- | | No /weak | RT-PCR[54, 71] |
| | ABCC3 | MRP3 | -- | | -- | | Yes | RT-PCR, Western blotting and immunohistochemistry [54] |
| | ABCC4 | MRP4 | -- | | -- | | Yes | Branched DNA technology[53] |
| | ABCC5 | MRP5 | -- | | -- | | Yes | RT-PCR, Western blotting and immunohistochemistry [54] |

# CHAPTER 4

# IDENTIFICATION AND LOCALIZATION OF ENT1 AND CNT3 IN THE NASAL MUCOSA

## 4.1. Introduction

Nucleosides are the precursors for the synthesis of nucleic acids which are fundamental to the growth, maintenance and reproduction of all living systems [72]. Nucleosides and nucleobases (**Figure 4.1**) also play diverse roles inside and outside the cells; for example, they act as an energy source for the cell in the form of adenosine triphosphate (**ATP**), and they regulate enzyme activity, as in the case of the intracellular kinase, 5' AMP-activated protein kinase (**AMPK**) which is activated by cyclic adenosine monophosphate (**cAMP**) [73]. Nucleosides consist of a nucleobase (a purine or pyrimidine) and a ribose sugar; therefore, they are considered relatively large, polar substances [74, 75]. The flux of nucleosides across cellular membranes is controlled by membrane carriers called nucleoside transporters (**Figures 4.2-3**).

The pharmacological significance of nucleoside transporters originates from their ability to transport nucleoside-analog drugs into cells. Anti- cancer drugs such as cladribine and gemcitabine and/or anti-viral agents such as zidovudine and lamivudine share a common nucleoside-like structure and each is reported to be a substrate for at least one nucleoside transporter [73, 76, 77]. Nucleoside transporters also play a role in the treatment of some types of cardiovascular disease. For example, inhibiting nucleoside uptake into endothelial cells using a nucleoside transporter inhibitor, draflazine, increased and prolonged the cardiovascular effects of adenosine [73, 74, 78]. Other investigational uses for nucleoside analogues and nucleoside transporter inhibitors include treatment of parasitic and protozoan infections and as opioid adjuncts [74].

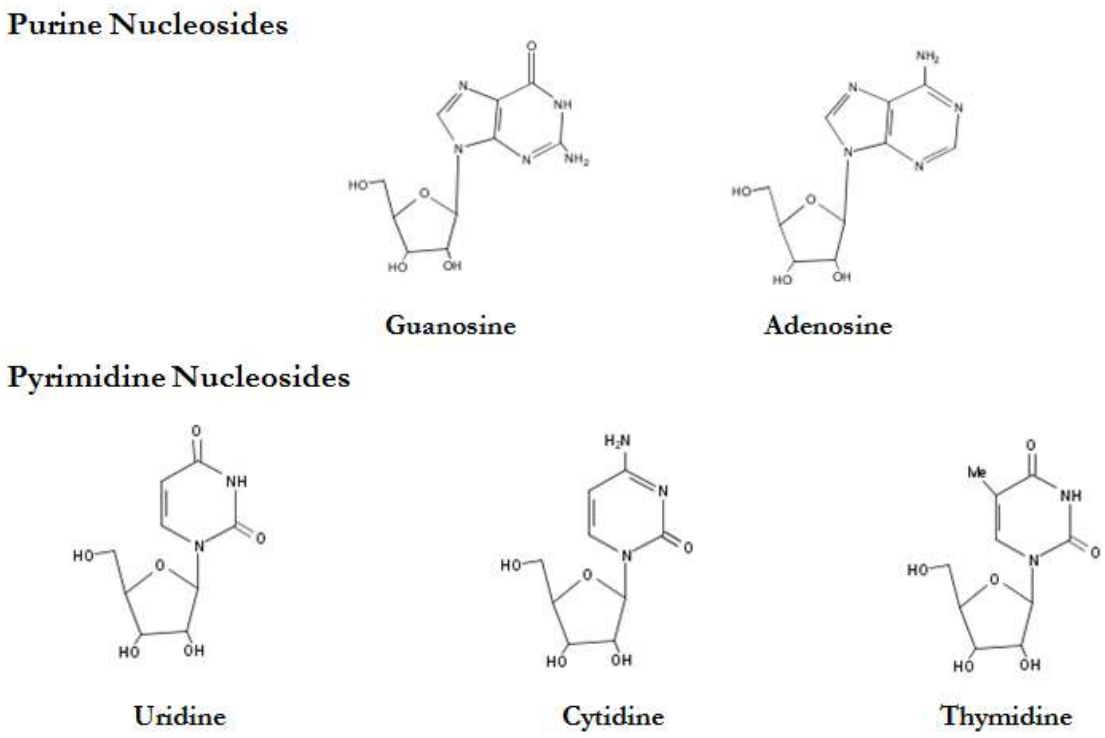


Figure 4.1: Chemical structures of endogenous nucleosides[75].

The two major classes of nucleoside transporters are: (1) equilibrative nucleoside transporters (**ENT, SLC29A**) and (2) concentrative nucleoside transporters (**CNT, SLC28A**). The ENTs are bidirectional, facilitative carriers and are subdivided to two subtypes based on their sensitivity to the specific inhibitor, nitrobenzylmercatopurine ribonucleoside (**NBMPR**) (**Figure 4.3B**). Es or ENT1, "equilibrative inhibitor sensitive", is potentially inhibited by NBMPR ($K_i$= 0.1to 10 nM) while ei or ENT2, "equilibrative inhibitor insensitive", is not inhibited by NBMPR at concentrations below 1 mM[72-74, 76, 79-81]. ENT3 and ENT4 are novel members of the nucleoside transporter family identified from the human genome project. ENT3 is an intracellular, low-affinity nucleoside transporter, and ENT4 exhibits a novel substrate specificity by functioning as a polyspecific organic cation

transporter [74, 78]. Most drug uptake studies have not focused on either of these novel transporters.

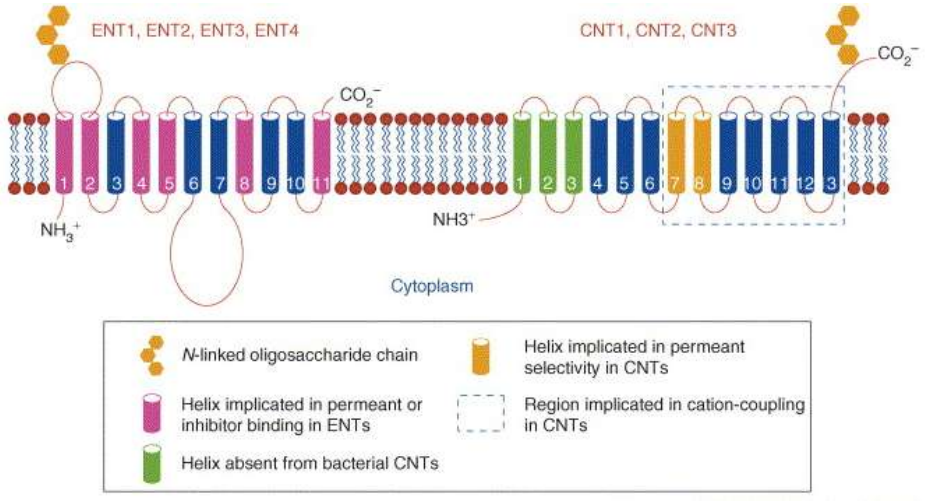


Figure 4.2: Predicted transmembrane topologies of mammalian members of the ENT and CNT families [74].

CNTs are inwardly directed $Na^+$/nucleoside co-transporters, i.e. concentrative systems. CNTs are insensitive to NBMPR and are subdivided based on their affinity to specific nucleotides. The cif or CNT1 subtype is mainly purine selective; the cit or CNT2 subtype is pyrimidine selective; and the cib or CNT3 subtype is broadly selective, transporting both purine and pyrimidine nucleosides [72-74, 76, 79-81](**Figure 4.3,Table 4.1**).

ENTs are low affinity transporters with $K_m$ values in the high micromolar range (>100 μM). They transport both purines and pyrimidines and are widely distributed in a variety of tissues. CNTs are high affinity transporters with $K_m$ values in the low micromolar range (<100 μM). They have been reported to be present in the intestinal and renal epithelia and, along with other specialized cells; they function in tandem with the ENTs in absorbing, distributing and eliminating nucleosides [72-74, 76, 79-81].

The nasal route has been shown to be a promising route to transport drugs, including chemotherapeutic agents, directly to the brain to treat conditions such as HIV-induced CNS complications [82]. The nasal administration of the antiviral agent, zidovudine, a nucleoside analogue, in rats led to a higher CSF to plasma ratio compared to IV infusion suggesting direct brain delivery following nasal administration [83]. ENTs have been localized in the brain of humans and rats, and they are also present in the nasal mucosa of both species [40, 53, 84, 85]. Analysis of microarray data obtained from NCBI's Gene Expression Omnibus for humans, mice and rats indicates that at least two of the nucleoside transporters, namely ENT1 and CNT3, are expressed in the nasal mucosa in all the three species (**Chapter 3**). Little information is known about the presence of transporters, including nucleoside transporters, in cows, and the current studies aim to investigate the expression of ENT1 and CNT3 in the bovine nasal mucosa to evaluate the potential use of this *in vitro* tissue explant model to elucidate the mechanism of nucleoside transport in the nasal respiratory and olfactory mucosa.

Of the two broadly selective ENTs, ENT1 was investigated due to its reported extensive tissue distribution and its susceptibility to inhibition by several compounds such as NBMPR. CNT3 was also selected for investigation based on its broader selectivity compared to the other CNTs, which improves the selection of potential substrate drug compounds.

Additional aims of this study were to identify the location of these two nucleoside transporters, ENT1 and CNT3, in the bovine nasal mucosa and to determine the contribution of these transporters in the permeation of nucleoside analogue drugs through the nasal mucosa (**Chapter 5**). Identifying the location of the transporters in the nasal mucosa, especially within the epithelial cell layers will help to evaluate their contribution to drug uptake and transport.

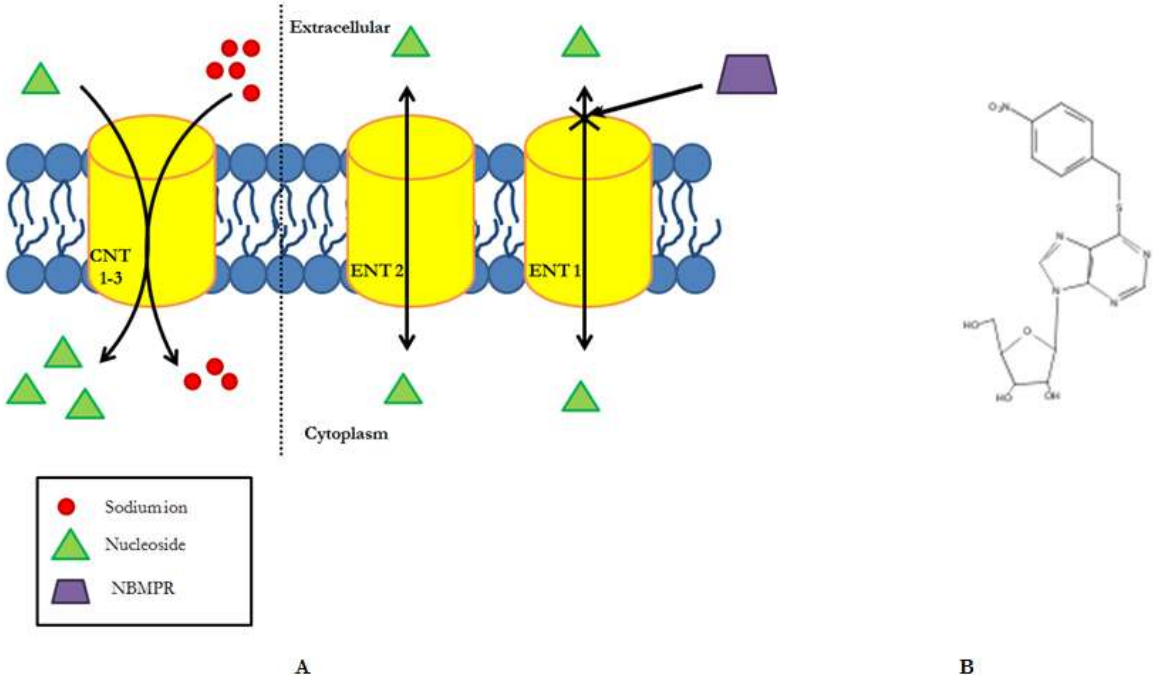


Figure 4.3**:** (**A**) Mammalian nucleoside transport systems of the equilibrative nucleoside transporter (ENT) and concentrative nucleoside transporter (CNT) protein families. (**B**) Chemical structure of nitrobenzylmercatopurine ribonucleoside (NBMPR) [78].

Table 4.1**:** Classifications and characterization of human nucleoside transporter subtypes[72-74, 76, 79-81].

| **Class** | **ENT** | | **CNT** | | |
|---|---|---|---|---|---|
| Subclass | ENT1 (es) | ENT2 (ei) | CNT1 (cit) | CNT2 (cif) | CNT 3 (cib) |
| Inhibition by NBMPR | Yes | No | No | | |
| Sodium ion: Nucleoside coupling ratio | -- | -- | 1:1 | 1:1 | 2:1 |
| Selectivity | Purine and pyrimidine nucleoside | Purine and pyrimidine nucleoside and nucleobases | Purine and uridine nucleoside | Pyrimidine and adenosine nucleoside | broad |
| Chromosomal location | 6p1.1-21.2 | 11q13 | 5q25-56 | 15q15(15q13-14) | 9q22.2 |
| Number of amino acids in transporter | 465 | 465 | 650 | 658 | 691 |
| Molecular weight (kDa) | 52 | 52 | 71 | 72 | 77 |

## 4.2. Materials and methods

### 4.2.1. Reagents and materials

#### 4.2.1.1. RNA extraction, cDNA production and RT-PCR

Materials were described in **Chapter 3**.

#### 4.2.1.2 Western blotting

Triton X, sodium chloride, glycine, and Tris HCl were purchased from Fisher Scientific (Hampton, NH), protease inhibitor cocktail was from Fermentas (Thermo Scientific, Waltham, MA) and a Micro BCA Protein Assay Kit was from Thermo Scientific (Waltham, MA). Other materials and reagents used include: phosphate buffered saline (**PBS**) (Gibco, Life Technologies, Carlsbad, CA), sodium dedocyl sulfate (**SDS**), 2-mercaptoethanol, bovine serum albumin (**BSA**) and anti-goat IgG peroxidase conjugate developed in rabbit antibody (Sigma-Aldrich, St. Louis, MO); Laemmli buffer and Precision PlusProtein™ Dual Xtra Standard (Molecular Weight Standards; Bio-Rad, Life Research Clinical Diagnostics, Hercules, CA); Amersham™ ECL™ Western Blotting Detection Reagents (GE Healthcare Life Sciences, Piscataway Township, NJ); KODAK GBX Developer and Replenisher (Carestream Kodak® processing chemicals for autoradiography films, Sigma-Aldrich, St. Louis, MO) and classic X-ray film for autoradiography (Research Products International Corp, Mount Prospect, IL).

#### 4.2.1.3Bright field imaging and immunohistochemistry

Primary antibodies against ENT1and CNT3were purchased from Santa Cruz Biotechnologies, Inc (Santa Cruz, CA), goat IgG from Sigma-Aldrich (St. Louis, MO), TO-PRO®-3 and donkey anti-goat Alexa Fluor® 488 from Invitrogen (Life Technologies, Carlsbad, CA). Additional materials and reagents include: Solvent 100 mounting medium

(IMEB Inc, San Marcos, CA); Vectashield® mounting media (Vector Laboratories, Burlingame, CA); tissue freezing media (Triangle Biomedical Science, Durham, NC); Surgipath® Em-400 Embedding Medium™ Paraffin (Leica Biosystems, Richmond, IL); ethanol (AAPER Alcohol & Chemical Co., Shelbyville, KY); Pro-Par Clearant and zinc formalin (Anatech Ltd., Battle Creek, MI); eosin (Sigma-Aldrich, St. Louis, MO); normal donkey serum, BSA, xylene, hematoxyline, glacial acetic acid, hydrochloride acid, and magnesium sulfate (Research Products International Corp., Mount Prospect, IL); and pholxine B, sodium bicarbonate, sucrose and acetone (Fisher Scientific, Hampton, NH).

### 4.2.2. Methods

#### 4.2.2.1. RNA extraction and cDNA production

Respiratory and olfactory nasal tissues excised from 5 cows were snap frozen using liquid nitrogen.The RNA extraction was performed as described in **Chapter 3**. The volume of water used to reconstitute the RNA depended on the size of the pellet; the volumes used ranged from 10 to 100 uL. The volume typically used was 40 μL, except for pellets that appeared smaller where 20 μL was used.

Two microliter samples were withdrawn from each RNA sample, mixed with 1 μl of the loading dye, and electrophoresis using 1% agarose gel was performed to check the quality of the RNA and for semi-quantitative analysis. Another 2 μL sample was withdrawn and using a Nanodrop spectrophotometer (Thermo Scientific, Waltham, MA), the concentration (ng/μL) of RNA was determined always from absorption at 260 nm and the ratio between absorbance at 260 and 280 nm was used to confirm the purity of the sample. The remaining RNA samples were stored at -80℃. For samples that were shown to be contaminated with genomic DNA, DNase treatment was performed by adding 2 units per

10 ug of RNA followed by incubation in a thermal cycler (Techne Genius, Houston, TX) at 37º C for 10 min. The DNase was deactivated by the addition of 0.05 M EDTA along with heating at 75 ºC for 10 min.

cDNA was synthesized from the RNA as described in **Chapter 3**.

4.2.2.2. RT-PCR

Primers for ENT1 and CNT3 (Integrated DNA Technologies, Coralville, IA) were designed using Primer3-web 0.4.0 software from the *Bos taurus* sequences (designing conditions are described in **Table B.1** (**Appendix B**) and specificity was checked using BLAST on NCBI (**Table 4.2**). These investigations were performed prior those described in **Chapter 3,** which Primer-Blast was used to design the primers. Primer-Blast is based on Primer 3, however it has additional integrated options including BLAST, avoiding known SNPs and primer selection spanning exon-exon junctions.

cDNA containing mixtures were prepared as described in **Chapter 3** and placed in the thermal cycler. PCR was performed using 35 cycles (**Tables 4.3 and 4**). Samples containing no cDNA were used as negative controls. The expression of the glyceraldehyde 3-phosphate dehydrogenase gene (**GAPDH**), a housekeeping gene, was used as an internal positive control. The PCR products (10 μL) were analyzed using 2% agarose gel electrophoresis and the gel was imaged using an AlphaImager 2200, V5.5 (Alpha Innotech Corporation, San Leandro, CA).

To study the level of expression, PCR was also performed over different cycle numbers. To avoid evaporation while sampling, 50 μL of mineral oil was added to the mixture before placing it in the thermal cycler. Samples (7 μL) were withdrawn after 27 and 31 cycles, in addition to the 35 cycle sample. All of the samples were replaced in the thermal cycler for

the final elongation. The PCR products (5 μL) were analyzed by 2% agarose gel electrophoresis.

Table 4.2: Primers designed for bovine ENT1 and CNT3 using Primer 3

| Trans-porter | Gene | NCBI reference number | Primer | Primer sequence |
|---|---|---|---|---|
| ENT1 | SLC29A1 | NM_001034398.1 | Sense | GAGGAGAGAGCCTCTGTGGAT |
| | | | Anti-sense | GGCAGACAGACAAGACACACA |
| CNT3 | SLC28A3 | NM_001192167.1 | Sense | TCCTTCAAGAAAGCGTGACAT |
| | | | Anti-sense | TTCTGACTAAGCCGGAGTTGA |

Table 4.3**:** Mixture used for PCR.

| **Material** | **Volume (μL) for one sample** |
|---|---|
| cDNA<br>(from olfactory and respiratory samples) | 1 or 2 |
| Forward and reverse primer 1:1 mix<br>(ENT1,CNT3 or GAPDH) | 2 |
| 10X Standard *Taq* Reaction Buffer<br>(100 mM Tris-HCl, pH 8.3 at room temperature; 500 mM KCl; 15 mM $MgCl_2$ ) | 2.5 |
| dNTP | 0.5 |
| Taq polymerase | 1 |
| DNase and RNase water | Up to 25 μL total volume |

Table4. 4**:** PCR conditions for determination of ENT1 and CNT3 from bovine samples.

| | | **Temperature (ºC)** | **Duration** |
|---|---|---|---|
| **Step 1: Initialization** | | 95 | 5 min |
| **Step 2:** | **Denaturation** | 95 | 30 sec |
| | **Annealing** | 55 | 30 sec |
| | **Elongation** | 72 | 30 sec |
| **Step 3: Final elongation** | | 72 | 10 min |

4.2.2.3. Protein extraction and BCA assay

Efficient protein extraction is required for sample preparation and subsequent analysis by Western blotting. Since the transporters of interest are located within the cell membrane, a membrane protein extraction protocol adopted from Abcam Protocols using Triton X-100 was used[86]. Sections of snap frozen bovine respiratory and olfactory tissues were washed with 500 µL cold PBS containing protease inhibitors and mixed using a scalpel with gradual addition of cold lysis buffer (about 600 µL total) (**Table 4.5**). Sections of bovine intestine and mouse heart was used as positive controls for ENT1 and bovine liver and mouse liver were used as positive controls for CNT3. The samples were left on a shaker for 2 hours (Vortex Gene-2, Scientific Industries Inc, Bohemia, NY) at 4°C (cold room) then centrifuged for 20 min at 12000 x g at 4 °C (Eppendorf centrifuge 5810R, Hauppauge, NY). The supernatant was aspirated, aliquoted and stored at -20 ºC.

The total amount of protein extracted was quantified using a Micro BCA Protein Assay kit. In a 96-well plate, serial dilutions of BSA standard solution (2 mg/mL) were made using PBS as the diluent to prepare the standards for the calibration curve. The highest working concentration was 100 µg/mL and 2-fold serial dilutions were made to the lowest concentration of 0.0977 µg/mL. PBS alone was used as a negative control. Serial dilutions

were also prepared from the extracted protein samples. A mixture of solutions of A, B, and C (**Table 4.6**) in a ratio of 25:24:1 were prepared and added to each sample in a volume equal to that of the protein containing mixture (total volume 200 µL). The plate was incubated at 37℃ for 2 hours (VMR incubator orbital shaker, Radnor, PA). The absorbance was measured at 562 nm using a SpectraMax Plus384 Absorbance Microplate Reader (Molecular Devices, Sunnyvale, CA).

Table 4.5: Lysis buffer component (pH 9.0) (Abcam Protocols [86]).

| **Material** | **Amount** |
|---|---|
| NaCl | 150 mM |
| TritonX 100 | 1.0% |
| TrisHCl | 50 mM |
| Protease inhibitor cocktail (added prior use) | 1% |

Table 4.6**:** BCA protein assay reagents.

| **Reagent** | **Contents** |
|---|---|
| A | Alkaline tartrate-carbonate buffer |
| B | Bicinchoninic acid solution |
| C | Copper sulfate solution |

4.2.2.4. Western blotting and immunoblotting

Membrane proteins were separated by SDS-PAGE electrophoresis. A volume containing 100 µg of protein was taken and mixed with an equal volume of laemmli buffer. To denature the proteins, the mixture was heated at 95 ºC for 5 min. The samples were loaded on a 10% SDS polyacrylamide gel (Bio-Rad Ready Gel, Life Research Clinical

Diagnostics, Hercules, CA) that was placed in a Mini-Protein 3 Cell (Bio-Rad, Life Research Clinical Diagnostics, Hercules, CA) filled with running buffer (**Table 4.7**). Molecular weight standards (10 μL) were also loaded onto one of the lanes. The electrophoresis was run at 20 mA and 75 V for 3 hours at room temperature. The separated proteins were transferred to a nitrocellulose membrane (Bio-Rad, Life Research Clinical Diagnostics, Hercules, CA) overnight at 90 mA and 30 V at 4℃ using a Mini Tran-Blot electrophoresis transfer cell (Bio-Rad, Life Research Clinical Diagnostics, Hercules, CA) filled with a freshly-prepared, cooled transfer buffer (**Table 4.8** ).

The nitrocellulose membranes were treated with a blocking solution (3% BSA in PBS) for 1 hour at room temperature. The membranes were incubated with goat polyclonal antibodies against ENT1 or CNT3 for 2 hours at room temperature. The dilutions used were 1:50 and 1:100, respectively, using 0.3% BSA in PBS as a diluent. The blots were washed 3 times with 0.03% Tween 20 in PBS and were incubated with rabbit antigoat antibody conjugated with horseradish peroxidase (at a dilution of 1:5000 in 0.3% BSA in PBS) for 1 hour at room temperature. The blots were washed, and equal volumes of the detection reagents (Luminol substrate and a peroxide solution) were added. The treated membranes were dried and autoradiography films were placed over them (in the dark room); and they were left in a closed cartridge to develop the image for 2 min. While remaining in the dark room, the films were placed in the developer solution for 2 min, washed with tap water, and placed in fixer solution for few minutes until the image appeared. The films were washed and then left to dry.

Table 4.7**:** Running buffer components (Abcam protocols book[86]).

| Material | Amount |
|---|---|
| Tris base | 25 mM |
| Glycine | 190 mM |
| Sodium dodecyl sulfate (**SDS**) | 0.1 % |

Table 4.8: Transfer buffer component (Abcam protocols book[86]).

| Material | Amount |
|---|---|
| Tris base | 25 mM |
| Glycine | 190 mM |
| Methanol | 20 % |

4.2.2.5. Bright field imaging

Sections of respiratory and olfactory bovine tissues were fixed in Zn-formalin solution for 48 hours with shaking at room temperature, dehydrated with a graded series of solutions containing ethanol, cleared with Pro-Par (xylene substituent) and infiltrated with paraffin wax according to an automated process in the Central Microscopy Facility (University of Iowa, Iowa City, IA) (**Table C.1**, **Appendix C**) and then embedded in paraffin. The paraffin blocks were cut into 7 μm sections using a microtome, and the sections were placed in 0.25 M ammonium hydroxide solution, picked up onto the surface of a glass slide, then dipped in a hot water bath (55-65 ºC) to flatten the sections, and left to dry on a hot plate overnight. The sections were stained using hemotoxylin and eosin (**H&E**) after being placed in an oven (58 ºC) for 10 min to allow the paraffin to melt. The staining procedure performed by the autostainer is described in **Tables B 2-4** (**Appendix C**).The slides were mounted using Solvent 100 mounting medium (IMEB Inc, San Marcos, CA) and bright field images were

taken using an Olympus BX-51 Light Microscope (Olympus Microscopes and Imaging Systems Inc., Melville, NY).

4.2.2.6. Immunohistochemistry and confocal imaging

Sections of bovine respiratory and olfactory nasal tissues were fixed in Zn-formalin for at least 48 hours while shaking at room temperature. They were cryofixed in tissue freezing media using liquid nitrogen after being gradually impregnated with sucrose (using 10, 20 and 30% sucrose solutions). Sucrose works as cryoprotectant that prevents the formation of ice-crystal artifacts and ensures good microscopic morphology. Sections (10 μm) were obtained by cutting the blocks using a CryoJane® microtome (Microm Ltd, Bicester, UK) at -35 ºC. The CryoJane® involves the use of a special window tape and hand roller to capture the frozen section as it is being cut. CryoJane®, even though it is time consuming, produces flatter and more wrinkle-free sections and it allows more homogenous staining compared to a conventional cryostat (**Figure 4.4**). For immunostaining, the sections were incubated in cold acetone for 10 min and then treated with a blocking agent (10% normal donkey serum diluted in 10% bovine serum albumin solution) for 20 min. After the blocking step, the sections were treated with goat polyclonal antibody against ENT1 or CNT3, which was also diluted in 10% bovine serum albumin solution at 4 ºC overnight. The working dilutions used were 1:50, 1:100, 1:250, and 1:500 for both antibodies initially, and then 1:10 and 1:25 dilutions were also used for the ENT1 antibody. Sections treated with no primary antibody or with goat IgG (the same amount as used for the primary antibody) were used as negative controls and isotype matched negative controls, respectively. Donkey anti-goat Alexa Fluor® 488 (1:500) was used as the secondary antibody. Each 30 min incubation was followed by TO-PRO®-3 staining (1:2000) (5 min) to visualize cell nuclei. PBS was used as a washing solution between steps and as a diluent for the antibodies. The slides were mounted in

Vectashield® mounting media and images were taken using a Bio-Rad MRC-1024 confocal microscope (Bio-Rad, Berkeley, CA) using the green (495 nm) and the far red (642 nm) fluorescence channels. The images were merged using Image J software (NIH).

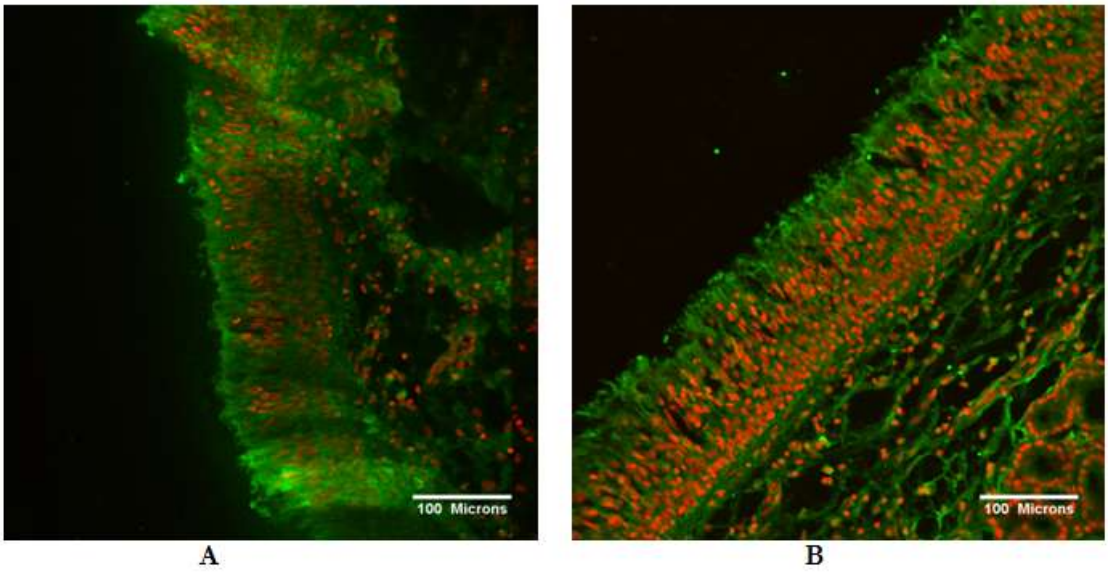


Figure 4.4: Bovine nasal tissue sectioned using (**A**) conventional cryostat and (**B**) CryoJane®. Both sections were immunostained against CNT3 (green signal).

## 4.3. Results and discussion

### 4.3.1. RNA extraction and cDNA production

RNA integrity is an important parameter to check for the efficiency of the RNA extraction step before proceeding to studying gene expression by PCR. One of the most common and simple methods to evaluate RNA integrity is to use agarose gel electrophoresis followed by staining with ethidium bromide. Typically, the gel image shows 2 bands corresponding to the 18S and 28S ribosomal RNA subunits (rRNA), the most abundant types of cellular RNA. As expected, two bands were observed in the purified RNA samples

(**Figure 4.5**). However, in some of the samples, another high intensity band appeared above the two bands. This band is an indication of DNA contamination. Those samples were treated with DNase before further processing.

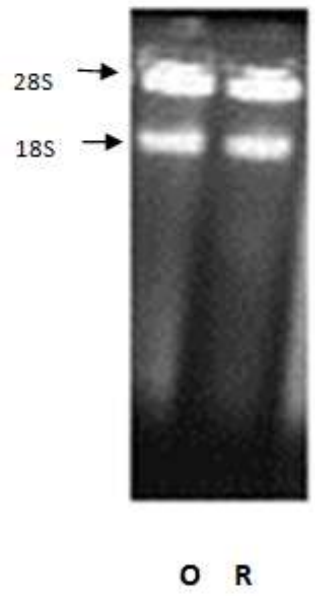


Figure 4.5**:** Example of RNA gel image showing the two characteristic bands of 18S and 28S rRNA subunits for one of the bovine olfactory (O) and respiratory (R) samples.

Nucleic acids are traditionally quantified using UV absorption. RNA has a maximum UV absorption at 260 nm. Proteins have a maximum absorption at 280 nm, thus, the ratio of absorption at 260 and 280 nm can be used as assess RNA purity. A value between 1.8 and 2 indicates the RNA is sufficiently pure for further processing. For the bovine mucosal samples, the RNA concentration was between 300-600 ng/μL and the 260/280 ratio was determined to be between 1.8 and 1.9.

4.3.2. RT-PCR

Primers were designed to amplify segments of the coding regions for ENT1 and CNT3. The size of these segments are 142bp (ENT1) and 167 bp (CNT3). After running the PCR products on gel electrophoresis, the gel images showed bands with sizes between 100 and 200 bp which indicates that ENT1 and CNT3 are expressed in the bovine respiratory and olfactory nasal tissues and the expression of ENT1 was higher than CNT3 (**Figure 4.6**). The negative controls showed no bands, indicating that there was no DNA contamination. In addition, the gel image of GAPDH showed the expected bands between 400 and 500 bp (**Figure 4.6**).

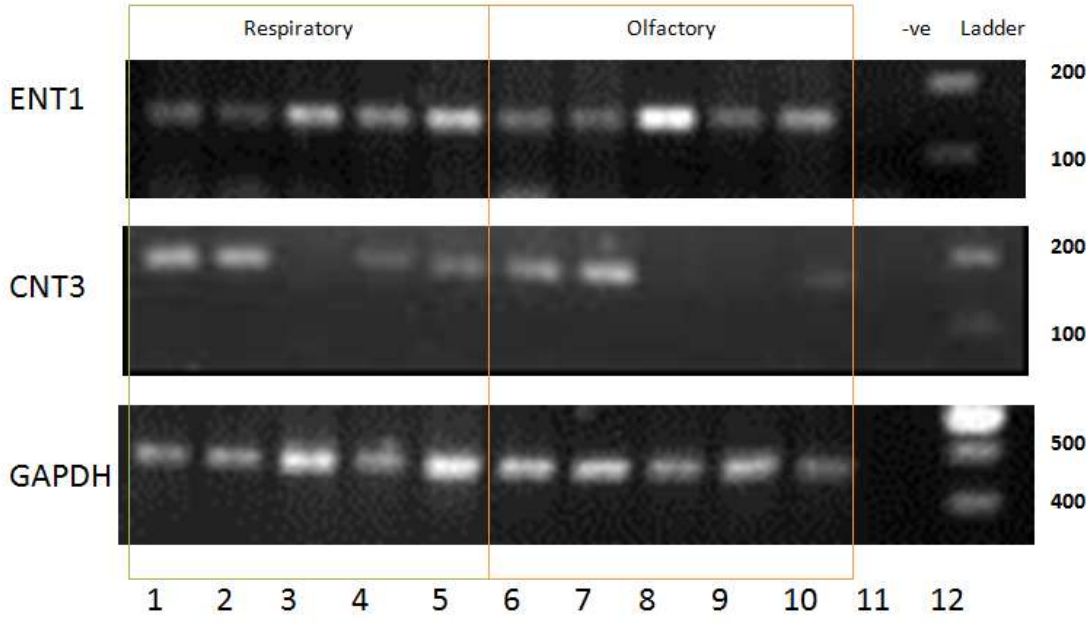


Figure 4.6**:** Gel image of the RT-PCR products indicating the expression of ENT1, CNT3, and GAPDH genes in bovine respiratory and olfactory samples. Lanes (1-5): respiratory Samples; Lanes (6-10): olfactory Samples; Lane 11: negative (-ve) control (with no cDNA); Lane 12:100 bp Ladder.

In the case of CNT3, the gel image for the PCR products showed an additional band between 400 and 500 bp (**Figure 4.7**). In order to identify the band, the PCR products were sent to The DNA Sequencing Facility, University of Iowa to be sequenced (**Appendix D**). By comparing the resulting sequence to sequence reported from the Gene Bank (NM_001192167.1), the additional DNA sequence was identified (**Figure 4.8**) and determined to either due to amplification of genomic DNA that was not completely cleared by DNase treatment or to another, unidentified isoform of CNT3. Identification of this potential new isoform was not pursued.

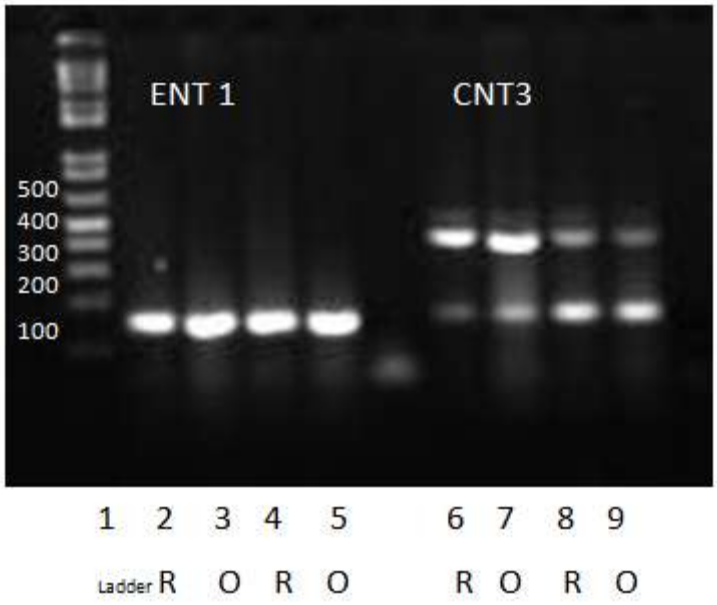


Figure 4.7: Gel image for the RT-PCR showing the presence of 2 bands for CNT3 samples. Lane 1: 100 bp ladder; Lanes (2,4,6,8):respiratory Samples (R); Lanes (3,5,7,9):olfactory Samples (O).

**The expected DNA sequence of the amplified region according to the Gene bank**

TCCTTCAAGAAAGCGTGACATCACCGCAGGAGCAATGAGAGCTCTGATTGCGGGGACCATCGCCTGCTTCCTGACAGC
CTGCATCGCAGGCATGCTTACCAACACTCCTGTAGACATCAACTGCCACCACATTTTGGAGAATGCCTCCGGCTTAGTCAGAA

**The DNA sequence of the amplified region**

NNNNNTGAGAGCTCTGATTGCGGGGACATCGCCTGCTTCCTGACAGCCTGCATCGCAGGTATTATATTGTGTTGTTTGT
GTCCTGTCTCCCTGCACTCACAGGATGGCAACATTGGGGGGGACAGTGCCCACCACTAACATACACAGCATATGTTGCTGTAGAG
AGCTGAGAGGCAGAGCTGCTCTTAAGCATACTGTGATGTGAAATGTGTGGAGCATGGTGGAGAAGTCAAGAATAGAAGAAGA
GTTCGGTGACATCATTAATTAAATAAATGGCACTCTGTTCCACTTCTAGGCATGCTTACCAACACTCCTGTAGACATCAACTGCCA
CCACATTTTGGAGAATGCCTTCAACTCNNGNNAANTCAGAAANN

Figure 4.8**:** The DNA sequence of the amplified region of CNT3 as expected according to GeneBank (CNT3: NM_001192167.1) and the sequence of the PCR products of the bovine nasal samples. Shaded area resembles an additional DNA sequence.

Traditional PCR is not a quantitative technique; however, semi-quantitative data can be generated by analyzing the products after varying numbers of PCR cycles. This allows identification of the quantitative portions of the amplification cycles, and by comparing the intensity of the bands from the same cycle from two different tissues, the relative abundance of mRNA can be estimated. From the gel images (**Figure 4.9**), the bands were hard to visualize at 27 cycles, and at 35 cycles the polymerase enzyme may be saturated, thus 31 cycles was selected as the optimum number needed for the expression comparison. At 31 cycles, both genes were expressed at nearly the same levels in both the bovine respiratory and olfactory nasal tissues.

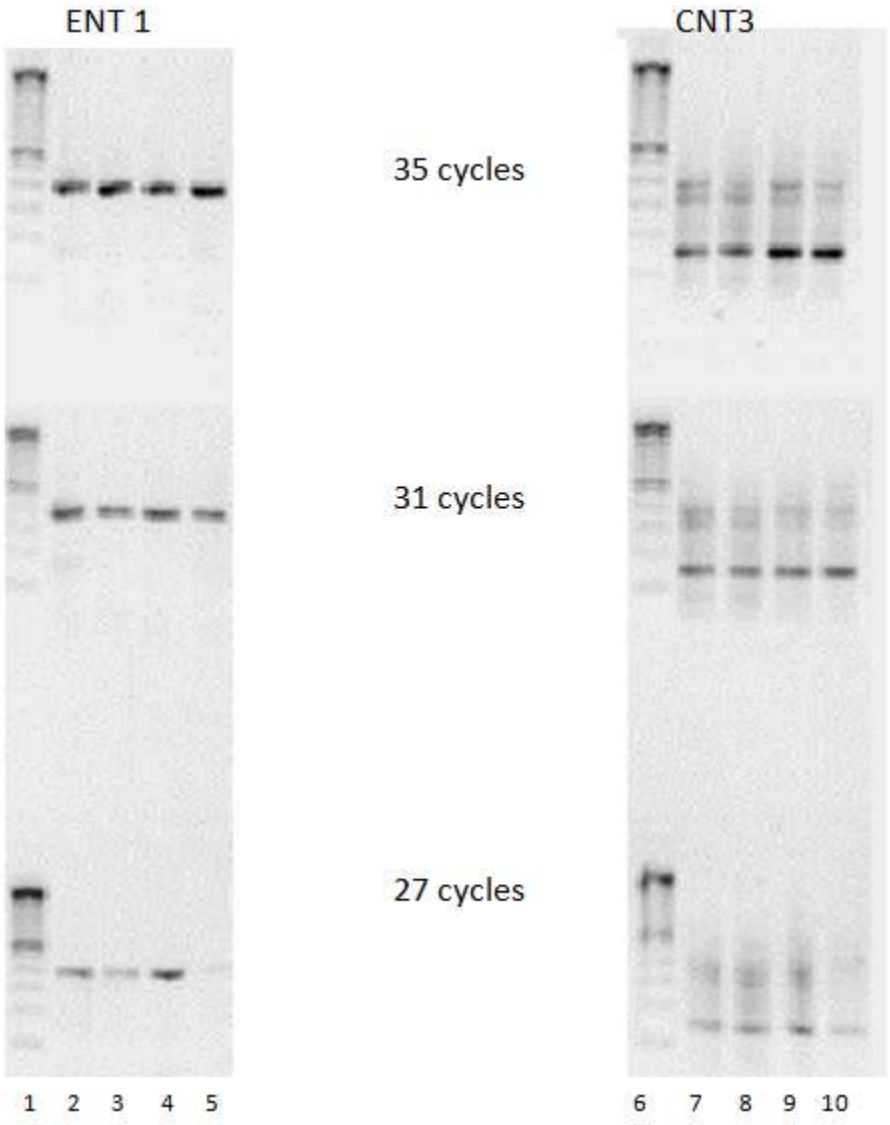


Figure 4.9: Gel images for the RT-PCR conducted over a number of different cycles. Lanes (1,6): 100basepair Ladder; Lanes (2,4,7,9):respiratory samples; Lanes (3,5,8,10):olfactory samples.

### 4.3.3. Protein extraction and BCA assay

In order to quantify the amount of protein extracted, a Micro BCA protein assay was used. This assay is based on using bicinchoninic acid as a detecting agent for the $Cu^{1+}$ which is formed from the reduction of $Cu^{2+}$ by proteins in an alkaline environment. The colored product has an absorbance at 562 nm. The intensity of the color produced by this reaction is

stable and increasing proportionally with increased protein concentration. BSA was used as a protein standard to prepare the calibration curve [87].

To develop a calibration curve for protein content, the absorbance (562 nm) of the blank was subtracted from the absorbance of the prepared BSA standards. After plotting the absorbance versus the concentration, a linear relationship was obtained over the range of 2-50 µg/mL with a determination coefficient of 0.995 (**Figure 4-10**). The concentrations of the extracted proteins from both tissues were calculated using this standard curve.

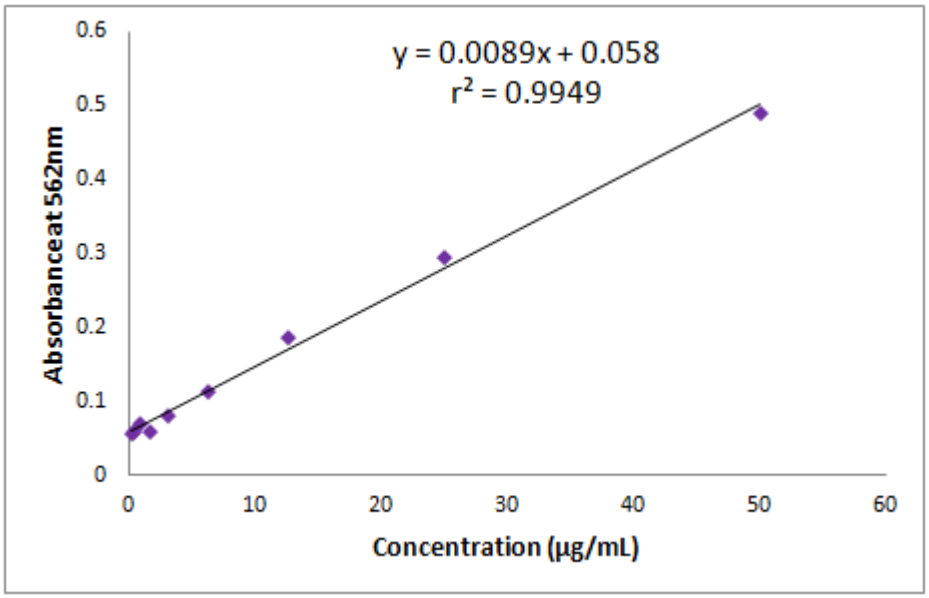


Figure 4.10**:** Calibration curve for BSA in PBS using the Micro BCA Protein Assay kit. Absorbance was measured at 562 nm.

4.3.4. Western blot and immunoblotting

The primary antibodies used for immunoblotting were goat polyclonal antibodies raised against epitopes of ENT1 or CNT3 of human origin. However, according to the antibodies manufacturer, these antibodies can react with other mammalian species including

cows, due to sequence homology. Moreover, two NCBI tools, HomoloGene and BLASTP 2.2.28, were used to check the homology of the ENT1 and CNT3 proteins between humans and cows by comparing nucleoside (HomoloGene) and amino acid (BLASTP 2.2.28) sequences (**Appendix E**) and the proteins showed high similarities. The ENT1 band should appear between 50-60 kDa (molecular weight = 55 kDa) and CNT3 at about 80kDa (molecular weight = 77 kDa). Bands were seen at these molecular weights for both proteins in the respiratory and olfactory tissues and the positive controls (**Figure 4.11**). This suggests that the proteins are present at low levels in both tissues. However, the experimental conditions used, especially the protein extraction, need to be further optimized for improved quality of the immunoblots. The appearance of protein bands corresponding to ENT1 and CNT3, while faint, do indicate that the mRNA detected by RT-PCR is transcribed into the corresponding protein in the nasal mucosa.

### 4.3.5. Bright field imaging

In order to understand the barriers a drug may face when crossing the nasal mucosa, bright field images for the olfactory and respiratory tissues were taken after H&E staining. **Figure 4.12** shows that both the respiratory and the olfactory mucosa possess the expected epithelial layer resting on a basement membrane over a supporting lamina propria. The epithelium consists of pseudostratified columnar cells with goblet cells (only in respiratory epithelia) interspersed between the columnar cells. The underlying lamina propria contains blood vessels and Bowman's glands which secrete mucus.

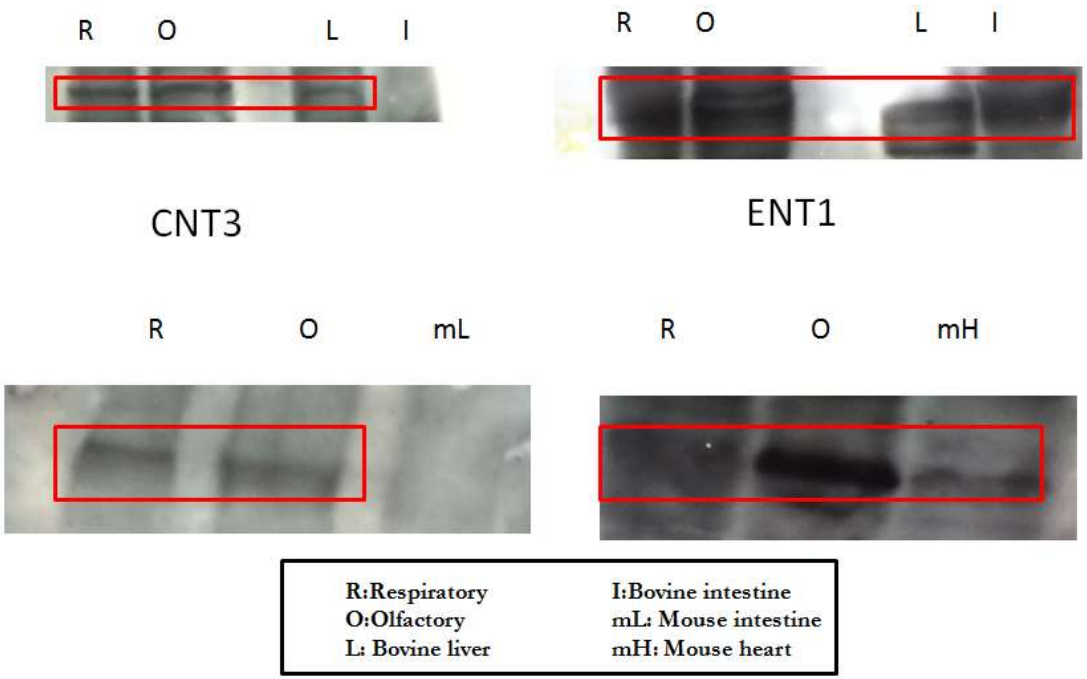


Figure 4. 11: Western blotting showing a band for ENT1 in the bovine respiratory and olfactory samples as well as positive control the bovine liver but not in mice and a band for CNT3 in the bovine respiratory and olfactory samples as well as positive controls .

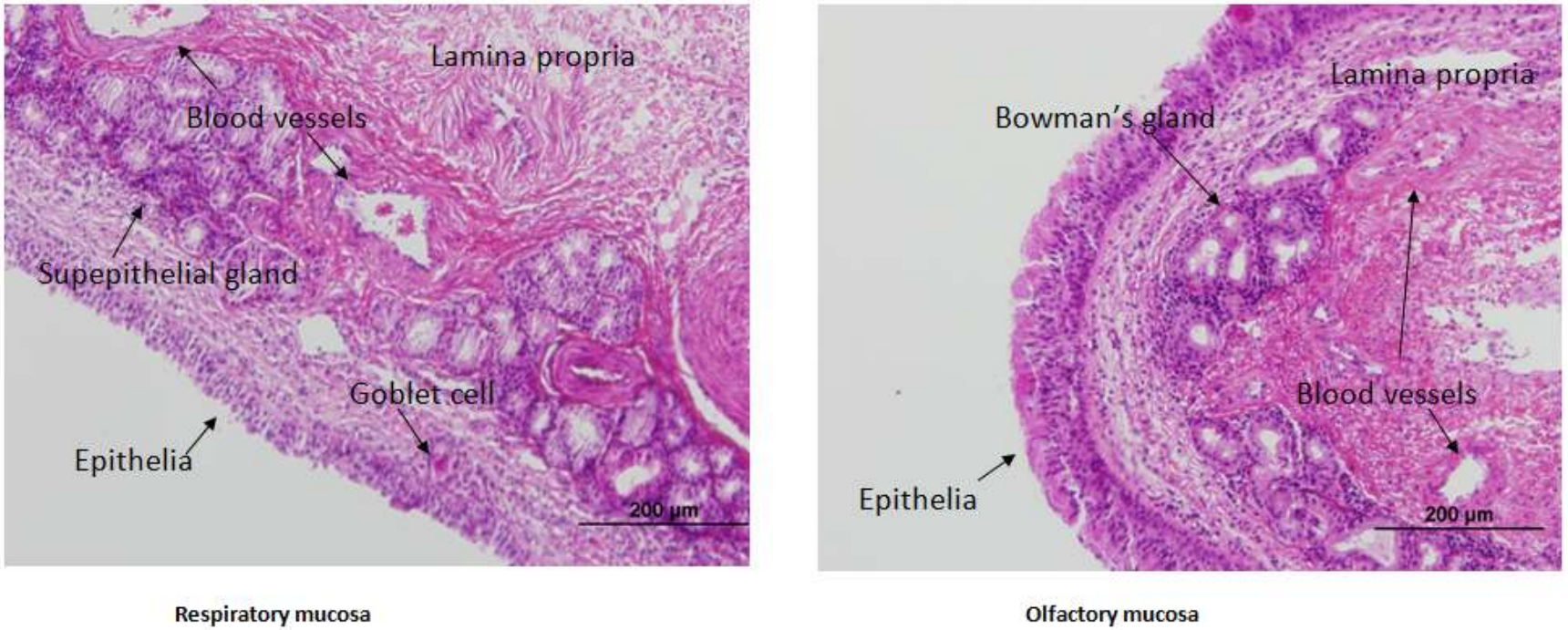


Figure 4.12: Bright field images for H&E stained bovine respiratory (A) and olfactory (B) mucosa showing the pseudostratified columnar epithelium and the lamina propria.

### 4.3.6. Immunohistochemistry and confocal imaging

Immunohistochemistry is widely used to identify, in situ, various components of tissues, including transporter proteins. The technique relies on the specific interaction of an antibody (immunoglobin) and an antigen (e.g. transporter protein). Early immunohistochemistry depended on directly labeling the primary antibodies with a fluorochrome or enzyme for detection. Later, an indirect method, where a labeled secondary antibody was used to detect the primary antibody, was introduced. The indirect method offers more versatility and is more sensitive than the direct method[88]. Donkey anti-goat IgG was used as the secondary antibody against the primary antibodies (goat IgG) to detect the presence of the transporters (ENT1 or CNT3). The secondary antibody was labeled by green-fluorescent Alexa Fluor 488 dye, thus, the green signal (495 nm excitation, 519 nm emission) implies the presence of the transporters. TO-PRO®-3 was used as nuclear stain and gave a red signal (642 nm excitation, 661 nm emission).

The preliminary results showed that the optimum dilutions of primary antibodies for use are (1:25) for ENT1 and (1:100) for CNT3. Samples treated with the primary antibodies showed a green signal in the epithelial region. Two sets of negative controls were used: (1) samples treated with no antibody to account for non-specific binding of the secondary antibody, and (2) samples treated with goat IgG instead of the primary antibody to account for the specificity of the primary antibody. The results show good agreement with the PCR results and confirm the presence of ENT1 and CNT3 in the bovine respiratory and olfactory tissues (**Figures 4.13-16**).

From the images (**Figures 4.13-16**), both transporters appear to be localized primarily in the epithelial region. It is expected that nucleoside transporters are concentrated in epithelial cells present at absorptive mucosal sites. CNTs in other epithelial tissues are

reported to be present on the apical membrane of polarized cells while ENTs have frequently been reported to present on the basal side in many absorptive tissues [72, 73]. However, in the bovine tissues, the antibody signal appears to be on the apical side of the membrane for both transporters. In General, Molina-acras et al. have reported that ENT1 is mainly localized in the basolateral membrane, although it can be also detected in the apical membrane, which supports the finding of this current study [81]. Moreover, Damjura et al. also showed that ENT1 was present on the apical surfaces of the proximal tubular epithelium and on both the apical and basal surfaces of the epithelium of the thick ascending loops of Henle and the collecting ducts of the human kidney [77]. Genter et al. also reported finding ENT1 on the apical surface of the olfactory mucosa in rats [53].

The presence of ENT1 and CNT3 in the nasal mucosa was investigated using a number of different techniques. Western blotting was used to verify the expression of these proteins in the bovine nasal tissues. Since there are no commercially available specific antibodies for bovine ENT1 and CNT3, Western blotting could not be used as the sole confirmation of protein expression. Thus, RT- PCR, which is a specific and less tedious method, was used to verify the expression of genes encoding for the bovine ENT1 and CNT3 proteins. As additional experimental confirmation, immunohistochemistry was performed on mucosal tissue sections to both verify the expression of the transporter proteins and identify their localization in the tissues. The bovine microarray study also confirmed the presence of mRNA for these transporters and it showed that there is at least one other nucleoside transporter, ENT2, expressed in the bovine nasal respiratory and olfactory mucosa. The microarray analyses presented in **Chapter 3** also showed that ENT1 and CNT3 are expressed in nasal mucosa of humans and other commonly used animal

models, including mice and rats. The microarray results suggest that all of these species appear to have lower expression levels than in cows.

The presence of nucleoside transporters on the apical surface of the nasal mucosa suggests the need for nucleoside uptake by the nasal epithelial cells. Nucleoside transporters play a key role in salvaging nucleosides for nucleic acid synthesis [72]. Moreover, extracellular adenosine is active in the regulation mucocillary clearance and is important in the maintenance of epithelial functions [89, 90,40].

The presence of nucleoside transporters in the nasal mucosa assists in the understanding of the absorption behavior of nucleoside-analogue drugs such as antiviral or anticancer agents, after intranasal administration. Further evaluation of their transport activities will improve the opportunities to use the nasal route to administer nucleoside-analogue drugs for systemic absorption or targeting the brain to treat CNS disorders.

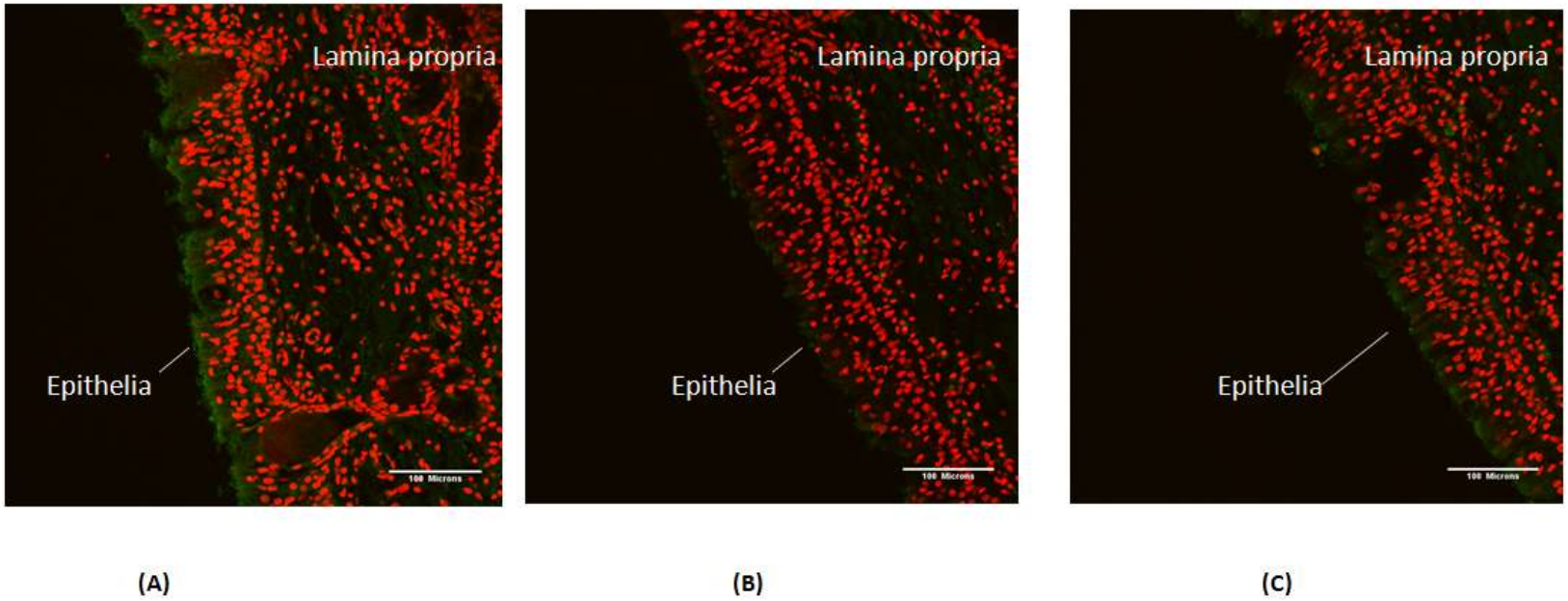


Figure 4. 13: (**A**) ENT1 expression (green signal seen mainly on the apical side of the epithelia) in the respiratory mucosa compared to (**B**) untreated mucosa (negative control) and (**C**) goat IgG treated mucosa (isotype matched negative control). Red signal represents the nuclei stained with TO-PRO®-3.

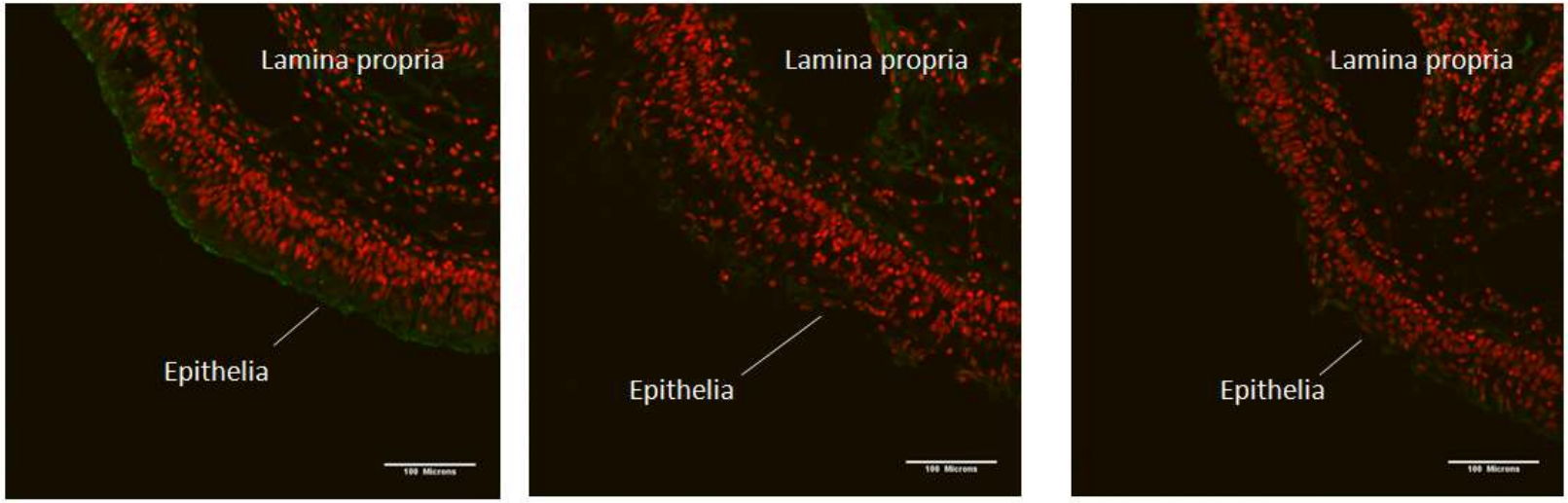


Figure 4.14: (**A**) ENT1 expression (green signal seen mainly on the apical side of the epithelia) in the olfactory mucosa compared to (**B**) untreated mucosa (negative control) and (**C**) goat IgG treated mucosa (isotype matched negative control). Red signal represents the nuclei stained with TO-PRO®-3.

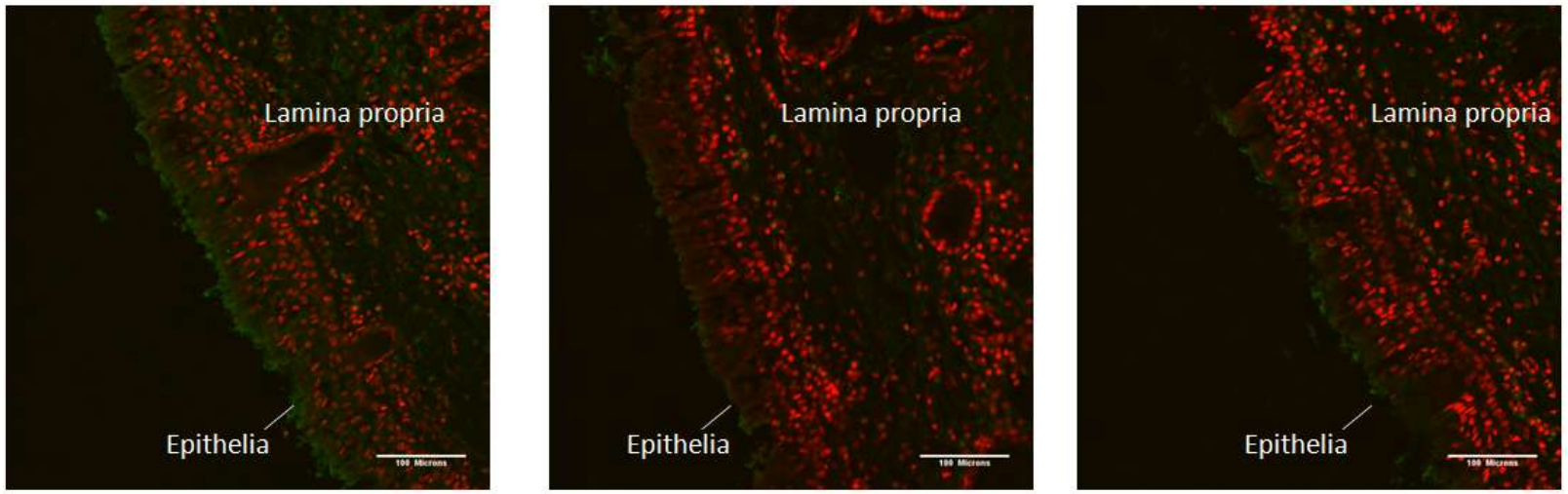


Figure 4.15**:** (**A**) CNT3 expression (green signal seen mainly on the apical side of the epithelia) in the respiratory mucosa compared to (**B**) untreated mucosa (negative control) and (**C**) goat IgG treated mucosa (isotype matched negative control). Red signal represents the nuclei stained with TO-PRO®-3.

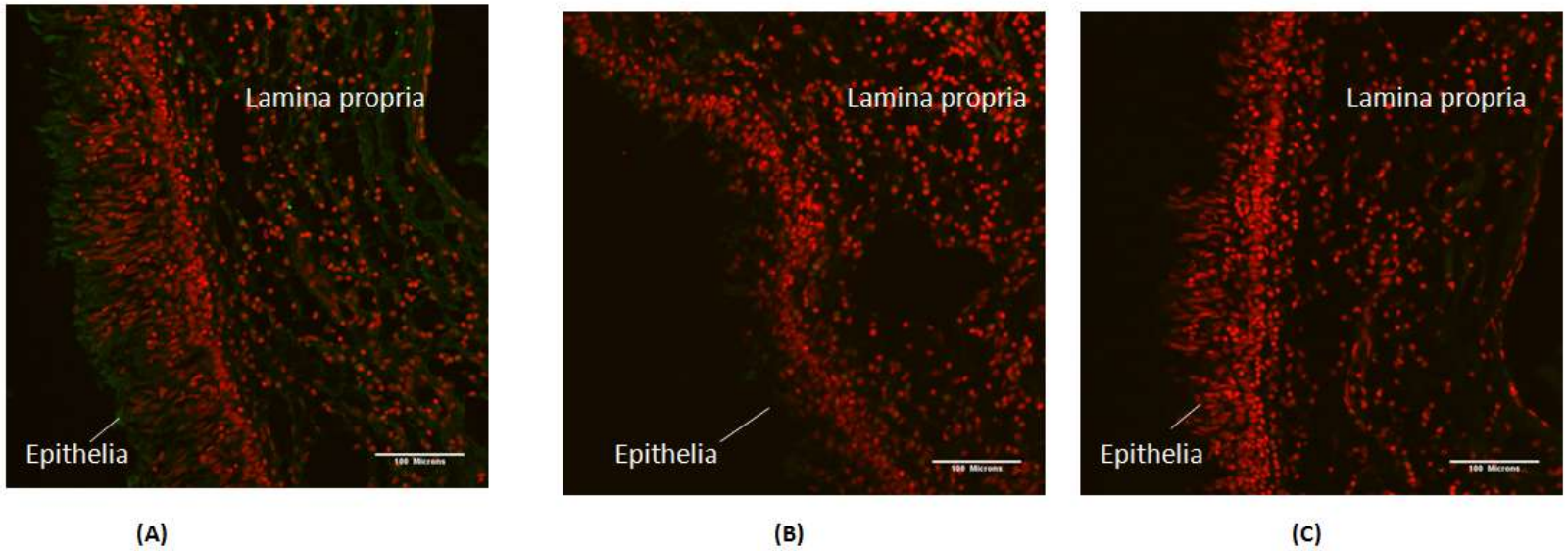


Figure 4.16**:** (**A**) CNT3 expression (green signal seen mainly on the apical side of the epithelia) in the olfactory mucosa compared to (**B**) untreated mucosa (negative control) and(**C**) goat IgG treated mucosa (isotype matched negative control). Red signal represents the nuclei stained with TO-PRO®-3.

# CHAPTER 5

# PERMEATION OF ALOVUDINE THROUGH THE NASAL MUCOSA

## 5.1. Introduction

Alovudine, a thymidine analog, (**Figure 5.1**) is a nucleoside-like drug compound that acts as a reverse transcriptase inhibitor. It exhibits its activity after being phosphorylated by a cellular thymidine kinase, and the active metabolite blocks viral replication by: (1) competing with deoxythymidine triphosphate (**dTTP**) for binding to viral reverse transcriptase; and (2) by incorporating itself into viral DNA causing chain-termination [91]. Therefore, alovudine can be used to inhibit human immunodeficiency virus (**HIV**) replication.

**Molecular weight:** 244.22 g/mole

**Predicted solubility (pH7, 25°C):** 2.2 g/L

**xlogP3**: -0.3

**pKa:** 9.55

Figure 5.1**:** Chemical structure and estimated physical properties of alovudine (3'-fluorodeoxythymidine) [92].

Alovudine has been investigated for the treatment of HIV infection, and it showed similar *in vitro* potency to zidovidine, one of the most potent agents against HIV infection. Alovudine also provides higher levels of intracellular active phosphorylated forms [93]. An initial clinical trial showed an alovudine-induced, concentration-dependent hematological toxicity which halted its further development in the early 1990s. However, later *in vitro* studies found that alovudine can suppress several multi-drug resistant HIV strains which are increasingly becoming a problem in the current treatment of HIV infection [94]. A more recent clinical study showed that adding alovudine efficiently reduced the HIV viral load for patients who have failed on multiple drug-regimens and have at least two thymidine-associated mutations (TAMs) [95]. Another study showed that a dose of alovudine as low as 2 mg/day can also significantly reduce the viral load in patients with a median of four TAMs[96]. In addition, both studies indicated that alovudine was well tolerated.

Currently, the $^{18}$F form of alovudine ($^{18}$F flurothymidine, **FLT**) is also used as a proliferation tracer in positron emission tomography (**PET**). Cell proliferation is a key target for tracing tumor development and growth. Labeled nucleosides such as $^{11}$C-thymidine can be used as cell proliferation tracers because they are used extensively for DNA replication. However, $^{11}$C-thymidine, which is widely used to assess tumor development, undergoes catabolism. $^{18}$F-alovudine, in comparison, has a more suitable nuclide half-life (109.8 min). FLT has been shown to accumulate in various tumors, including brain tumors [97].

Early preclinical studies suggested that, similar to thymidine, alovudine permeated cell membranes by a carrier-mediated mechanism. This was determined from inhibition of the influx of alovudine into HL-60 cells by the presence of NBMPR, an ENT 1 inhibitor [93]. Parproske et al. also studied the uptake of alovudine in *Xenopus lavevis* oocytes individually expressing ENT1, ENT2, CNT1, or CNT3. In all four types of oocytes, the uptake of

alovudine was concentration dependent, indicating the involvement of these nucleoside transporters (**Figure 5.2**). Examining their Michaelis-Menten kinetics ($V_{max}$ and $K_m$), ENT1 and ENT2 displayed a greater capacity ($V_{max}$) and lower affinity ($K_m$) than CNT1 and CNT3 [98].

Parproske et al. also studied alovudine uptake in various cell lines such as MCF-7, A549, and U251 in the presence of NBMPR. The uptake of alovudine in all of the cell lines was inhibited at least 50%. Real time PCR showed that nucleoside transporters were expressed in these cell lines with ENT 1 and ENT2 having the most abundant transcripts [98]. Their results suggest that nucleoside transporters are important determinants of cellular uptake of alovudine.

The nasal route could be used to deliver alovudine directly to the brain to treat HIV complications with potentially less systemic toxicity. HIV has the propensity to infect the brain and cause severe neurocognitive disorders such encephalitis and HIV-associated dementia [99]. Microdialysis studies of alovudine in rats have shown that alovudine has the ability to cross the blood brain barrier (**BBB**) after subcutaneous injection or intravenous infusion [100, 101]. The concentration of alovudine in the brain reached a maximum of 20 % of that in the blood. However, bearing in mind the possible bone marrow toxicity caused by alovudine, brain targeting using nasal administration could offer an improved route to treat HIV- associated neurocognitive disorders.

This chapter describes the permeation of alovudine across the nasal mucosa and evaluates the possible involvement of transporters, nucleoside transporters specifically. Along with the *in vitro* studies discussed in this chapter, *in vivo* studies have been conducted to determine the possible direct transport of alovudine to the brain after intranasal administration in rats[102, 103].

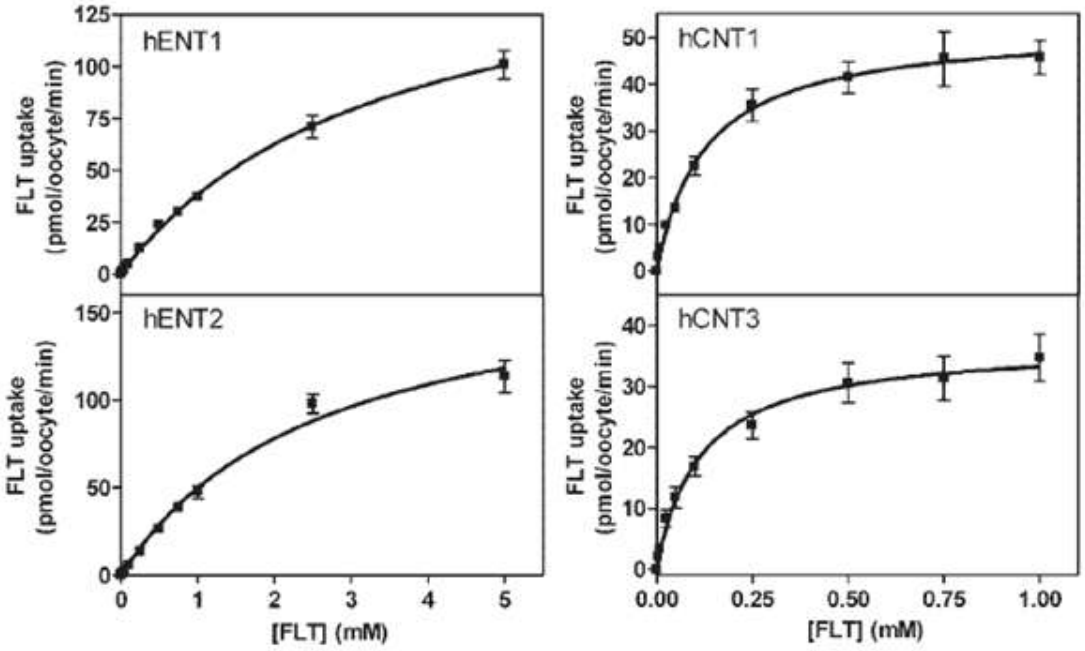


| hNT | $K_m$ mM | $V_{max}$ pmol/oocyte/min |
|---|---|---|
| **hENT1** | 3.4±0.2 | 169±4 |
| **hENT2** | 2.6±0.4 | 180±13 |
| **hCNT1** | 0.13±0.01 | 52±1 |
| **hCNT3** | 0.11±0.01 | 37±1 |

Figure 5.2**:** Concentration-dependent influx of $^{3}$H-alovudine (FLT) in oocytes producing human nucleoside transporter proteins and the kinetic parameters of [$^{3}$H] FLT influx are detailed in the table[98].

## 5.2. Materials and methods

### 5.2.1. Reagents and materials

Alovudine and NBMPR were purchased from Sigma-Aldrich (St. Louis, MO). Methanol, dimethyl sulfoxides (**DMSO**), and ammonium phosphate were obtained from Fisher Scientific (Chicago, IL). Kreb's Ringer's buffer (**KR**

**B**) salts (**Table 4.1**) were purchased from Research Products International Corp (Mount Prospect, IL), except for magnesium chloride (**$MgCl_2$**) and dibasic sodium phosphate (**$Na_2HPO_4$**) which were from Sigma-Aldrich (St. Louis, MO), and calcium chloride (**$CaCl_2$**) which was from EM Science (Gibbstown, NJ). The NaviCyte® vertical chamber systems were obtained from Harvard Apparatus (Holliston, MA). Each system consists of six vertical chambers, a gas manifold, and a heater block. The chambers are connected to a carbogen ($O_2/CO_2$ 95%/5%) cylinder. Each chamber consists of two piece assemblies held together with retaining rings (**Figure 4.3**). Tissue explants are fixed between the opposing faces of the two half-chambers using the pins that surround the opening. Each chamber can hold up to a 2 mL volume and the opening diameter is 0.9 cm, which provided a cross-sectional area of 0.64 $cm^2$.

Figure 5.3**:** Diffusion chambers used in transport studies. Each chamber consists of two pieces between which the tissue explants can be mounted. Electrodes for TEER measurement are shown in the back chamber [104].

KRB preparation

KRB's components are listed in **Table 4.1**. The buffer was prepared by dissolving all of the components, except for $CaCl_2$, in deionized water. Carbogen was bubbled in the solution for 10 min to lower the pH of the solution slightly, then $CaCl_2$ was added and the solution was exposed to carbogen again for 10 min. The pH of the buffer was approximately 7.4 with osmolality around 250 mmol/kg.

Table 5.1**:** Krebs-Ringer buffer (pH= 7.4).

| **Material** | **Concentration (mM)** |
|---|---|
| $MgCl_2$ | 1.67 |
| NaCl | 119.76 |
| KCl | 4.56 |
| $Na_2HPO_4$ | 0.83 |
| $NaH_2PO_4$ | 1.50 |
| $NaHCO_3$ | 15.00 |
| $CaCl_2$ | 1.20 |
| Glucose | 10.00 |

Stock and working alovudine solutions preparation

An alovudine stock solution (4000 μM) was prepared by dissolving the compound in KRB at room temperature. Alovudine solutions were prepared by diluting the stock solution with KRB to the desired concentration. NBMPR stock solution (5 μM; 200 mL) was prepared by dissolving NBMPR in KRB in the presence of 200 μL DMSO. DMSO was used as a co-solvent to enhance the aqueous solubility of NBMPR.

## 5.2.2. Methods

### 5.2.2.1. Preparation of mucosal tissues

Excised bovine respiratory and olfactory nasal tissues were obtained from Bud's Custom Meats (Riverside, IA). The tissue was collected immediately after decapitation. The nasal tissue was retrieved by removing the nasal septum to expose the nasal cavity. The dorsal and the ventral conchae are lined by the respiratory mucosa and the ethmoid and the middle conchae are lined by the olfactory mucosa. The conchae were excised using a sharp knife (**Figure 4.4**), and the tissues were placed in iced, sparged KRB for transportation to the lab (travel time was about 30 min).

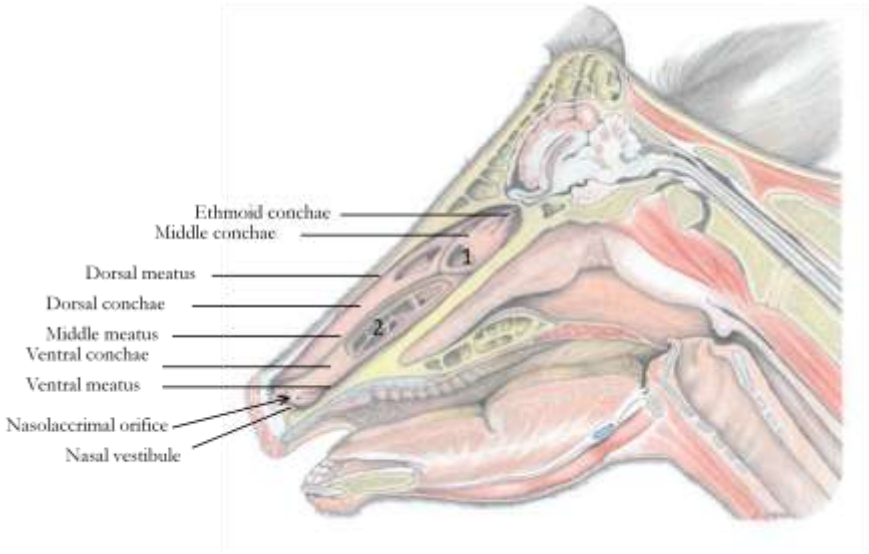


Figure 5.4: Diagrammatic representation of the cross-section of the bovine nasal cavity showing (1) the respiratory region and (2) the olfactory region [105].

### 5.2.2.2. *In vitro* bidirectional transport studies

The mucosal explants consisting of the epithelium and the underlying connective tissue were carefully separated from the cartilage using a pair of tweezers and were mounted into

the diffusion chambers. The tissues were equilibrated in KRB and sparged with carbogen ($O_2/CO_2$ 95%/5%) for at least 15 minutes. The KRB was replaced with 1 mL of the alovudine solution in the donor compartment and 1mL of KRB in the receiver compartment. To determine the transport of alovudine across the mucosa, 200 μL samples were withdrawn from the receiver compartment every 15 min for 2 hours and the samples withdrawn were replaced with fresh KRB to keep the total volume constant. The donor concentrations used were 50, 100, 200, 300, 1000, and 4000 μM alovudine prepared in KRB. The range of concentrations investigated was based on the report of Paproske [98]. The study was performed with triplicate tissue explants and the explants were mounted with either that the epithelial or connective tissue surface facing the donor solution. The chambers were sparged with carbogen ($O_2/CO_2$ 95%/5%) during the experiment.

5.2.2.3. Transport inhibition with NBMPR

In order to study the permeation of alovudine in the presence of ENT1 inhibitor, NBMPR, transport studies were performed at an alovudine concentration of 500 μM, which is below the estimated $K_m$ of alovudine to ensure that the ENT1 transporters were not saturated during the experiment. The NBMPR concentration used was 100 nM which was the highest concentration used to inhibit alovudine uptake in the Paproske study [98]. The transport study was performed as described in the previous section, however; NBMPR solution was used instead of KRB for the initial equilibration of the tissue. The alovudine solution was prepared in the NBMPR solution (donor chamber) and the NBMPR solution alone was used in the receiver chamber. As a control, a transport study using alovudine at a concentration of 500 μM without NBMPR was performed at the same time. Since DMSO is known to be permeation enhancer, the same amount of DMSO used to prepare the

NBMPR solution was used in the KRB and the alovudine solutions used in the control study.

5.2.2.4. Analytical method for alovudine quantification

The samples were analyzed according to the method described by Stahle et al. [106]. The analysis was performed using HPLC with UV detection at a wavelength of 254 nm. A Zorbax RX, C18 4.6x250 mm, 5 μm column (Agilent Technologies, Santa Clara, CA) was used. The mobile phase consisted of 0.05 M ammonium phosphate buffer (pH=6) containing 20% methanol. The flow rate was 1 mL/min, and the injection volume was 100 μL. The HPLC system consisted of an LC-600 liquid chromatography, SPD-6A UV spectrophotometric detector (Shimadzu Scientific Instruments, Columbia, MD) and a Waters 712 WISP autosampler (Waters Corporation, Milford, MA). The detector response was collected and analyzed by an integrator, a C-R5A Chromatopac integrator (Shimadzu Scientific Instruments, Columbia, MD).

A typical alovudine chromatogram is presented in **Figure 5.5**. The limit of detection was 0.1 μM. A calibration curve over the range of 0.4-25 μM was used (**Figure 5.6**). Linear regression analysis of the peak areas of alovudine vs. concentration gave a correlation coefficient of 0.9999. NBMPR was not detected (no peaks) at 254 nm which indicates that NBMPR did not interfere with the alovudine analysis.

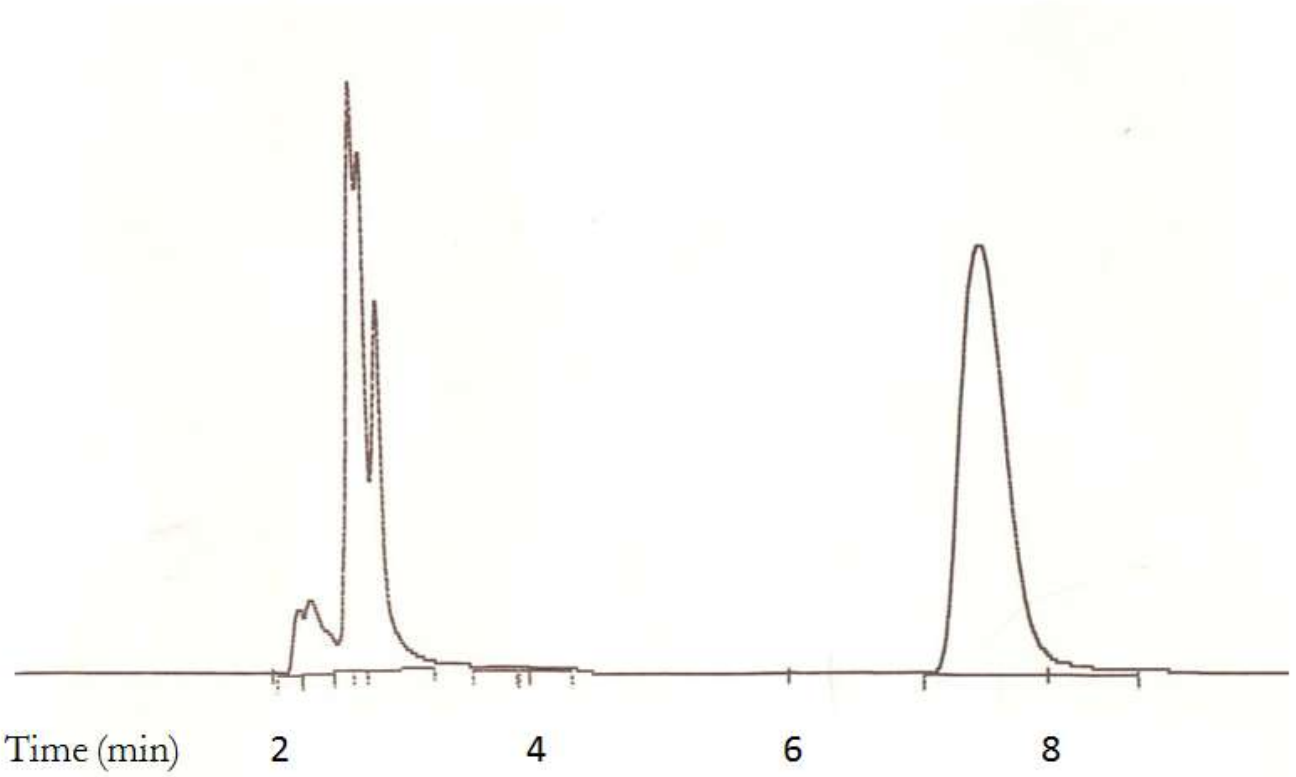


Figure 5.5: HPLC chromatograph of alovudine (7.5 min) in Kreb's Ringer buffer. Mobile phase: 0.05 M ammonium phosphate buffer (pH=6) containing 20% methanol; Column: Zorbax C18 4.6 x 250 mm, 5 μm; Flow rate: 1 mL/min; Wavelength: 254 nm.

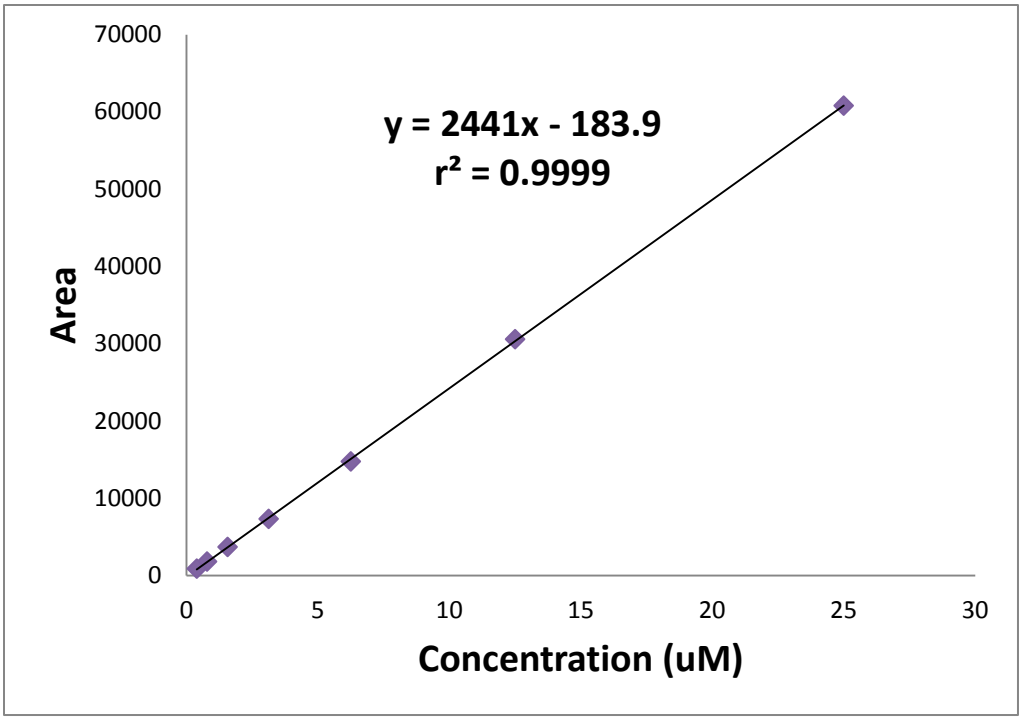


Figure 5.6**:** Calibration curve for alovudine in Kreb's Ringer buffer. Mobile phase: 0.05 M ammonium phosphate buffer (pH=6) containing 20% methanol; Column: Zorbax C18 4.6 x 250 mm, 5 μm; Flow rate: 1 mL/min; Wavelength: 254 nm.

5.2.2.5. Transepithelial electric resistance (TEER)

Viability testing is one of the requirements needed in *in vitro* experiments with excised tissue. Electrophysiological measurement is a powerful tool to test the viability of tissue and the integrity of membranes [36]. The integrity of the nasal mucosal tissues was monitored by measuring the transepithelial electric resistance (**TEER**) at the beginning and the end of the experiment using an EVOM volt-ohm meter (World Precision Instruments Inc., Sarcosta, FL). Two pairs of electrodes each contains silver/silver chloride pellet and a silver electrode were placed in each of the half-chambers. One pair was used to pass the current across the tissue and the other pair to measure the voltage. The volt-ohm meter

reports an electrical resistance which was recorded and used to assess tissue viability. Typical TEER values recorded for excised tissue are in the range of 100-200 Ω $cm^2$ for bovine respiratory mucosa and 100-160 Ω $cm^2$ for bovine olfactory mucosa. Values below 100 Ω $cm^2$ were taken as an indication of tissue damage and samples below this value were excluded from the study.

5.2.2.6. Flux measurement and permeability calculation

The concentration (μM) of alovudine in the sample withdrawn from the receiver chamber was calculated and the amount of alovudine in the receiver chamber (1 ml) at each sampling time was determined. The cumulative amount of drug in the receiver chamber was calculated by adding the amount removed from the previous 200 μL samples to the amount present in the receiver chamber. The cumulative amounts of alovudine transported were plotted against time and the slope was calculated from the linear portion of the curve. The flux was determined using Fick's first law by dividing the slope with the surface area of the tissue available for diffusion (0.64 $cm^2$). A Student's t-test was performed to compare the mean flux value at each concentration, and a value of $p \leq 0.05$ was considered statistically significant. All calculations were performed using Microsoft Excel 2007 (Microsoft Corp., Redwood City, WA).

## 5.3. Results and discussion

Viability testing is a crucial requirement for any *in vitro* study using excised tissue. Viability of the membranes is required for accurate transport results to ensure (1) the functional integrity of cellular and subcellular barriers, (2) the continued activity of transporters, and (3) the activity of metabolic enzymes. Several conditions used in these experiments help in maintaining the viability of membranes, including the addition of

glucose and perfusing the diffusion chambers with carbogen gas. Each of these helps in maintaining the biological functions of the tissue. The gas perfusion also assists with media circulation and stirring of the chamber contents[36]. Tissue viability was tested by measuring the TEER at the beginning (15 min after adding the drug solution) and the end (after 2 hours) of the experiment. The TEER values agreed with the typical values measured in our lab for bovine respiratory (100-200 $\Omega$ cm$^2$) and bovine olfactory mucosae (100-160 $\Omega$ cm$^2$). TEER values didn't fall below the limit value of 100 $\Omega$ cm$^2$ used by our laboratory after 2 hours, but they did show a significant decrease below this level after 4 hours. These observations were consistent with those of previous investigations and support the use of the two hour experimental interval. The TEER values obtained for each experiment are listed in **Appendix F**. The presence of NBMPR and DMSO did not lower the measured TEER values and thus are believed to have no direct effect on membrane barrier integrity.

The TEER values measured in these studies were higher than what had been measured by Schmidt et al.who reported values of 42 $\pm$ 12 $\Omega$ cm$^2$ for bovine nasal tissue [39]. One possible reason for this differences may be the difference in thickness of the tissues used in each laboratory. While the average thickness of the bovine respiratory and olfactory tissues measured in our lab is 0.75 mm and 0.4 mm, respectively, the thickness of the nasal tissue used by Schmidt et al. was reported to be ~0.1 mm.

These low TEER values also suggest that the nasal mucosa is similar to or leakier than various regions of the gastrointestinal mucosa. Specifically, the tight gastric mucosa shows typical TEER values of 2000 $\Omega$ cm$^2$, while the leakier regions of the jejunum and ileum have values between 50 and 100 $\Omega$ cm$^2$, and the colonic region is reported to give values 300-400 $\Omega$ cm$^2$ [107].

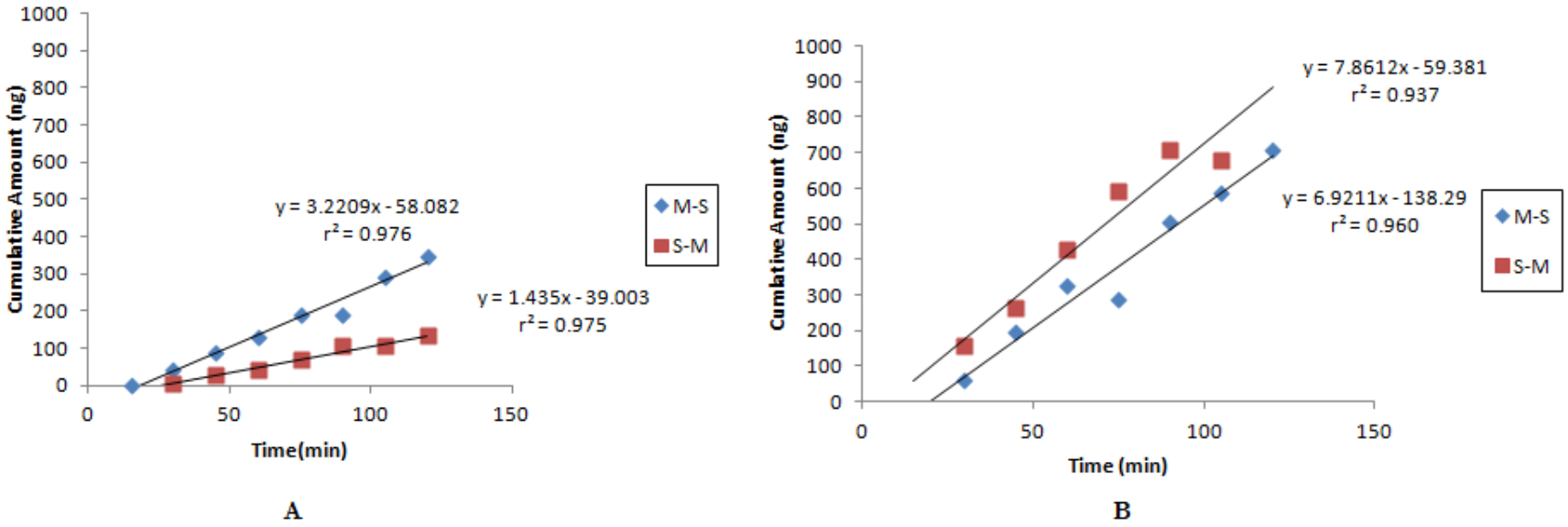


Figure 5.7**:** Representative plot of cumulative amount of drug (alovudine) appearing in the receiver chamber as a function of time during steady state period. Results for bovine respiratory (**A**) and olfactory (**B**) tissues with100 μM alovudine in the donor chamber. (M-S: mucosal to submucosal direction; S-M: submucosal to mucosal direction).

At steady state, the amount of material which crosses a barrier is constant with respect to time [108]. Thus, the cumulative amount of material permeating across the barrier should increase linearly with time. **Figure 5.7** shows an example of the cumulative amount of alovudine permeated across the nasal tissues at a donor concentration of 100 μM. The cumulative amount of alovudine permeated versus time plots for each donor concentration are included in **Appendix G**.

The flux across a membrane is defined as the amount of permeant transferred per unit area of membrane surface per unit time, and it is proportional to the concentration gradient of the permeant across the membrane (Fick's first law). Under sink conditions, where the receiver compartment was maintained at low (zero) concentration and the donor concentration remains constant, the flux is directly proportional to the donor concentration of the permeant [108]. When the average flux of alovudine (n=3) for 8 different concentrations was plotted against the donor concentration for the respiratory mucosa, a non-linear relationship over the 50-4000 μM concentration range was observed (**Figure 5.8**). The flux of alovudine increased with increasing the donor concentration up to 2000 μM, and above this concentration the flux remained essentially constant. This suggests the involvement of saturable transporters in the uptake of alovudine by the respiratory mucosa. However, the flux once again increased drastically at 4000 μM indicating the presence of other factors affecting its transport. It is possible that other transporters that were not saturated at or near 4000 μM play a role at these higher concentrations. The flux of alovudine through the olfactory mucosa (**Figure 5.9**) also showed a non-linear relationship over the 50-4000 μM concentration range. Compared to the respiratory results, the transport of alovudine through the olfactory mucosa was saturated at a lower concentration (1000 μM). This may be due to

differences in transporter expression between these tissues or due to a different distribution of transporters within the olfactory and respiratory mucosae.

The Michaelis-Menten equation (**Equation 1**) is one of the most well-known models used to describe enzyme kinetics. It can also be used to describe transporters kinetics.

$$V = \frac{Vmax\,[C]}{Km+[C]} \qquad \text{Equation 1}$$

Where,

V= the rate of transport= flux,

$V_{max}$=the maximum flux achieved by the system,

[C]= concentration of the substrate,

$K_m$=the concentration of the substrate at one-half $V_{max}$.

Fitting the Michaelis-Menten equation to the flux of alovudine was performed using GraphPad Prism 6 software (GraphPad Software, San Diego, CA) (**Figure 5.10**). Even though the $K_m$ value determined cannot be assigned to only one transporter in the nasal tissue, the values for $K_m$ in the bovine nasal respiratory (2191 μM (M-S) and 3830 μM (S-M)) and olfactory (2140 μM (M-S) and 1836 μM (S-M)) were similar to what was reported for ENT1 (3400 μM) and ENT2 (2600 μM) in *Xenopus lavevis* oocytes (**Figure 5.2**)[98].

The flux of alovudine in the mucosal to submucosal and submucosal to mucosal directions through the respiratory and olfactory mucosae was studied to examine the role of nucleoside transporters in the net uptake or efflux. It was expected that the flux in the mucosal direction would be higher than in the opposite direction because ENT1 and CNT3 were observed to be located on the apical side of the respiratory and the olfactory mucosa (**Chapter 4**). Based on the experimental results, flux in the mucosal to submucosal direction was not significantly greater than in the opposite direction (**Figures 5.8** and **5.9**), which

suggests that the facilitative nature of the equilibrative transporters allows for the nearly equivalent uptake and efflux of the substrate across the nasal mucosae.

Based on the total mass of alovudine transported , the flux of alovudine through the olfactory mucosa was greater than through the respiratory mucosa. One likely reason for this is due to the difference in thickness between the two tissues. Since the thickness of the respiratory tissue (0.75 mm) was greater than the olfactory tissue (0.4 mm), an additional analysis was conducted where the flux values were normalized to an equivalent tissue thickness of 1 cm (**Figure 5.11**). Under these conditions, the flux of alovudine through the olfactory mucosa was found to be comparable to the respiratory mucosa.

To examine the specific contribution of ENT1 to the permeability of alovudine, an ENT1 inhibitor was included in additional transport studies. These studies were performed using a 500 μM donor concentration of alovudine. This concentration was below the $V_{max}$ for both the bovine olfactory and respiratory mucosa and was selected to maximize the likelihood of observing inhibitory effects (**Figures 5.8-10**). Because the ENTs are inhibited by nanomolar concentrations of NBMPR, 100 and 200 nM concentrations were tested [72, 98]. At 200 nM, the flux of alovudine was 10-80 % lower in the presence of NBMPR, demonstrating the presence and activity of ENT1 (**Figure 5.12**). Even though the gene expression of the transporters did not show any differences between the bovine respiratory and the olfactory regions (**Chapter 3**), the flux of alovudine across the olfactory mucosa was decreased to a greater extent by NBMPR compared to the respiratory mucosa. Moreover, the flux in the submucosal to mucosal direction was inhibited to a greater extent by NBMPR than in the mucosal to submucosal direction. Finally, the incomplete inhibition of transport indicates that other transporters, such as CNT3, or additional transport mechanisms, including passive diffusion, are also involved in alovudine transport across the nasal mucosa.

Several studies evaluating the utility of the nasal route to deliver anti-HIV nucleoside analogue drugs to the brain have been reported. Yang et al. showed that stavudine reached the brain after intranasal administration in rats but did not show a significant distribution advantage over systemic administration [109]. On the other hand, zidovudine showed a higher CSF to plasma ratio after intranasal administration compared to intravenous administration in both rats and rabbits[83,110]. The mechanism by which the two drugs passed across the nasal mucosa and the involvement of transporters were not evaluated, however.

Ponto et al. studied the distribution of the $^{18}$F form of alovudine (**FLT**) into the brain after intranasal administration in rats [102, 103]. In this study, PET was used to quantitatively image the distribution of FLT over time, and computed tomography (**CT**) was used to co-localize anatomical landmarks with the PET analysis. A higher concentration of FLT was observed in the brain, especially in the olfactory bulb, after intranasal administration compared to intravenous administration [102, 103]. This indicated that FLT was preferentially transported to the brain from the nasal cavity. In addition, the intranasal co-administration of NBMPR decreased the concentration of FLT in the olfactory bulb, which appears to be a result from the inhibition of ENT1 uptake activity in the nasal mucosa. Interestingly, the concentration of FLT in the olfactory bulb increased when NBMPR was administered systemically. Moreover, FLT concentrations in other brain areas increased when NBMPR was co-administered with FLT, regardless the route of administration. This suggests the reduced FLT clearance from the brain was caused by NBMPR inhibitory effects on ENT1 at other tissue sites and underscores the unique role the nasal uptake pathway played in the transport of alovudine into the olfactory bulb and the surrounding tissue regions[102].

Since alovudine can only minimally cross the blood brain barrier [100, 101], the nasal route could be considered as potential route to deliver alovudine directly to the brain. *In vivo* studies showed that alovudine can access to the brain directly after intranasal administration and demonstrated that nucleoside transporters, namely ENT1, contributed to alovudine disposition in the brain. The *in vitro* studies demonstrated the involvement of nucleoside transporters in the transport of alovudine across the nasal mucosa. Furthermore, the expression of the nucleoside transporters and their localization in the epithelial cells of the nasal mucosal presented in the previous chapters helped to establish their likely role in the transport behavior of alovudine.

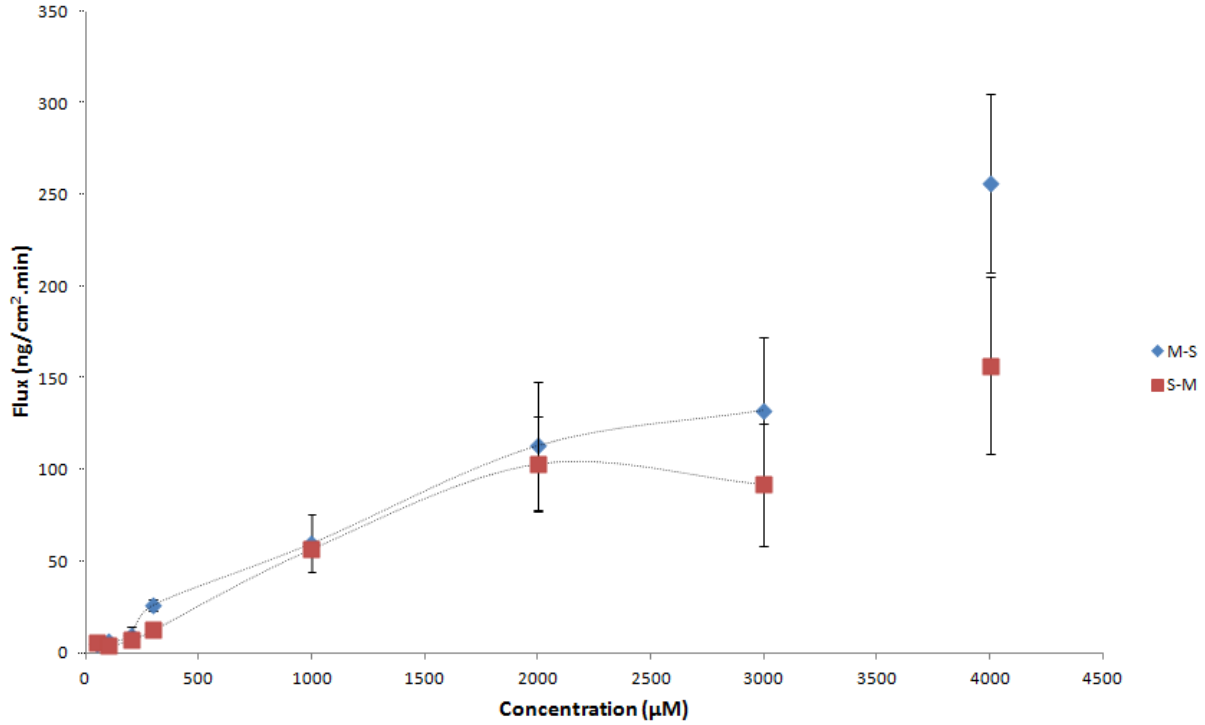


Figure 5.8: Flux of alovudine in the mucosal to submucosal (M-S) and submucosal to mucosal (S-M) directions across the bovine respiratory mucosa as a function of the alovudine concentration in the donor compartment (n=3). The curve indicates a non-linear increase in flux. Error bars indicate the standard deviation and at 300 µM the flux was statistically different between M-S and S-M ($p \leq 0.05$).

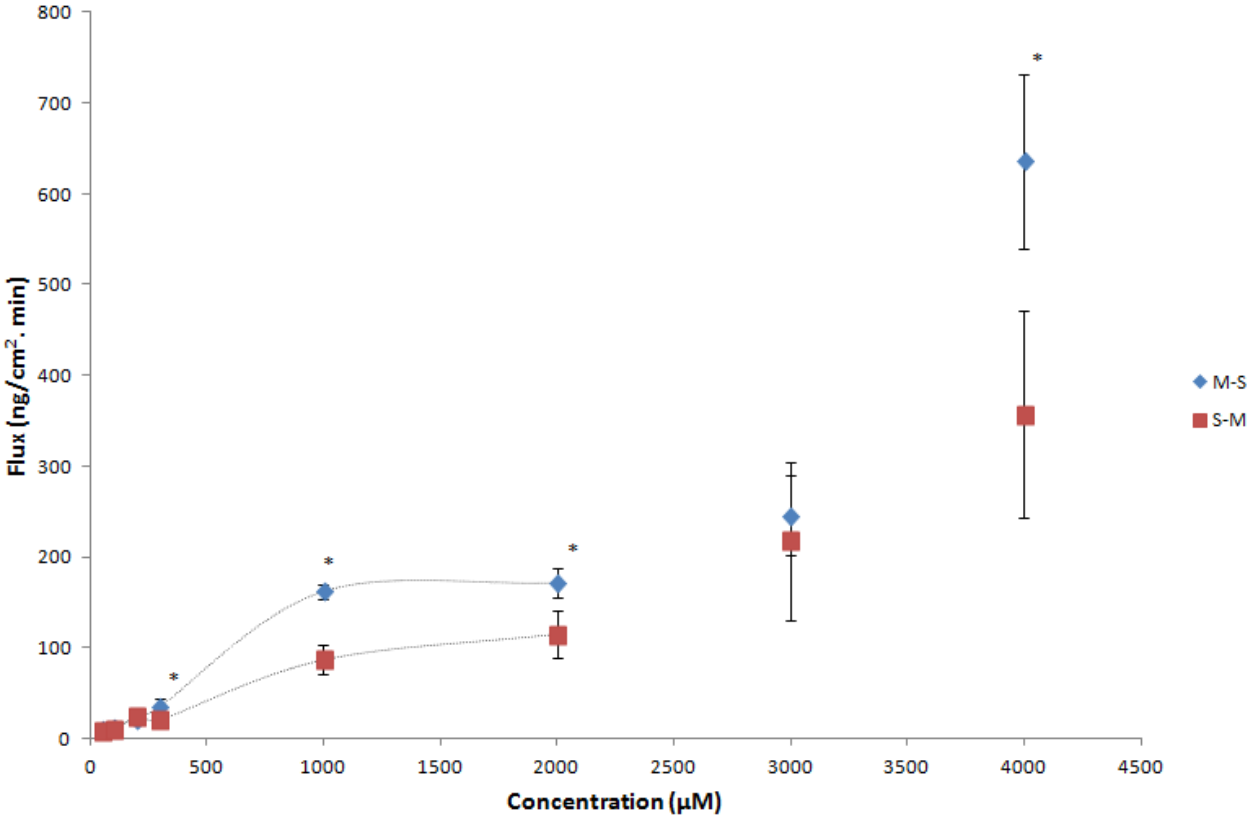


Figure 5.9: Flux of alovudine in the mucosal to submucosal (M-S) and submucosal to mucosal (S-M)) directions across the bovine olfactory mucosa as a function of the alovudine concentration in the donor compartment (n=3). The curve indicates a non-linear increase in flux. Error bars indicate the standard deviation and *indicates statistically significant difference between M-S and S-M flux values ($p \leq 0.05$).

Table 5.2**:** Flux values (mean and standard deviation, n=3) of alovudine in the mucosal to submucosal (M-S) and submucosal to mucosal (S-M) directions across the bovine respiratory and olfactory mucosa at different alovudine concentrations in the donor compartment.

| Concentration (μM) | Respiratory | | | | Olfactory | | | |
|---|---|---|---|---|---|---|---|---|
| | M-S | | S-M | | M-S | | S-M | |
| | Flux ng/cm².min | SD | Flux ng/cm².min | SD | Flux ng/cm².min | SD | Flux ng/cm².min | SD |
| 50 | 4.68 | 1.05 | 5.70 | 3.28 | 9.95 | 0.44 | 8.57 | 2.23 |
| 100 | 6.29 | 0.99 | 4.29 | 2.22 | 11.79 | 0.90 | 10.29 | 1.73 |
| 200 | 9.58 | 5.00 | 6.97 | 2.95 | 21.35 | 3.29 | 24.47 | 2.72 |
| 300 | 26.17 | 3.02 | 12.54 | 2.42 | 34.83 | 8.50 | 21.46 | 0.98 |
| 1000 | 59.69 | 15.81 | 56.65 | 0.22 | 162.27 | 8.20 | 86.73 | 16.19 |
| 2000 | 113.05 | 35.03 | 103.08 | 25.58 | 171.65 | 16.59 | 114.54 | 25.63 |
| 3000 | 132.40 | 39.77 | 91.92 | 33.44 | 245.59 | 43.81 | 217.27 | 86.31 |
| 4000 | 256.36 | 48.66 | 156.6 | 48.31 | 635.92 | 96.46 | 356.92 | 113.72 |

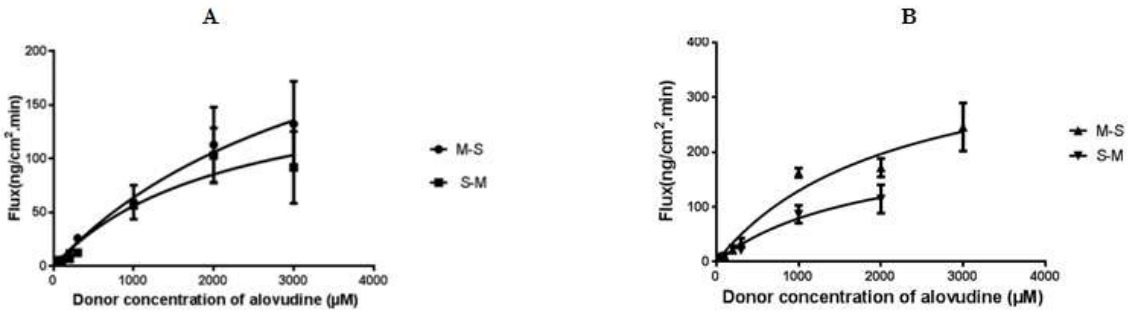


| Best-fit values | M-S | S-M |
|---|---|---|
| $V_{max}$ (ng/cm².min) | 309.0 | 179.1 |
| $K_m$ (µM) | 3830 | 2191 |
| $r^2$ | 0.9924 | 0.9462 |

| Best-fit values | M-S | S-M |
|---|---|---|
| $V_{max}$ (ng/cm².min) | 407.2 | 224.9 |
| $K_m$ (µM) | 2146 | 1836 |
| $r^2$ | 0.9608 | 0.9822 |

Figure 5.10**:** Alovudine transport in the mucosal to submucosal (M-S) and submucosal to mucosal (S-M) directions across the bovine respiratory (**A**) and olfactory (**B**) mucosa. Curves represent the best fit of the Michaelis-Menten equation to the data.

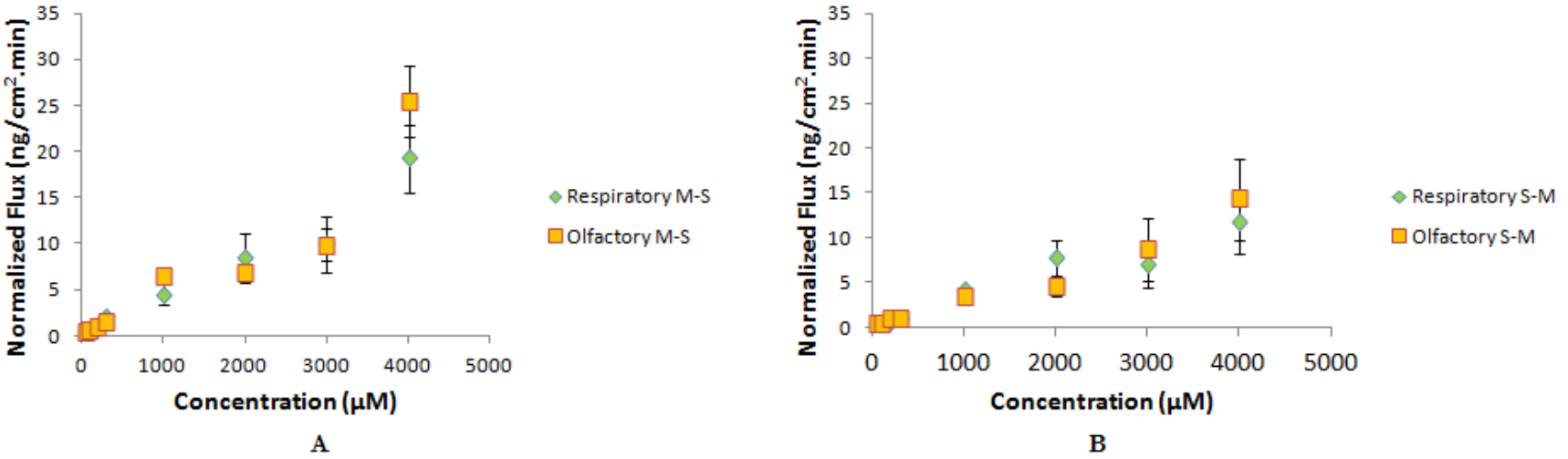


Figure 5.11: Comparative plot for alovudine flux through bovine respiratory and olfactory mucosa in the (**A**) mucosal to submucosal (M-S) and (**B**) submucosal to mucosal (S-M) directions after normalization of the flux to tissue thickness value of 1 cm (n=3).The error bars indicate the standard deviation .In A, at 1000 μM the flux was statistically different between respiratory and olfactory while in B at 200 μM the flux was statistically different between respiratory and olfactory ($p \leq 0.05$).

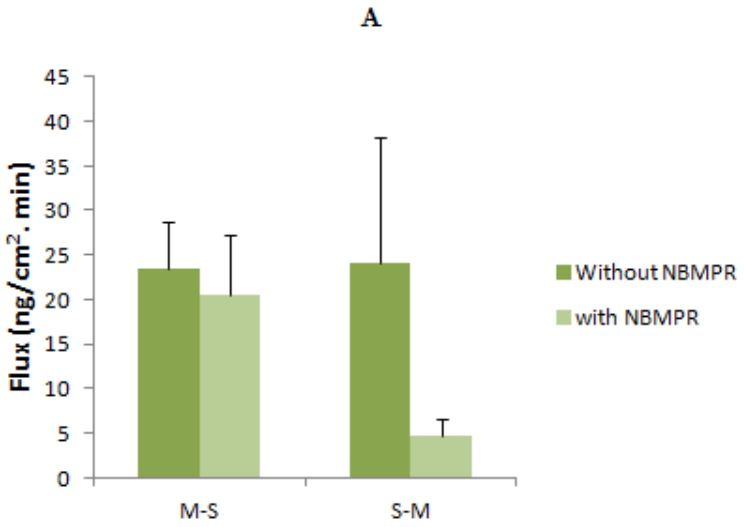


| | Without NBMPR | | With NBMPR | |
|---|---|---|---|---|
| | Avg | SD | Avg | SD |
| M-S | 23.48 | 5.2 | 20.59 | 6.7 |
| S-M | 24.15 | 14.01 | 4.7 | 1.8 |

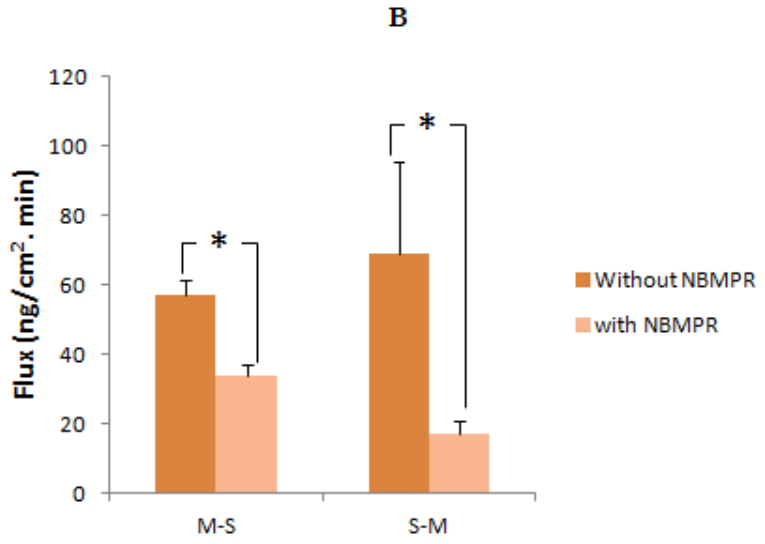


| | Without NBMPR | | With NBMPR | |
|---|---|---|---|---|
| | Avg | SD | Avg | SD |
| M-S | 57.32 | 4.06 | 33.77 | 3.14 |
| S-M | 69.15 | 26.52 | 16.80 | 4.04 |

Figure 5.12**:** Mean flux value (n=3) for alovudine through bovine respiratory (**A**) and olfactory (**B**) tissue at a500μM donor concentration in the presence and absence of 200 nM NBMPR, an ENT1 inhibitor. Error bars indicate the standard deviation and *indicates statistically significant difference ($p \leq 0.05$).

# CHAPTER 6

## SUMMARY

The nasal mucosa is an interesting drug administration site not only for systemic delivery of drugs but also for targeting to the CNS. Delivering drugs by the nasal route offers several advantages, including being painless, non-invasive, providing rapid drug absorption with quick onset of action and enhanced bioavailability by avoiding gastrointestinal and hepatic first-pass metabolism.

The two regions of the nasal cavity that are of most interest in drug absorption are the respiratory and olfactory regions. The respiratory epithelium, which consists primarily of pseudostratified columnar cells, covers the largest portion of the nasal cavity and is highly vascularized. This region is considered to be the main site of the nasal cavity for systemic absorption. The olfactory epithelium, which also consists of pseudostratified columnar cells, is also populated with olfactory nerves. The proximity of the olfactory region to the CNS makes it potential for direct drug transport to the CNS.

Mechanistic understanding of the factors which governs drug transport across the nasal mucosa, such as the role of transporters, is important in predicting drug absorption. Transporters are proteins that span cellular membranes and are responsible for the uptake and efflux of crucial compounds and drugs into and/or out the cells. The transporters of greatest current interest in drug absorption include: nucleoside transporters (ENT 1-2) and (CNT 1-3); organic cationic transporters (OCT 1-3) and (OCTN 1-2); organic anionic transporters (OAT 1-3) and (OATP 1-4); peptide transporters (PEPT 1-2); monocarboxylate transporters (MCT1-4) and (sMCT1-2); and large neutral amino acid transporters (LAT 1-2). These transporters all belong to the SLC transporter family. Efflux transporters from the

ABC family also play a major role in drug disposition. This family includes the multidrug resistance protein (MDR1), multidrug resistance proteins (MRP1-9), and breast cancer resistance protein (BCRP).

The presence of drug transporters in the nasal mucosa was determined by examining their gene expression. DNA microarray is among the most widely used methods of expression profiling of genes because it offers the advantage of analyzing a large number of genes in parallel. In addition, RT-PCR is a complementary technology for microarray that enables verification of gene expression and analysis of the most informative genes identified by microarray in more precise way.

Microarray analysis was used to compare the gene expression of transporters among human and animal models. Information regarding the expression of transporters in the nasal mucosa of humans and animal models can assist in the correct selection of model systems when the drug under investigation is a transporter substrate. In addition, interspecies differences in the level of expression of drug transporters should be considered when translating information obtained from animal models to humans.

After identifying the transporters that are expressed in the nasal mucosa, determining the cellular location of these nucleoside transporters is essential to evaluate their contribution in the permeation of a drug substrate through the nasal mucosa. Transporters can be found within the epithelial cells or in the lamina propria region of the nasal mucosa. Transporters found on the surfaces of the epithelial cells contribute the most to drug uptake following nasal administration.

If the nasal route is considered as a potential drug delivery site, it is important to understand the substrate behavior of drug compounds of interest. Knowledge of transporter

expression can help in understanding the permeation behavior of a drug substrate across its nasal mucosa and the subsequent systemic absorption and/or CNS targeting.

For example, alovudine is an anti-viral nucleoside–like drug that was reported to be a substrate for nucleoside transporters. Because alovudine can minimally cross the blood brain barrier, the nasal route was considered as a potential route to deliver alovudine directly to the brain. *In vitro* transporter studies demonstrated the involvement of nucleoside transporters in the permeation of alovudine across the nasal mucosa. In addition, *in vivo* studies showed that alovudine can access to the brain directly after intranasal administration and nucleoside transporters, namely ENT1, contributed to alovudine disposition in the brain. Finally, the expression of the nucleoside transporters and their localization in the epithelial cells of the nasal mucosal helped in assessing the transport behavior of alovudine.

# APPENDIX A

## GEL IMAGES FOR RCR PRODUCTS

Table A.1: RT-PCR performed at annealing temperature of 62℃.

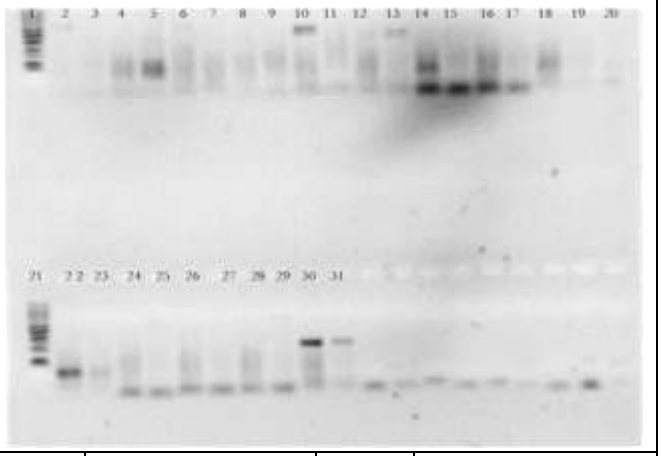

| | | | |
|---|---|---|---|
| 1 | Leader | 20 | -- |
| 2 | Resp-ENT1 | 21 | Leader |
| 3 | Olf-ENT1 | 22 | Resp-MRP5 |
| 4 | Resp-ENT2 | 23 | Olf-MRP5 |
| 5 | Olf ENT2 | 24 | Resp-BCRP |
| 6 | Resp-CNT1 | 25 | Olf EBCRP |
| 7 | Olf-CNT 1 | 26 | Resp-OCT3 |
| 8 | Resp-CNT2 | 27 | Olf-OCT3 |
| 9 | Olf-CNT2 | 28 | Resp-PEPT2 |
| 10 | Resp-CNT3 | 29 | Olf-PEPT2 |
| 11 | Olf-CNT3 | 30 | Resp-PEPT1 |
| 12 | Resp -MRP1 | 31 | Olf-PEPT1 |
| 13 | Olf- MRP1 | | |
| 14 | Resp-MRP2 | | |
| 15 | Old-MRP2 | | |
| 16 | Resp-MRP3 | | |
| 17 | Olf- MRP3 | | |
| 18 | Resp-MRP4 | | |
| 19 | Old-MRP4 | | |

Table A.2 : RT-PCR (trial 1 1) performed at annealing temperature of 55℃.

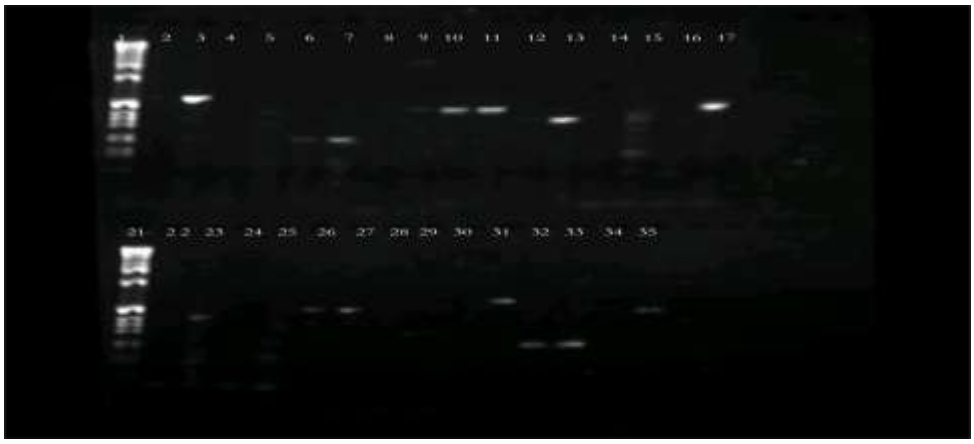

| | | | |
|---|---|---|---|
| 1 | Leader | 21 | Leader |
| 2 | Resp-ENT1 | 22 | Resp-MRP4 |
| 3 | Olf-ENT1 | 23 | Old-MRP4 |
| 4 | Resp-ENT2 | 24 | Resp-MRP5 |
| 5 | Olf ENT2 | 25 | Olf-MRP5 |
| 6 | Resp-CNT1 | 26 | Resp-BCRP |
| 7 | Olf-CNT 1 | 27 | Olf BCRP |
| 8 | Resp-CNT2 | 28 | Resp-OCT3 |
| 9 | Olf-CNT2 | 29 | Olf-OCT3 |
| 10 | Resp-CNT3 | 30 | Resp-PEPT2 |
| 11 | Olf-CNT3 | 31 | Olf-PEPT2 |
| 12 | Resp -MRP1 | 32 | Resp-PEPT1 |
| 13 | Olf- MRP1 | 33 | Olf-PEPT1 |
| 14 | Resp-MRP2 | | |
| 15 | Old-MRP2 | | |
| 16 | Resp-MRP3 | | |
| 17 | Olf- MRP3 | | |
| 18 | -- | | |
| 19 | -- | | |
| 20 | -- | | |

Table A..3: RT-PCR (trial 2) performed at annealing temperature of 55℃.

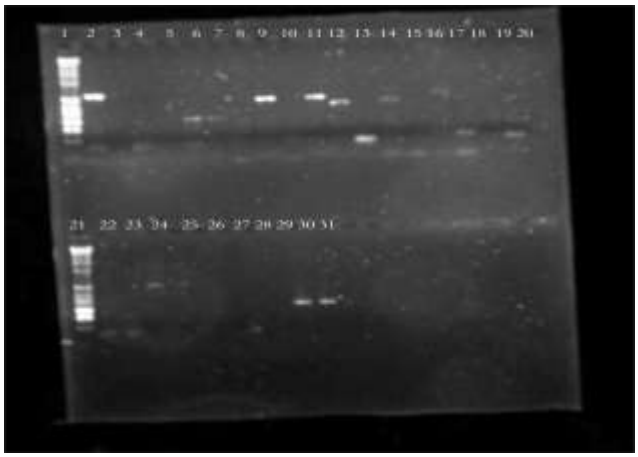

| | | | |
|---|---|---|---|
| 1 | Leader | 21 | Leader |
| 2 | Resp-ENT1 | 22 | Resp-MRP5 |
| 3 | Olf-ENT1 | 23 | Olf-MRP5 |
| 4 | Resp-ENT2 | 24 | Resp-BCRP |
| 5 | Olf ENT2 | 25 | Olf -BCRP |
| 6 | Resp-CNT1 | 26 | Resp-OCT3 |
| 7 | Olf-CNT 1 | 27 | Olf-OCT3 |
| 8 | Resp-CNT2 | 28 | Resp-PEPT1 |
| 9 | Resp-CNT3 | 29 | Olf-PEPT1 |
| 10 | Olf-CNT2 | 30 | Resp-PEPT2 |
| 11 | Olf-CNT3 | 31 | Olf-PEPT2 |
| 12 | Resp -MRP1 | | |
| 13 | Olf- MRP1 | | |
| 14 | Resp-MRP2 | | |
| 15 | Old-MRP2 | | |
| 16 | Resp-MRP3 | | |
| 17 | Olf- MRP3 | | |
| 18 | Resp-MRP4 | | |
| 19 | Olf-MRP4 | | |
| 20 | -- | | |

Table A.4: RT-PCR performed at annealing temperature of 58℃.

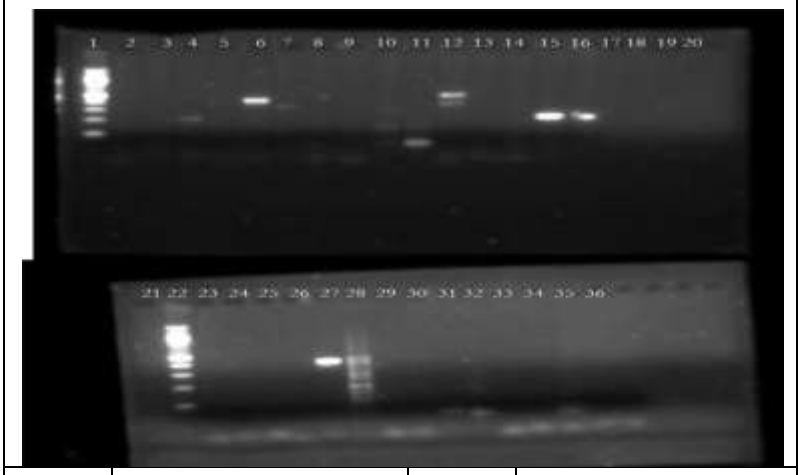

| | | | |
|---|---|---|---|
| 1 | Leader | 20 | -- |
| 2 | Resp-ENT1 | 21 | Leader |
| 3 | Resp-ENT2 | 22 | Olf-ENT1 |
| 4 | Resp-CNT1 | 23 | Olf ENT2 |
| 5 | Resp-CNT2 | 24 | Olf-CNT 1 |
| 6 | Resp-CNT3 | 25 | Olf-CNT2 |
| 7 | Resp -MRP1 | 26 | Olf-CNT3 |
| 8 | Resp-MRP2 | 27 | Olf- MRP1 |
| 9 | Resp-MRP3 | 28 | Olf-MRP2 |
| 10 | Resp-MRP4 | 29 | Olf- MRP3 |
| 11 | Resp-MRP5 | 30 | Olf-MRP4 |
| 12 | Resp-BCRP | 31 | Olf-MRP5 |
| 13 | Resp-OCT3 | 32 | Olf BCRP |
| 14 | Resp-PEPT1 | 33 | Olf-OCT3 |
| 15 | Resp-PEPT2 | 34 | Olf-PEPT1 |
| 16 | Resp-GAPDH | 35 | Olf-PEPT2 |
| 17 | -- | 36 | Olf-GAPDH |
| 18 | -- | | |
| 19 | -- | | |
| 20 | -- | | |

Table A.5: RT-PCR performed at annealing temperatures of 55 and 58℃.

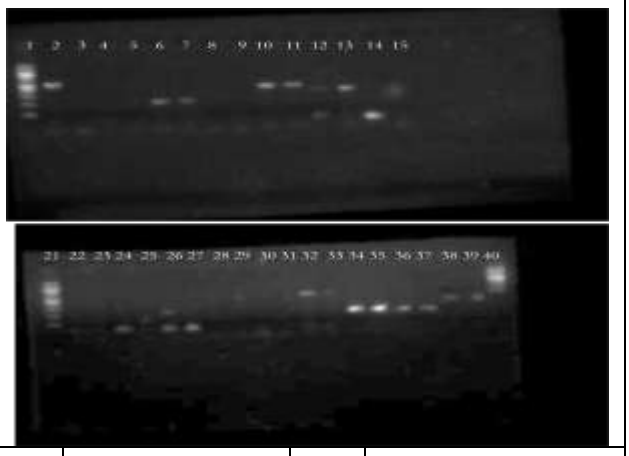

| | | | |
|---|---|---|---|
| 1 | Leader | 21 | Leader |
| 2 | Resp-ENT1 (55) | 22 | Resp-MRP3(55) |
| 3 | Olf-ENT1(55) | 23 | Olf- MRP3(55) |
| 4 | Resp-ENT2(55) | 24 | Resp-MRP4(55) |
| 5 | Olf ENT2(55) | 25 | Olf-MRP4(55) |
| 6 | Resp-CNT1(55) | 26 | Resp-MRP5(58) |
| 7 | Olf-CNT 1(55) | 27 | Olf-MRP5(58) |
| 8 | Resp-CNT2(55) | 28 | Resp-BCRP(55) |
| 9 | Resp-CNT3(55) | 29 | Olf -BCRP(55) |
| 10 | Olf-CNT2(55) | 30 | Resp-OCT3(55) |
| 11 | Olf-CNT3(55) | 31 | Olf-OCT3(55) |
| 12 | Resp -MRP1(55) | 32 | Resp-PEPT1(58) |
| 13 | Olf- MRP1(55) | 33 | Olf-PEPT1(58) |
| 14 | Resp-MRP2 (58) | 34 | Resp-PEPT2(58) |
| 15 | Olf-MRP2(58) | 35 | Olf-PEPT2(58) |
| 16 | -- | 36 | Resp-GAPDH(58) |
| 17 | -- | 37 | Olf-GAPDH(58) |
| 18 | -- | 38 | |
| 19 | -- | 39 | |
| 20 | -- | 40 | |

Table A.6: RT-PCR performed at annealing temperature of 55 C.

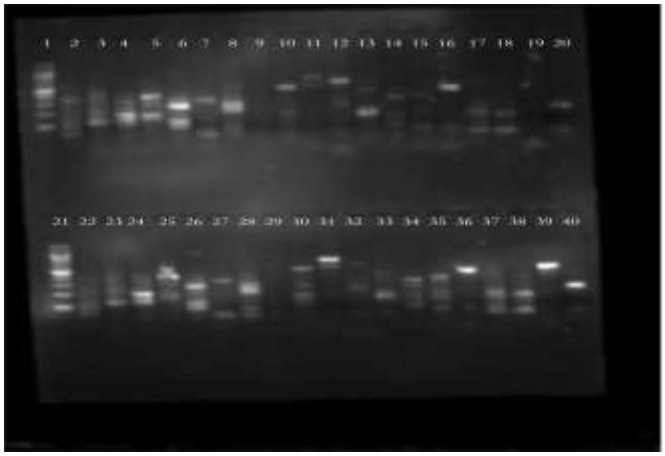

| | | | |
|---|---|---|---|
| 1 | Leader | 21 | Leader |
| 2 | Resp-MCT1 | 22 | Olf-MCT1 |
| 3 | Resp-MCT2 | 23 | Olf -MCT2 |
| 4 | Resp-MCT3 | 24 | Olf-MCT3 |
| 5 | Resp-MCT4 | 25 | Olf-MCT4 |
| 6 | Resp-sMCT1 | 26 | Olf-sMCT1 |
| 7 | Resp-sMCT2 | 27 | Olf -sMCT2 |
| 8 | Resp- y+LAT1 | 28 | Olf- y+LAT1 |
| 9 | Resp- LAT2 | 29 | Olf- LAT2 |
| 10 | Resp- $b^{0+}$ AT | 30 | Olf- $b^{0+}$ AT |
| 11 | Resp- Asc-1 | 31 | Olf- Asc-1 |
| 12 | Resp-xCT | 32 | Olf-xCT |
| 13 | Resp-MDR1 | 33 | Olf-MDR1 |
| 14 | Resp -MRP1 | 34 | Olf -MRP1 |
| 15 | Resp-MRP2 | 35 | Olf-MRP2 |
| 16 | Resp-MRP3 | 36 | Olf-MRP3 |
| 17 | Resp-MRP4 | 37 | Olf-MRP4 |
| 18 | Resp-MRP5 | 38 | Olf-MRP5 |
| 19 | Resp-BCRP | 39 | Olf-BCRP |
| 20 | Resp-GAPDH | 40 | Olf-GAPDH |

Table A.7: RT-PCR performed at annealing temperature of 55 ℃.

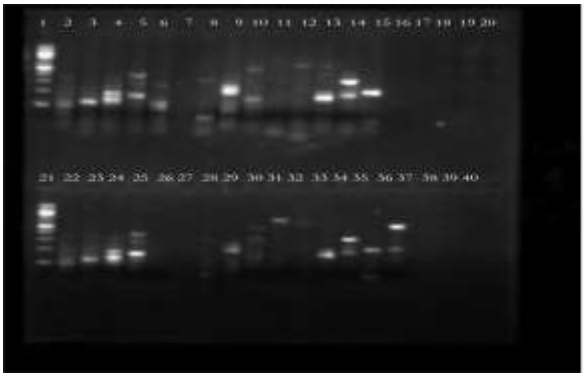

| | | | |
|---|---|---|---|
| 1 | Leader | 21 | Leader |
| 2 | Resp-MCT1 | 22 | Olf-MCT1 |
| 3 | Resp-MCT2 | 23 | Olf -MCT2 |
| 4 | Resp-MCT3 | 24 | Olf-MCT3 |
| 5 | Resp-MCT4 | 25 | Olf-MCT4 |
| 6 | Resp-sMCT1 | 26 | Olf-sMCT1 |
| 7 | -- | 27 | -- |
| 8 | Resp-sMCT2 | 28 | Olf -sMCT2 |
| 9 | Resp- y+LAT1 | 29 | Olf- y+LAT1 |
| 10 | Resp- $b^{0+}AT$ | 30 | Olf- $b^{0+}AT$ |
| 11 | Resp- Asc-1 | 31 | Olf- Asc-1 |
| 12 | Resp-xCT | 32 | Olf-xCT |
| 13 | Resp-MDR1 | 33 | Olf-MDR1 |
| 14 | Resp- LAT1 | 34 | Olf –LAT1 |
| 15 | -- | 35 | Olf-ENT1 |
| 16 | -- | | |
| 17 | -- | | |
| 18 | -- | | |
| 19 | -- | | |
| 20 | -- | | |

Table A.8: RT-PCR performed at annealing temperature of 55 ℃.

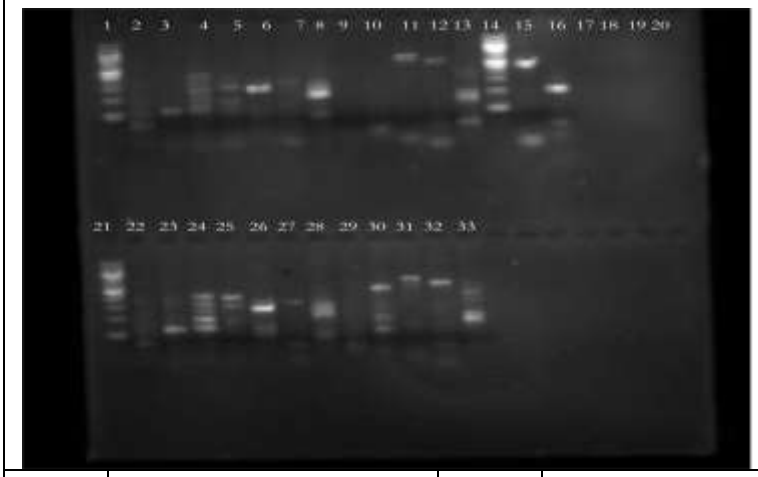


| | | | |
|---|---|---|---|
| 1 | Leader | 21 | Leader |
| 2 | Resp-MCT1 | 22 | Olf-MCT1 |
| 3 | Resp-MCT2 | 23 | Olf -MCT2 |
| 4 | Resp-MCT3 | 24 | Olf-MCT3 |
| 5 | Resp-MCT4 | 25 | Olf-MCT4 |
| 6 | Resp-sMCT1 | 26 | Olf-sMCT1 |
| 7 | Resp-sMCT2 | 27 | Olf -sMCT2 |
| 8 | Resp- y+LAT1 | 28 | Olf- y+LAT1 |
| 9 | Resp- LAT2 | 29 | Olf- LAT2 |
| 10 | Resp- $b^{0+}AT$ | 30 | Olf- $b^{0+}AT$ |
| 11 | Resp- Asc-1 | 31 | Olf- Asc-1 |
| 12 | Resp-xCT | 32 | Olf-xCT |
| 13 | Resp-MDR1 | 33 | Olf-MDR1 |
| 14 | Leader | | |
| 15 | Resp-BCRP (55) | | |
| 16 | Resp-GAPDH (55) | | |
| 17 | -- | | |
| 18 | -- | | |
| 19 | -- | | |
| 20 | -- | | |

# APPENDIX B

## CONDITIONS SET FOR PRIMER DESIGN

Table B.1: Conditions set for primer design using Primer3-web 0.4.0 software for *Bos taurus* sequences of ENT1 (SLC29A1) and CNT3 (SLC28A3)

| | |
|---|---|
| NCBI reference sequence | ENT1: BC102846.1<br>CNT3: NM_001192167.1 |
| Primer Size | Minimum : 20 Optimum: 21 |
| Primer melting temperature | Minimum : 57 Optimum: 60<br>Maximum:63 |
| Primer GC% | Minimum : 40 Optimum: 50<br>Maximum:60 |
| Maximum self complementarity | 8 |
| Maximum 3'self complementarity | 3 |

# APPENDIX C

## PARAFFIN PROCESSING FOR BRIGHT FIELD IMAGING

Table C.1: Paraffin processing procedure

| Station | Time | Solution | Temperature | Vacuum | Pressure |
|---|---|---|---|---|---|
| 1 | 6 hrs | Zn-Formalin | Room temperature | 15 | 7 |
| 2 | 6 hrs | Pen-Fix | Room temperature | 15 | 7 |
| 3 | 20 min | 80% Ethanol | Room temperature | 15 | 7 |
| 4 | 20 min | 95% Ethanol | Room temperature | 15 | 7 |
| 5 | 20 min | 95% Ethanol | Room temperature | 15 | 7 |
| 6 | 20 min | 100% Ethanol | Room temperature | 15 | 7 |
| 7 | 20 min | 100% Ethanol | Room temperature | 15 | 7 |
| 8 | 20 min | Pro-Par (Xylene Substitute) | Room temperature | 15 | 7 |
| 9 | 30 min | Pro-Par | Room temperature | 15 | 7 |
| 10 | 30 min | Pro-Par | Room temperature | | 7 |
| 11 | 30 min | Em-400 Embedding Media Paraffin | 60℃ | 15 | 7 |
| 12 | 1 hr | Em-400 Embedding Media Paraffin | 60℃ | 15 | 7 |
| 13 | 30 min | Em-400 Embedding Media Paraffin | 60℃ | 15 | 7 |

Table C.2: Station components

| Station 1 | Station 2 | Station 3 | Station 4 | Station 5 | Station 6 | Station21 |
|---|---|---|---|---|---|---|
| Xylene | Xylene | Xylene | 100% ethanol | 100% ethanol | 95% ethanol | Wash |
| Station 7 | Station 8 | Station 9 | Station 10 | Station 11 | Station 12 | Station 20 |
| 70% ethanol | Hematoxyline | Acid alcohol | 80% ethanol | Working eosin | 95% ethanol | Wash |
| Station 13 | Station 14 | Station 15 | Station 16 | Station 17 | Station 18 | Station 19 |
| 100% ethanol | 100% ethanol | 100% ethanol | Xylene | Xylene | Xylene | Scott's tap water |

Table C.3: Solutions used for staining

| Solution | Components |
|---|---|
| Stock eosin | Eosin 2 g<br>Double distilled water to 200 mL |
| Pholoxine | Phloxine B 1 g<br>Double distilled water to 100 mL |
| Working eosin | Stock eosin 122 mL<br>Phloxine 12 mL<br>Glacial acetic acid 8 mL<br>95% ethanol up to 1 L |
| Acid alcohol | 95% ethanol 675 mL<br>Hydrochloric acid (37%) 25 mL |
| Scott's tap water | Sodium bicarbonate 2 g<br>Magnesium sulfate anhydrous 20 g<br>Tap water 1000 mL |

Table C.4: Staining procedure

| Station Number | Time |
|---|---|
| 1 | 3min |
| 2 | 3min |
| 3 | 3min |
| 4 | 3min |
| 5 | 3min |
| 6 | 1min |
| 7 | 1min |
| 21 | 2min |
| 8 | 6min |
| 20 | 1min |
| 9 | 5sec |
| 21 | 3min |
| 19 | 30sec |
| 20 | 10sec |
| 10 | 5sec |
| 11 | 1min |
| 12 | 1min |
| 13 | 1min |
| 14 | 1min |
| 15 | 1min |
| 16 | 1min |
| 17 | 1min |
| 18 | 1min |

# APPENDIX D

## DNA SEQUENCING

The sequencing of PCR-generated DNA is performed by the use of the dye-terminator chemistry. Dye-terminator chemistry permits the use of standard oligonucleotide primers, "Universal" primers or the primers used in PCR, which are complementary to one of the strands of the DNA template. The sequencing is an amplification of the single strand DNA in the presence of dNTPs and a small portion of fluorescently labeled dideoxynucleotides. Dideoxynucleotides lack a 3' hydroxyl group, thus cannot form phosphodiester bonds at the 3' carbon atom, thereby causing termination of chain synthesis. Similar to dNTPs, four types of dideoxynucleotides are used but they are labeled with different fluorophores. As a result, a collection of labeled DNA fragments of different sizes are produced that can be separated electrophoretically followed by fluorescence detection.

For the DNA sequencing of the PCR products of our study, 1 μL containing about 10 ng of the amplified products was diluted with 9.5 μL DNase RNase free water and 0.5 μL of the sense or antisense primer (10 pmole) was added. The DNA sequencing was automated and BigDye® Terminator Cycle Sequencing Kit (Applied Biosystems, Life Technologies, Carlsbad, CA) was used [111].

# APPENDIX E

## AMINO ACID ALIGNMENTS OF HUMAN ENT1AND CNT3 AGAINST COWS

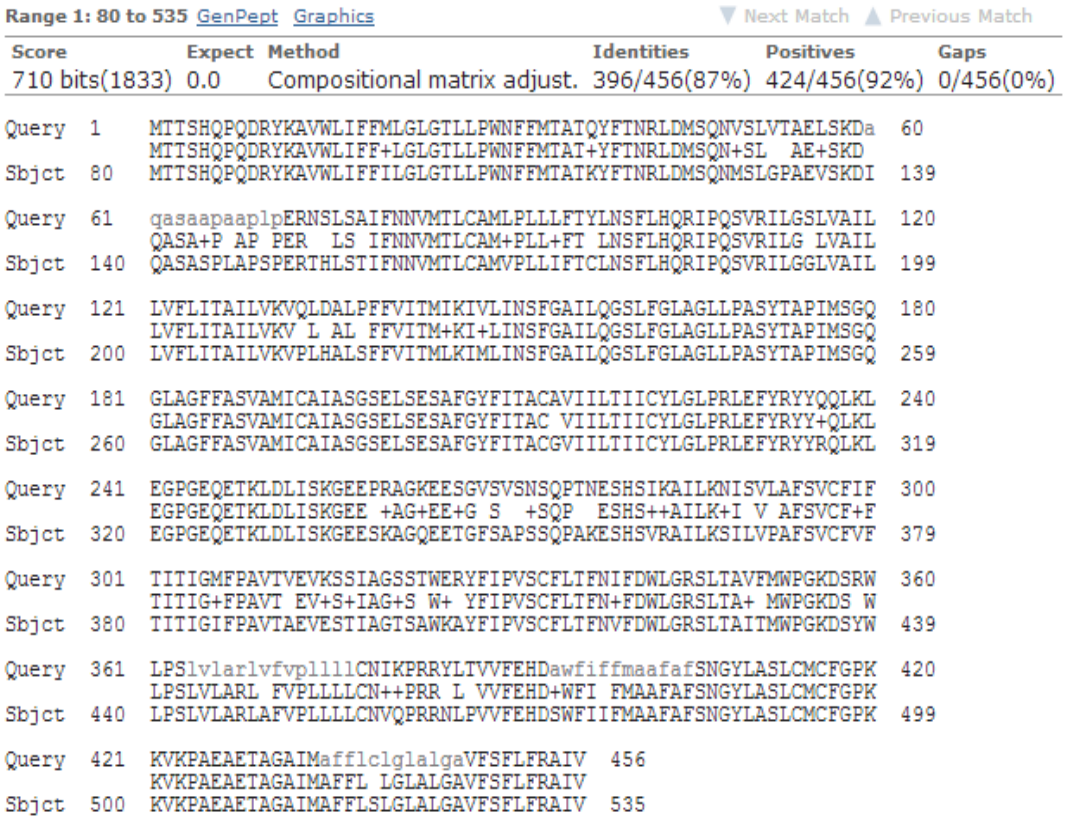

**Range 1: 80 to 535** GenPept Graphics ▼ Next Match ▲ Previous Match

| Score | Expect | Method | Identities | Positives | Gaps |
|---|---|---|---|---|---|
| 710 bits(1833) | 0.0 | Compositional matrix adjust. | 396/456(87%) | 424/456(92%) | 0/456(0%) |

```
Query  1    MTTSHQPQDRYKAVWLIFFMLGLGTLLPWNFFMTATQYFTNRLDMSQNVSLVTAELSKDa  60
            MTTSHQPQDRYKAVWLIFF+LGLGTLLPWNFFMTAT+YFTNRLDMSQN+SL  AE+SKD
Sbjct  80   MTTSHQPQDRYKAVWLIFFILGLGTLLPWNFFMTATKYFTNRLDMSQNMSLGPAEVSKDI  139

Query  61   qasaapaaplpERNSLSAIFNNVMTLCAMLPLLLFTYLNSFLHQRIPQSVRILGSLVAIL  120
            QASA+P AP PER  LS IFNNVMTLCAM+PLL+FT LNSFLHQRIPQSVRILG LVAIL
Sbjct  140  QASASPLAPSPERTHLSTIFNNVMTLCAMVPLLIFTCLNSFLHQRIPQSVRILGGLVAIL  199

Query  121  LVFLITAILVKVQLDALPFFVITMIKIVLINSFGAILQGSLFGLAGLLPASYTAPIMSGQ  180
            LVFLITAILVKV L AL FFVITM+KI+LINSFGAILQGSLFGLAGLLPASYTAPIMSGQ
Sbjct  200  LVFLITAILVKVPLHALSFFVITMLKIMLINSFGAILQGSLFGLAGLLPASYTAPIMSGQ  259

Query  181  GLAGFFASVAMICAIASGSELSESAFGYFITACAVIILTIICYLGLPRLEFYRYYQQLKL  240
            GLAGFFASVAMICAIASGSELSESAFGYFITAC VIILTIICYLGLPRLEFYRYY+QLKL
Sbjct  260  GLAGFFASVAMICAIASGSELSESAFGYFITACGVIILTIICYLGLPRLEFYRYYRQLKL  319

Query  241  EGPGEQETKLDLISKGEEPRAGKEESGVSVSNSQPTNESHSIKAILKNISVLAFSVCFIF  300
            EGPGEQETKLDLISKGEE +AG+EE+G S  +SQP  ESHS++AILK+I V AFSVCF+F
Sbjct  320  EGPGEQETKLDLISKGEESKAGQEETGFSAPSSQPAKESHSVRAILKSILVPAFSVCFVF  379

Query  301  TITIGMFPAVTVEVKSSIAGSSTWERYFIPVSCFLTFNIFDWLGRSLTAVFMWPGKDSRW  360
            TITIG+FPAVT EV+S+IAG+S W+ YFIPVSCFLTFN+FDWLGRSLTA+ MWPGKDS W
Sbjct  380  TITIGIFPAVTAEVESTIAGTSAWKAYFIPVSCFLTFNVFDWLGRSLTAITMWPGKDSYW  439

Query  361  LPSlvlarlvfvpllllCNIKPRRYLTVVFEHDawfiffmaafafSNGYLASLCMCFGPK  420
            LPSLVLARL FVPLLLLCN++PRR L VVFEHD+WFI FMAAFAFSNGYLASLCMCFGPK
Sbjct  440  LPSLVLARLAFVPLLLLCNVQPRRNLPVVFEHDSWFIIFMAAFAFSNGYLASLCMCFGPK  499

Query  421  KVKPAEAETAGAIMafflclglalgaVFSFLFRAIV  456
            KVKPAEAETAGAIMAFFL LGLALGAVFSFLFRAIV
Sbjct  500  KVKPAEAETAGAIMAFFLSLGLALGAVFSFLFRAIV  535
```

Figure E.1: Amino acid alignments of human ENT1 (NP_004946.1) against cows ENT1 (NP_001029570.2) showing 87% identical amino acid sequences.

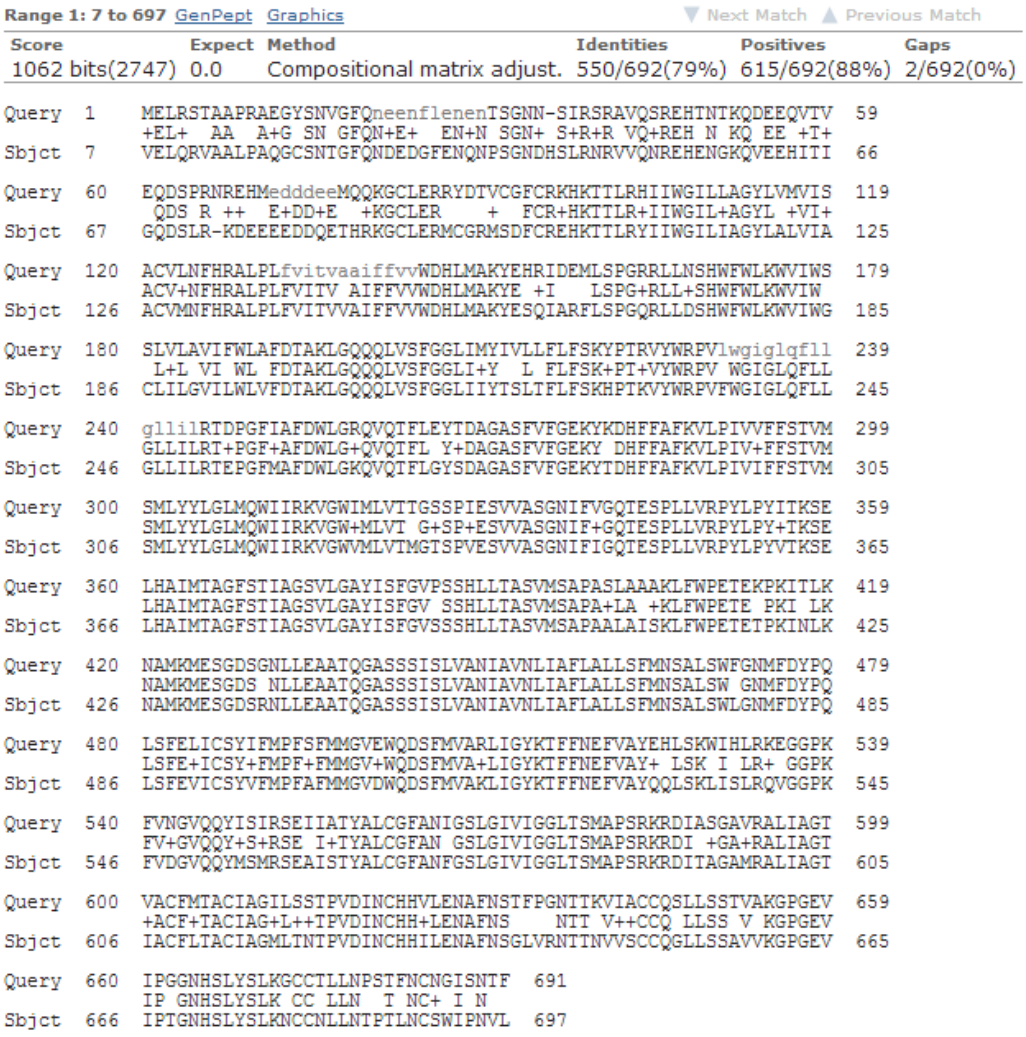

Range 1: 7 to 697 GenPept Graphics Next Match Previous Match

| Score | Expect | Method | Identities | Positives | Gaps |
|---|---|---|---|---|---|
| 1062 bits(2747) | 0.0 | Compositional matrix adjust. | 550/692(79%) | 615/692(88%) | 2/692(0%) |

```
Query  1    MELRSTAAPRAEGYSNVGFQneenflenenTSGNN-SIRSRAVQSREHTNTKQDEEQVTV  59
            +EL+  AA  A+G SN GFQN+E+  EN+N SGN+ S+R+R VQ+REH N KQ EE +T+
Sbjct  7    VELQRVAALPAQGCSNTGFQNDEDGFENQNPSGNDHSLRNRVVQNREHENGKQVEEHITI  66

Query  60   EQDSPRNREHMedddeeMQQKGCLERRYDTVCGFCRKHKTTLRHIIWGILLAGYLVMVIS  119
             QDS R ++  E+DD+E  +KGCLER    +  FCR+HKTTLR+IIWGIL+AGYL +VI+
Sbjct  67   GQDSLR-KDEEEEDDQETHRKGCLERMCGRMSDFCREHKTTLRYIIWGILIAGYLALVIA  125

Query  120  ACVLNFHRALPLfvitvaaiffvvWDHLMAKYEHRIDEMLSPGRRLLNSHWFWLKWVIWS  179
            ACV+NFHRALPLFVITV AIFFVVWDHLMAKYE +I   LSPG+RLL+SHWFWLKWVIW
Sbjct  126  ACVMNFHRALPLFVITVVAIFFVVWDHLMAKYESQIARFLSPGQRLLDSHWFWLKWVIWG  185

Query  180  SLVLAVIFWLAFDTAKLGQQQLVSFGGLIMYIVLLFLFSKYPTRVYWRPVlwgiglqfll  239
             L+L VI WL FDTAKLGQQQLVSFGGLI+Y  L FLFSK+PT+VYWRPV WGIGLQFLL
Sbjct  186  CLILGVILWLVFDTAKLGQQQLVSFGGLIIYTSLTFLFSKHPTKVYWRPVFWGIGLQFLL  245

Query  240  gllilRTDPGFIAFDWLGRQVQTFLEYTDAGASFVFGEKYKDHFFAFKVLPIVVFFSTVM  299
            GLLILRT+PGF+AFDWLG+QVQTFL Y+DAGASFVFGEKY DHFFAFKVLPIV+FFSTVM
Sbjct  246  GLLILRTEPGFMAFDWLGKQVQTFLGYSDAGASFVFGEKYTDHFFAFKVLPIVIFFSTVM  305

Query  300  SMLYYLGLMQWIIRKVGWIMLVTTGSSPIESVVASGNIFVGQTESPLLVRPYLPYITKSE  359
            SMLYYLGLMQWIIRKVGW+MLVT G+SP+ESVVASGNIF+GQTESPLLVRPYLPY+TKSE
Sbjct  306  SMLYYLGLMQWIIRKVGWVMLVTMGTSPVESVVASGNIFIGQTESPLLVRPYLPYVTKSE  365

Query  360  LHAIMTAGFSTIAGSVLGAYISFGVPSSHLLTASVMSAPASLAAAKLFWPETEKPKITLK  419
            LHAIMTAGFSTIAGSVLGAYISFGV SSHLLTASVMSAPA+LA +KLFWPETE PKI LK
Sbjct  366  LHAIMTAGFSTIAGSVLGAYISFGVSSSHLLTASVMSAPAALAISKLFWPETETPKINLK  425

Query  420  NAMKMESGDSGNLLEAATQGASSSISLVANIAVNLIAFLALLSFMNSALSWFGNMFDYPQ  479
            NAMKMESGDS NLLEAATQGASSSISLVANIAVNLIAFLALLSFMNSALSW GNMFDYPQ
Sbjct  426  NAMKMESGDSRNLLEAATQGASSSISLVANIAVNLIAFLALLSFMNSALSWLGNMFDYPQ  485

Query  480  LSFELICSYIFMPFSFMMGVEWQDSFMVARLIGYKTFFNEFVAYEHLSKWIHLRKEGGPK  539
            LSFE+ICSY+FMPF+FMMGV+WQDSFMVA+LIGYKTFFNEFVAY+ LSK I LR+ GGPK
Sbjct  486  LSFEVICSYVFMPFAFMMGVDWQDSFMVAKLIGYKTFFNEFVAYQQLSKLISLRQVGGPK  545

Query  540  FVNGVQQYISIRSEIIATYALCGFANIGSLGIVIGGLTSMAPSRKRDIASGAVRALIAGT  599
            FV+GVQQY+S+RSE I+TYALCGFAN GSLGIVIGGLTSMAPSRKRDI +GA+RALIAGT
Sbjct  546  FVDGVQQYMSMRSEAISTYALCGFANFGSLGIVIGGLTSMAPSRKRDITAGAMRALIAGT  605

Query  600  VACFMTACIAGILSSTPVDINCHHVLENAFNSTFPGNTTKVIACCQSLLSSTVAKGPGEV  659
            +ACF+TACIAG+L++TPVDINCHH+LENAFNS    NTT V++CCQ LLSS V KGPGEV
Sbjct  606  IACFLTACIAGMLTNTPVDINCHHILENAFNSGLVRNTTNVVSCCQGLLSSAVVKGPGEV  665

Query  660  IPGGNHSLYSLKGCCTLLNPSTFNCNGISNTF  691
            IP GNHSLYSLK CC LLN  T NC+ I N
Sbjct  666  IPTGNHSLYSLKNCCNLLNTPTLNCSWIPNVL  697
```

Figure E.2: Amino acid alignments of human CNT3 (NP_001186562.1) against cows CNT3 (NP_001179096.1) showing 79% identical amino acid sequences.

# APPENDIX F

## TEER VALUES FOR BOVINE NASAL MUCOSA

Table F.1: TEER values for bovine respiratory and olfactory nasal mucosa tissues after the exposure to alovudine in KRB at 15 min (start of experiment) and 2 hours (end of experiment).

| Alovudine concentration (μM) | Respiratory ($\Omega$ cm$^2$) | | Olfactory ($\Omega$ cm$^2$) | |
|---|---|---|---|---|
| | Start | End | Start | End |
| 50 | 176 | 162 | 128 | 145 |
| | 184 | 170 | 145 | 152 |
| | 157 | 142 | 153 | 152 |
| | 173 | 145 | 174 | 166 |
| | 175 | 158 | 154 | 176 |
| | 145 | 135 | 128 | 108 |
| 100 | 176 | 187 | 151 | 151 |
| | 191 | 204 | 160 | 144 |
| | 207 | 222 | 165 | 150 |
| | 197 | 197 | 164 | 141 |
| | 222 | 229 | 144 | 180 |
| | 190 | 136 | 173 | 154 |
| 200 | 168 | 167 | 121 | 104 |
| | 162 | 158 | 139 | 125 |
| | 200 | 217 | 111 | 108 |
| | 177 | 175 | 121 | 112 |
| | 162 | 172 | 105 | 102 |
| | 214 | 224 | 139 | 127 |

Table F.1 continued

| | | | | |
|---|---|---|---|---|
| 300 | 204 | 187 | 110 | 111 |
| | 191 | 184 | 125 | 140 |
| | 203 | 203 | 157 | 144 |
| | 240 | 241 | 166 | 139 |
| | 209 | 226 | 161 | 160 |
| | 194 | 204 | 177 | 146 |
| 1000 | 212 | 171 | 133 | 133 |
| | 206 | 169 | 115 | 150 |
| | 165 | 177 | 125 | 175 |
| | 158 | 195 | 155 | 148 |
| | 170 | 166 | 160 | 171 |
| | 122 | 164 | 141 | 165 |
| 2000 | 200 | 199 | 171 | 170 |
| | 205 | 190 | 153 | 151 |
| | 191 | 200 | 140 | 149 |
| | 180 | 170 | 125 | 133 |
| | 147 | 140 | 180 | 194 |
| | 144 | 154 | 148 | 100 |
| 3000 | 145 | 139 | 170 | 142 |
| | 150 | 142 | 135 | 142 |
| | 118 | 156 | 180 | 165 |
| | 146 | 190 | 150 | 148 |
| | 155 | 144 | 200 | 179 |
| | 140 | 109 | 138 | 110 |
| 4000 | 264 | 245 | 143 | 150 |
| | 269 | 241 | 190 | 179 |
| | 254 | 236 | 180 | 178 |
| | 263 | 252 | 174 | 230 |
| | 256 | 255 | 156 | 190 |
| | 225 | 211 | 156 | 191 |
| Avg | 187.5 | 184.6 | 149.8 | 149.6 |
| SD | 37 | 35.7 | 22.3 | 27.4 |

Table F.2: TEER values for bovine respiratory and olfactory nasal mucosa tissues after the exposure to alovudine in KRB containing DMSO at 15 min (start of experiment) and 2 hours (end of experiment).

| | Respiratory ($\Omega$ cm$^2$) | | Olfactory ($\Omega$ cm$^2$) | |
|---|---|---|---|---|
| Alovudine concentration ($\mu$M) | Start | End | Start | End |
| 500 | 208 | 211 | 110 | 112 |
| | 170 | 208 | 117 | 125 |
| | 198 | 230 | 122 | 127 |
| | 192 | 207 | 118 | 123 |
| | 197 | 208 | 109 | 109 |
| | 137 | 164 | 109 | 121 |
| 500 with 200nM NBMPR | 185 | 181 | 175 | 157 |
| | 215 | 215 | 191 | 150 |
| | 170 | 169 | 170 | 171 |
| | 187 | 187 | 166 | 177 |
| | 209 | 218 | 178 | 183 |
| | 215 | 215 | 195 | 206 |
| Avg | 190.3 | 201.1 | 146.7 | 146.8 |
| SD | 22.8 | 20.8 | 35.1 | 31.9 |

# APPENDIX G

## TRANSPORT STUDIES DATA

Following are plots of cumulative amount of alovudine vs time at different donor concentrations of alovudine.

Abbreviations:

Resp: Respiratory

Olf: Olfactory

M-S: Mucosal to submucosal

S-M: Submucosal to Mucosal

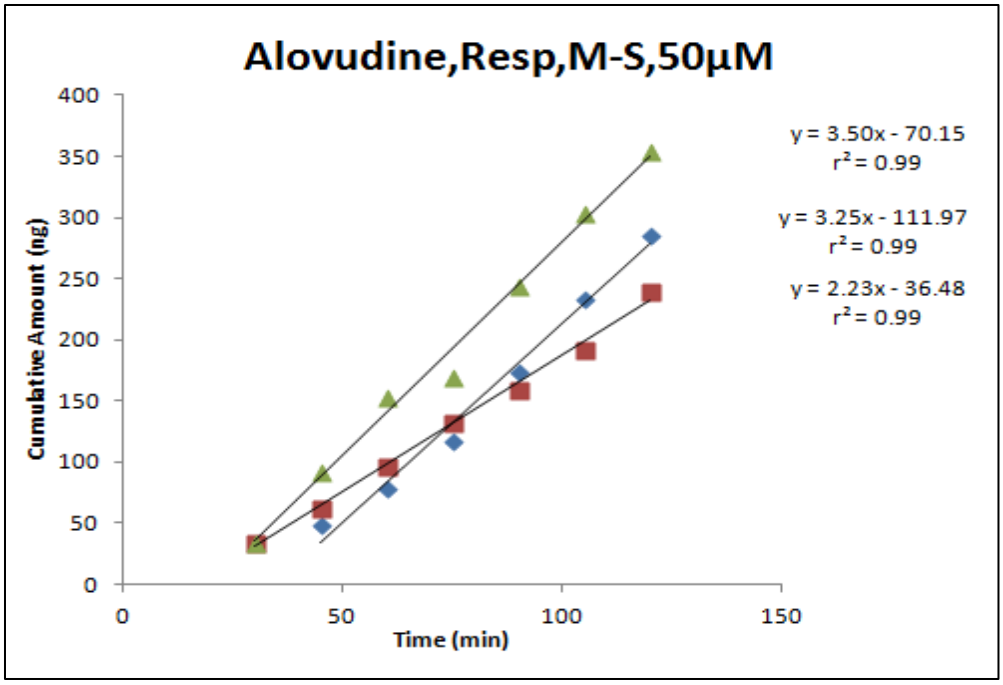
Alovudine,Resp,M-S,50µM
Cumulative Amount (ng)
Time (min)
0
50
100
150
200
250
300
350
400
y = 3.50x - 70.15
r² = 0.99
y = 3.25x - 111.97
r² = 0.99
y = 2.23x - 36.48
r² = 0.99

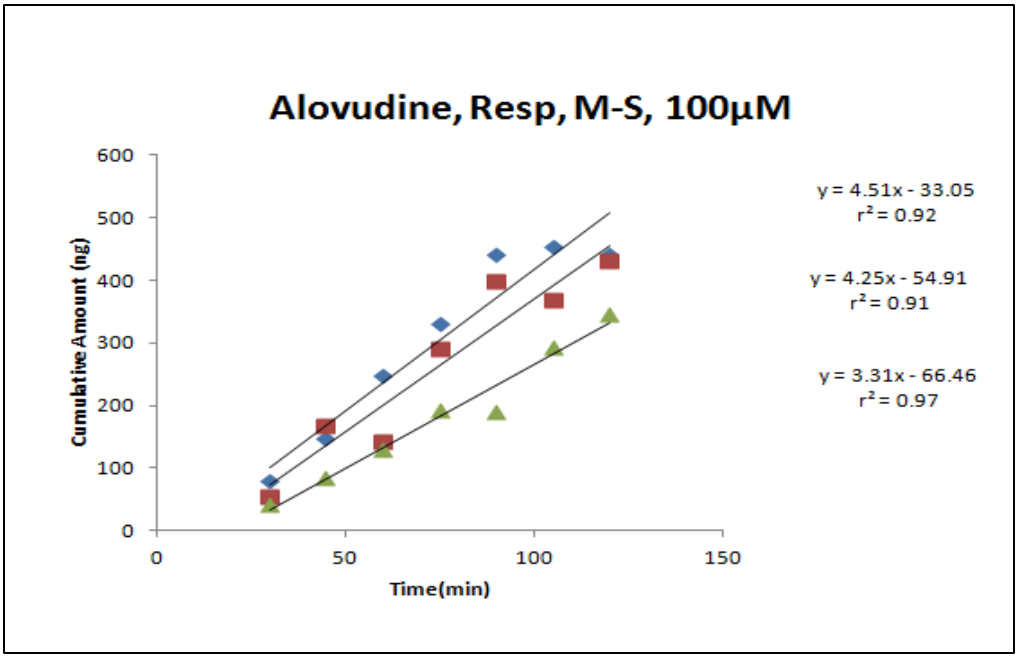
Alovudine, Resp, M-S, 100µM
Cumulative Amount (ng)
Time(min)
0
50
100
150
200
300
400
500
600
y = 4.51x - 33.05
r² = 0.92
y = 4.25x - 54.91
r² = 0.91
y = 3.31x - 66.46
r² = 0.97

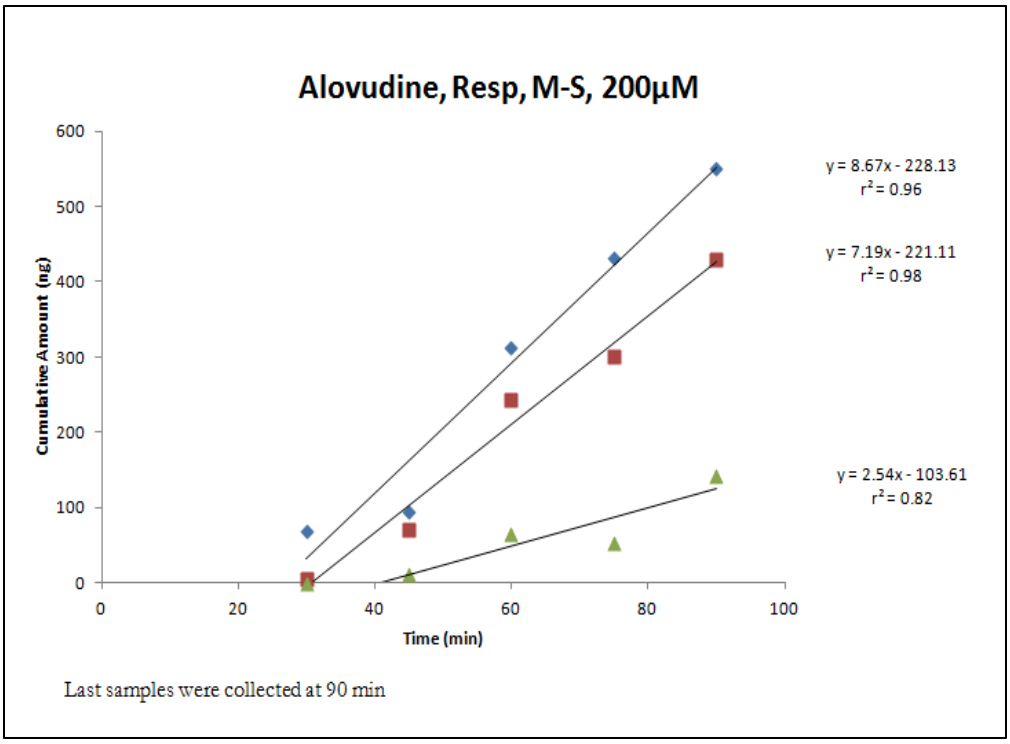


Last samples were collected at 90 min

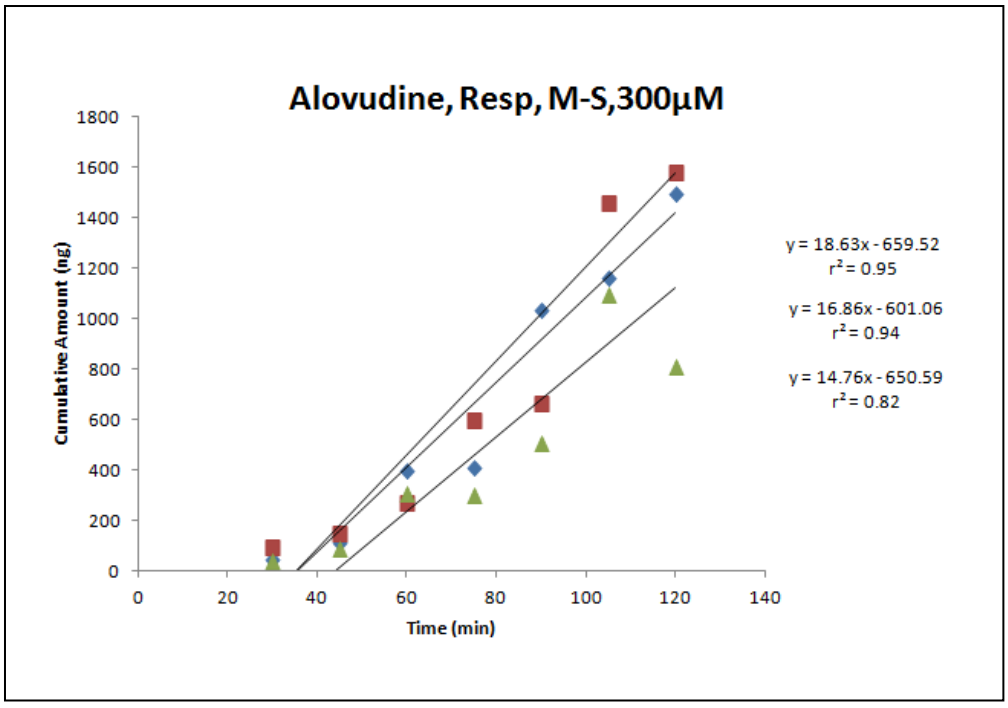

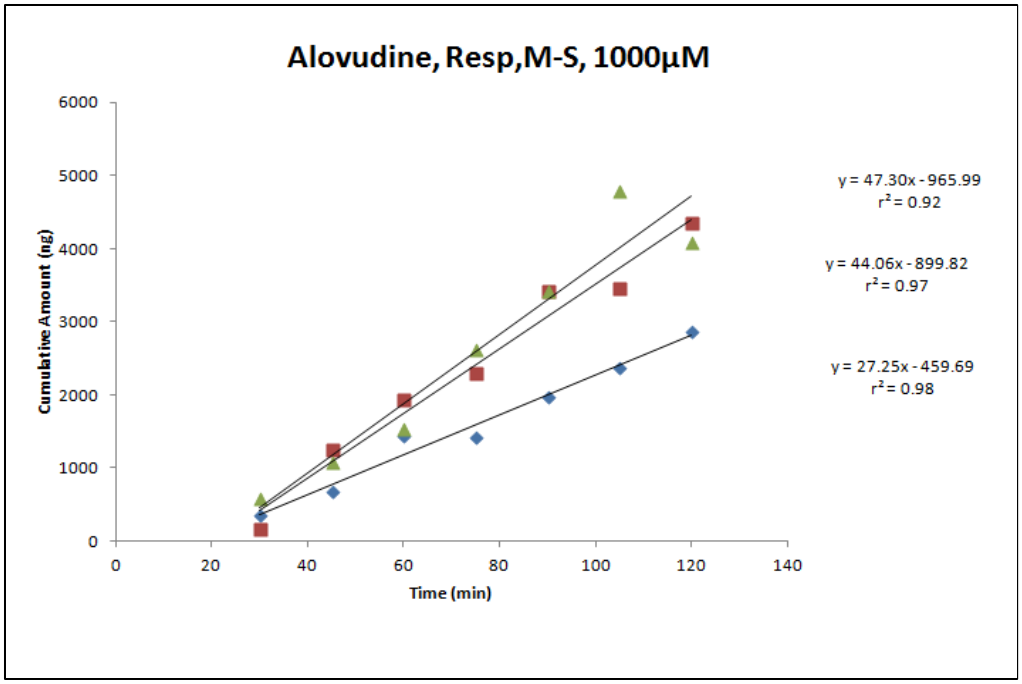
Alovudine, Resp,M-S, 1000µM
Cumulative Amount (ng)
Time (min)
y = 47.30x - 965.99
r² = 0.92
y = 44.06x - 899.82
r² = 0.97
y = 27.25x - 459.69
r² = 0.98

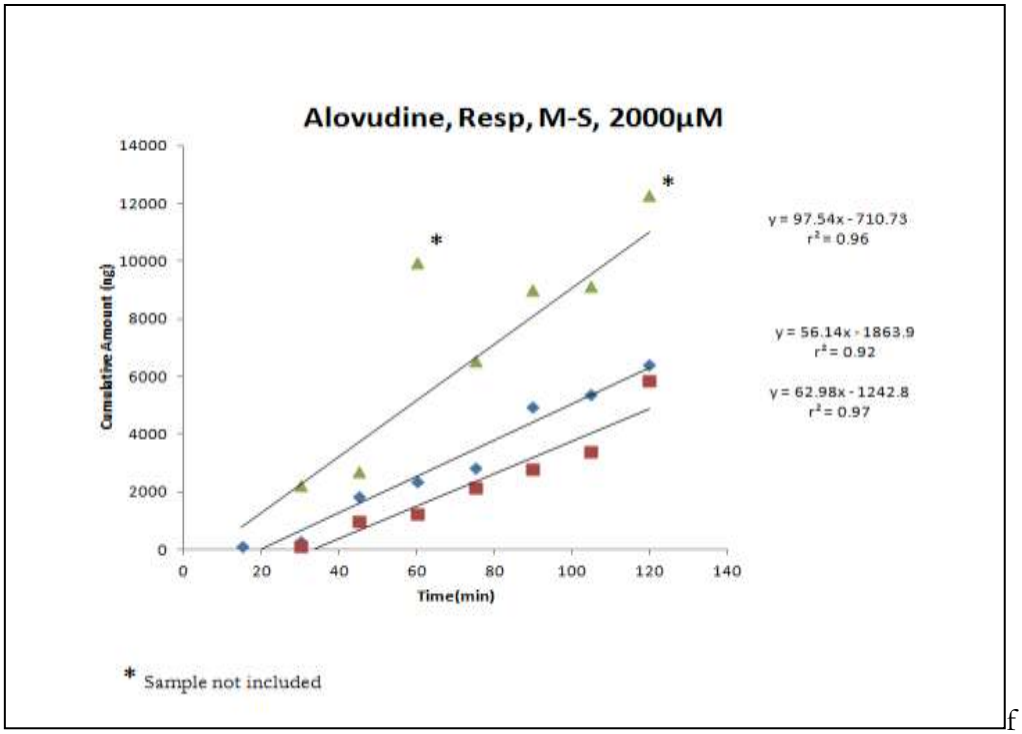
Alovudine, Resp, M-S, 2000µM
Cumulative Amount (ng)
Time(min)
y = 97.54x - 710.73
r² = 0.96
y = 56.14x - 1863.9
r² = 0.92
y = 62.98x - 1242.8
r² = 0.97
* Sample not included

f

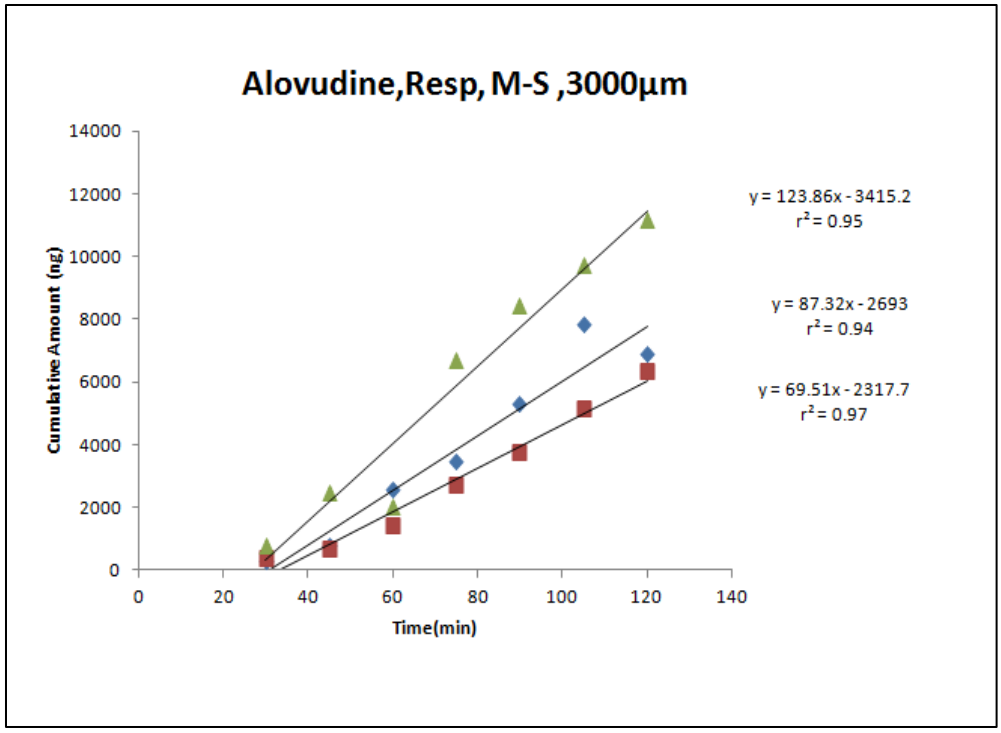
Alovudine,Resp, M-S ,3000µm
Cumulative Amount (ng)
Time(min)
y = 123.86x - 3415.2
r² = 0.95
y = 87.32x - 2693
r² = 0.94
y = 69.51x - 2317.7
r² = 0.97

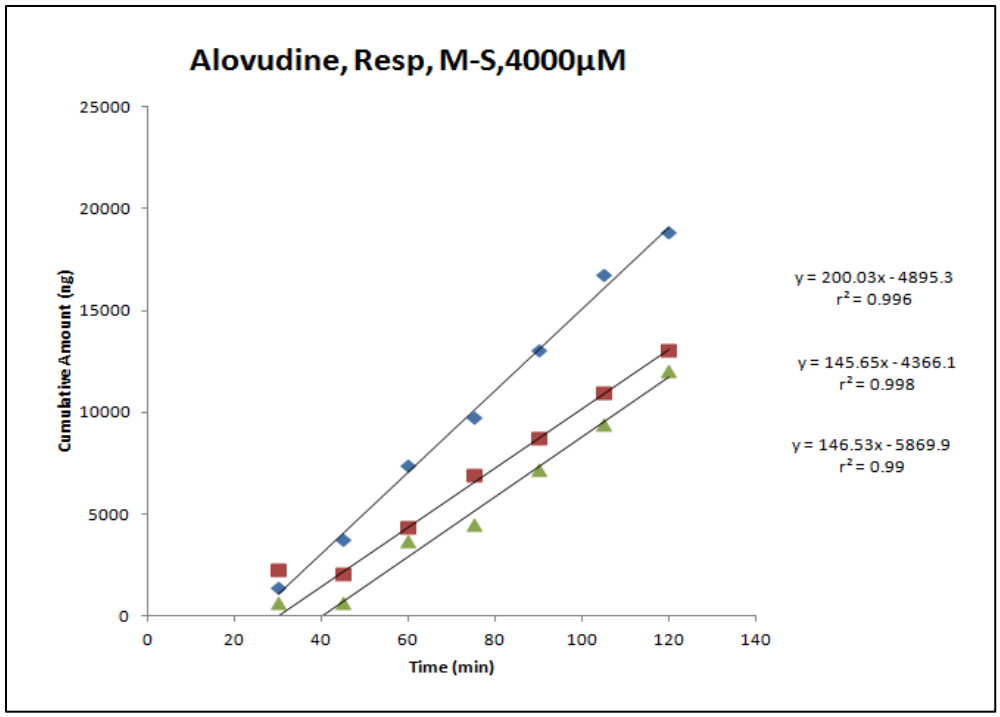
Alovudine, Resp, M-S,4000µM
Cumulative Amount (ng)
Time (min)
y = 200.03x - 4895.3
r² = 0.996
y = 145.65x - 4366.1
r² = 0.998
y = 146.53x - 5869.9
r² = 0.99

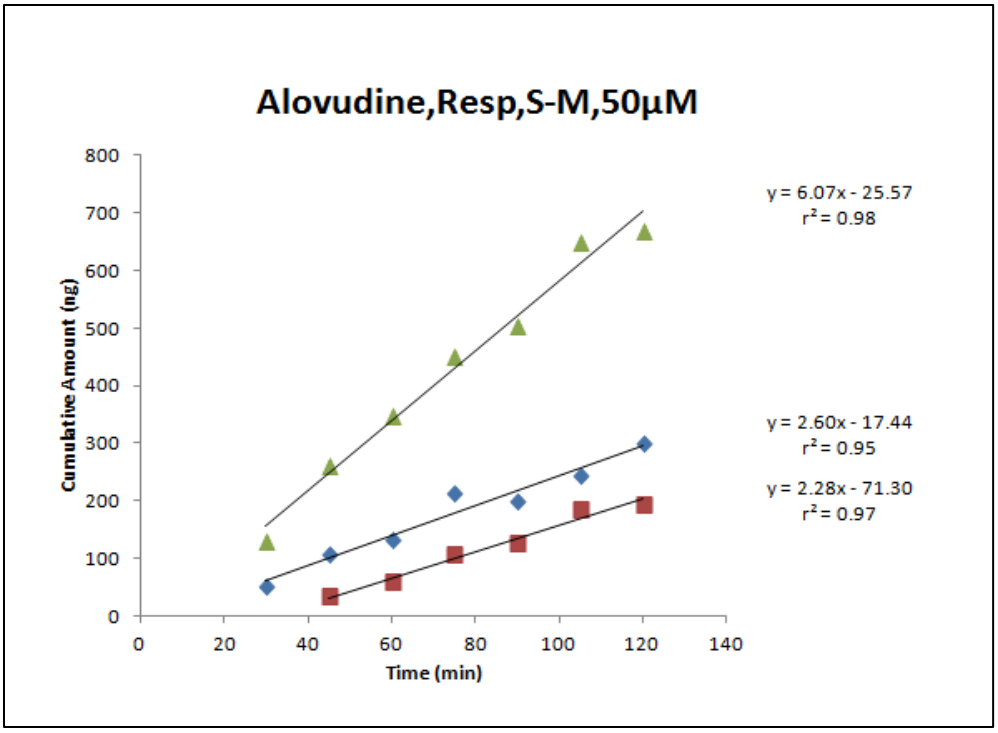
Alovudine,Resp,S-M,50µM
Cumulative Amount (ng)
Time (min)
y = 6.07x - 25.57
r² = 0.98
y = 2.60x - 17.44
r² = 0.95
y = 2.28x - 71.30
r² = 0.97

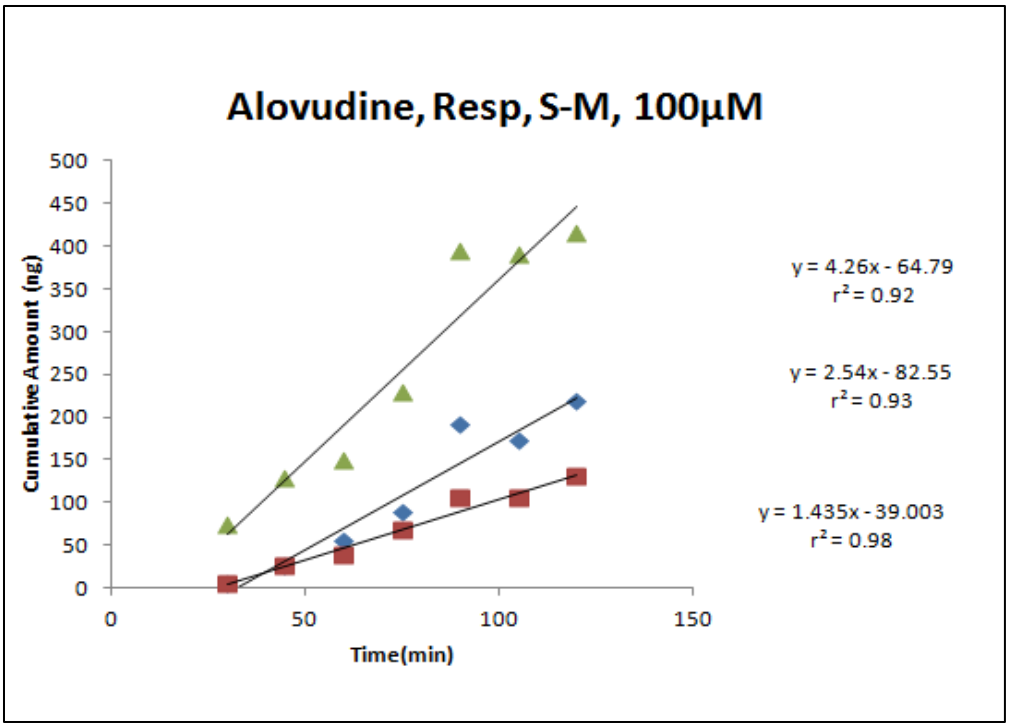
Alovudine, Resp, S-M, 100µM
Cumulative Amount (ng)
Time(min)
y = 4.26x - 64.79
r² = 0.92
y = 2.54x - 82.55
r² = 0.93
y = 1.435x - 39.003
r² = 0.98

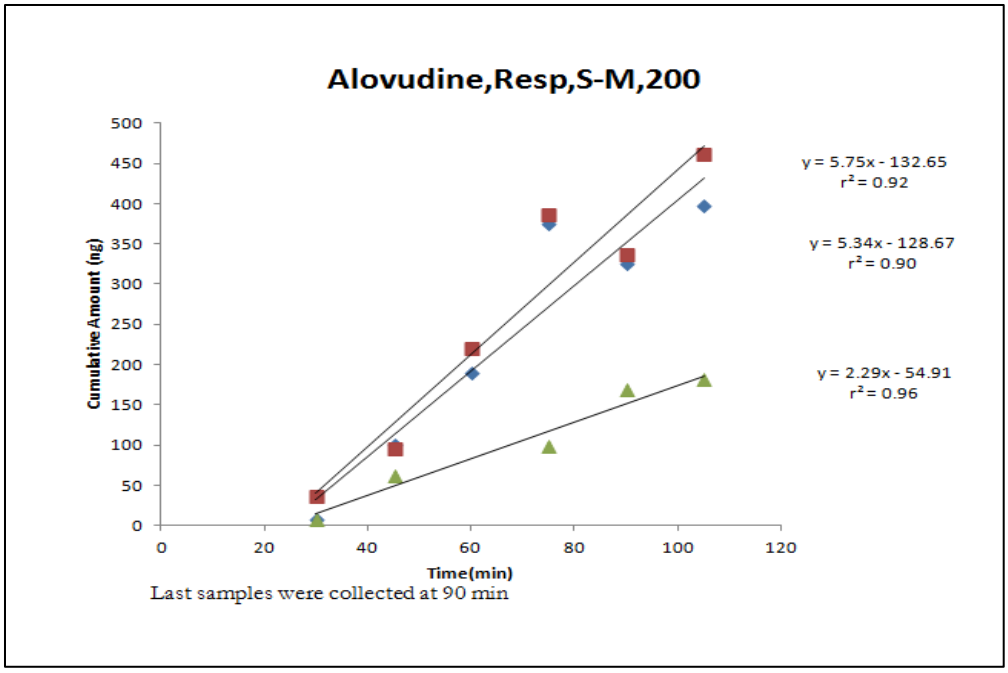

Last samples were collected at 90 min

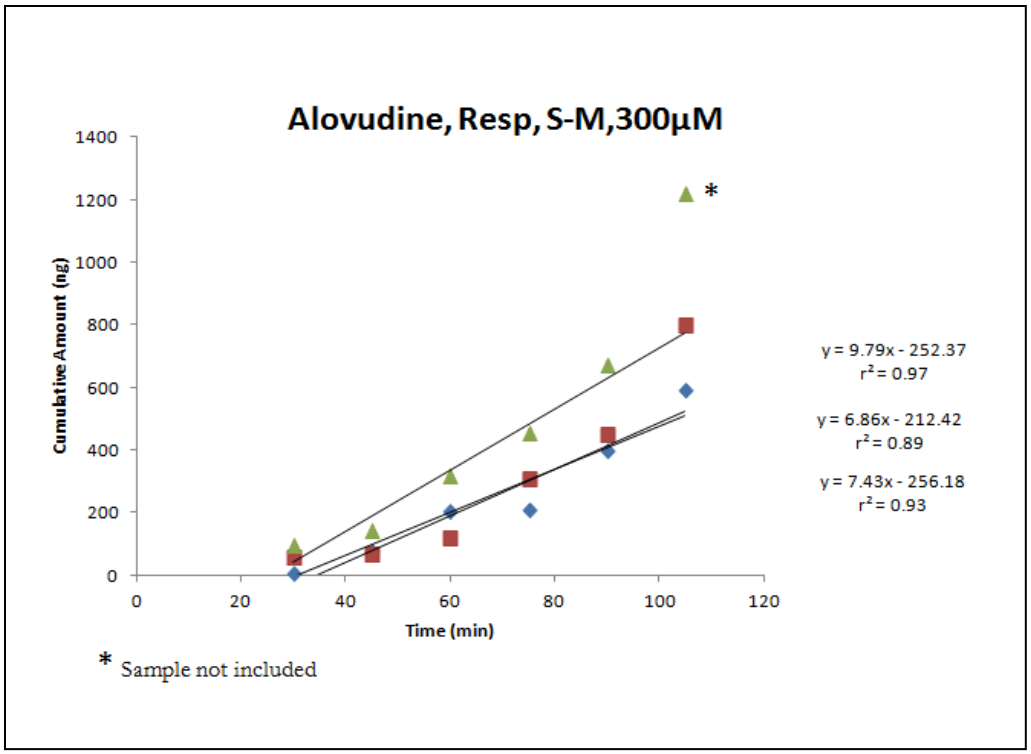

* Sample not included

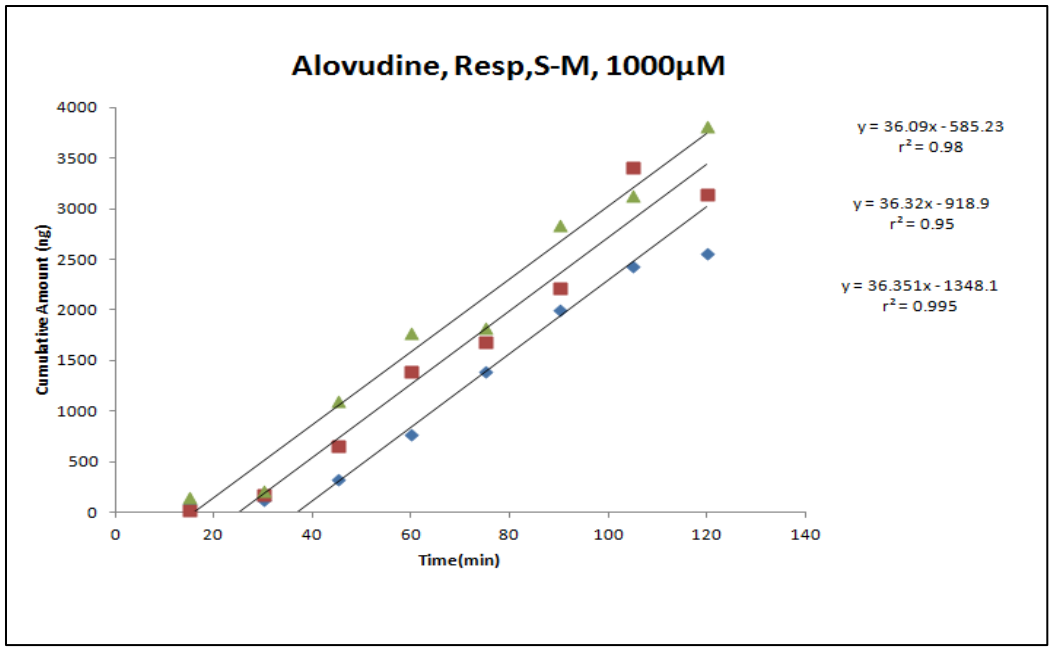
Alovudine, Resp,S-M, 1000µM
Cumulative Amount (ng)
Time(min)
y = 36.09x - 585.23
r² = 0.98
y = 36.32x - 918.9
r² = 0.95
y = 36.351x - 1348.1
r² = 0.995

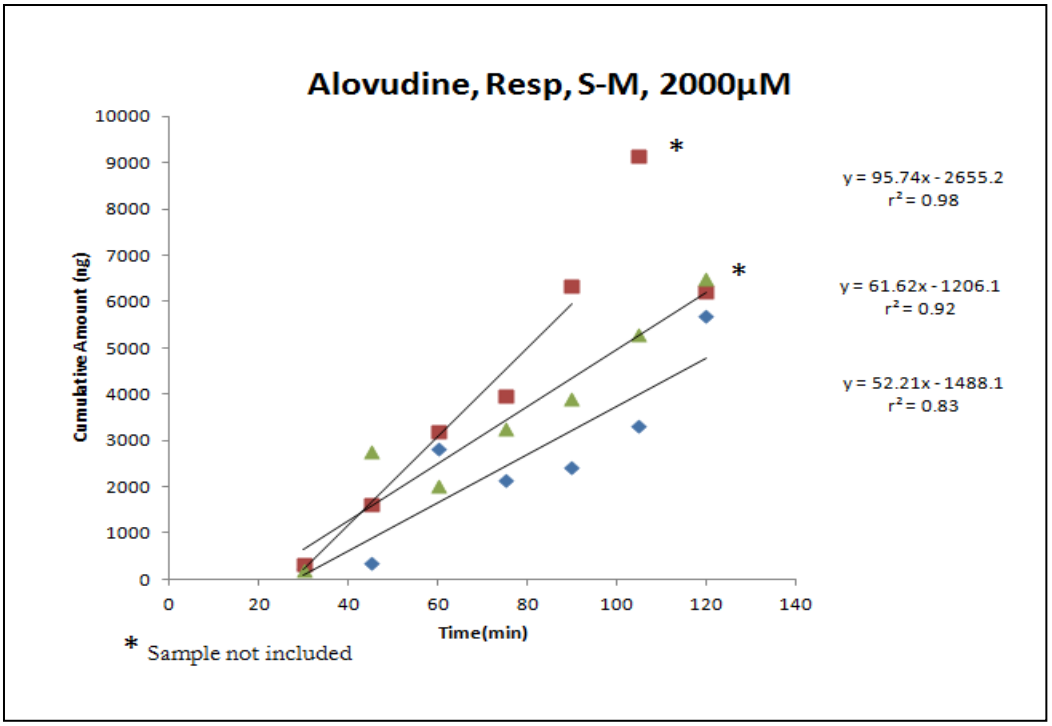
Alovudine, Resp, S-M, 2000µM
Cumulative Amount (ng)
Time(min)
y = 95.74x - 2655.2
r² = 0.98
y = 61.62x - 1206.1
r² = 0.92
y = 52.21x - 1488.1
r² = 0.83
* Sample not included

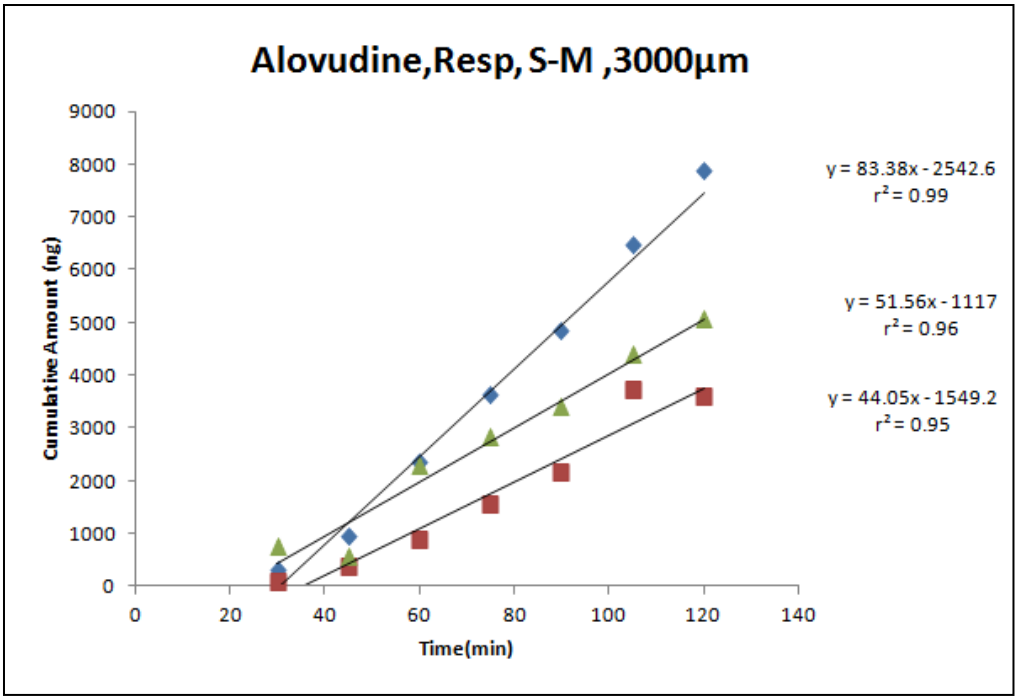
Alovudine,Resp, S-M ,3000µm
Cumulative Amount (ng)
Time(min)
y = 83.38x - 2542.6
r² = 0.99
y = 51.56x - 1117
r² = 0.96
y = 44.05x - 1549.2
r² = 0.95

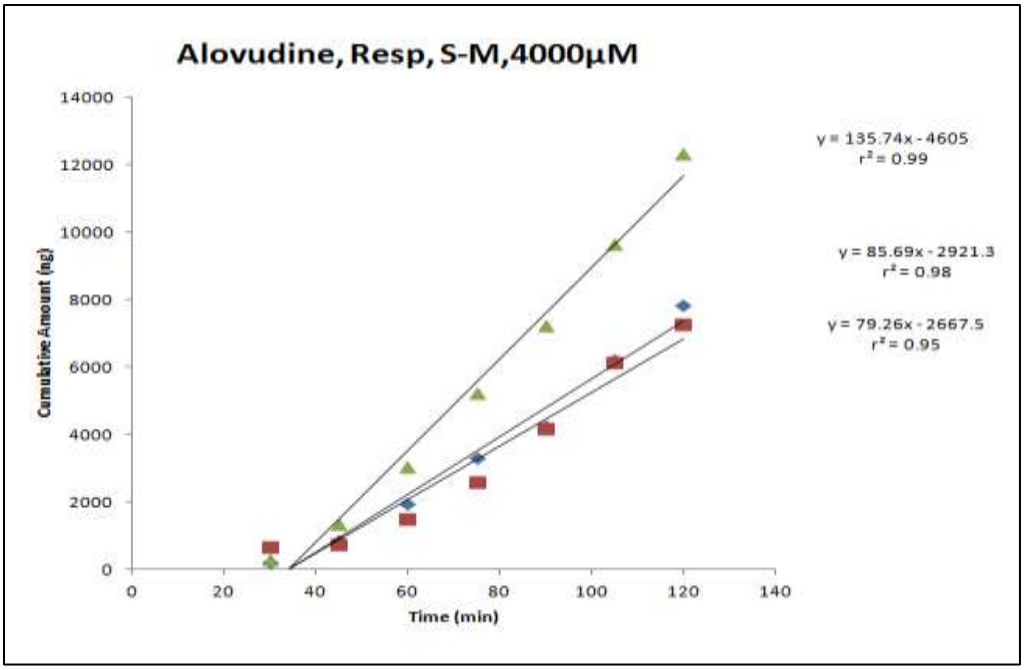
Alovudine, Resp, S-M,4000µM
Cumulative Amount (ng)
Time (min)
y = 135.74x - 4605
r² = 0.99
y = 85.69x - 2921.3
r² = 0.98
y = 79.26x - 2667.5
r² = 0.95

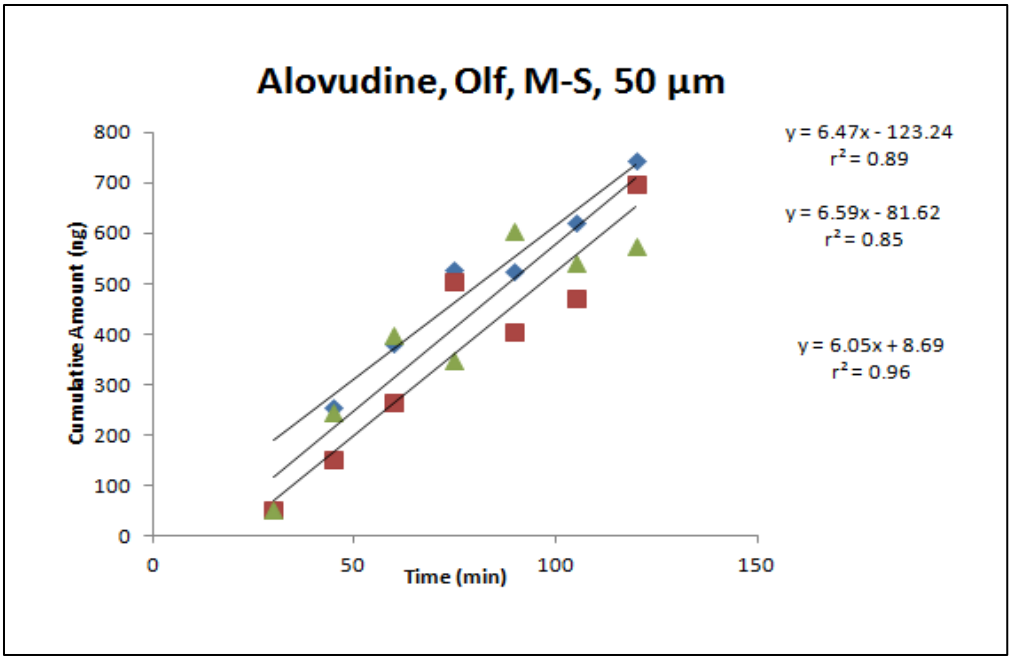
Alovudine, Olf, M-S, 50 µm
Cumulative Amount (ng)
Time (min)
0
100
200
300
400
500
600
700
800
0
50
100
150
y = 6.47x - 123.24
r² = 0.89
y = 6.59x - 81.62
r² = 0.85
y = 6.05x + 8.69
r² = 0.96

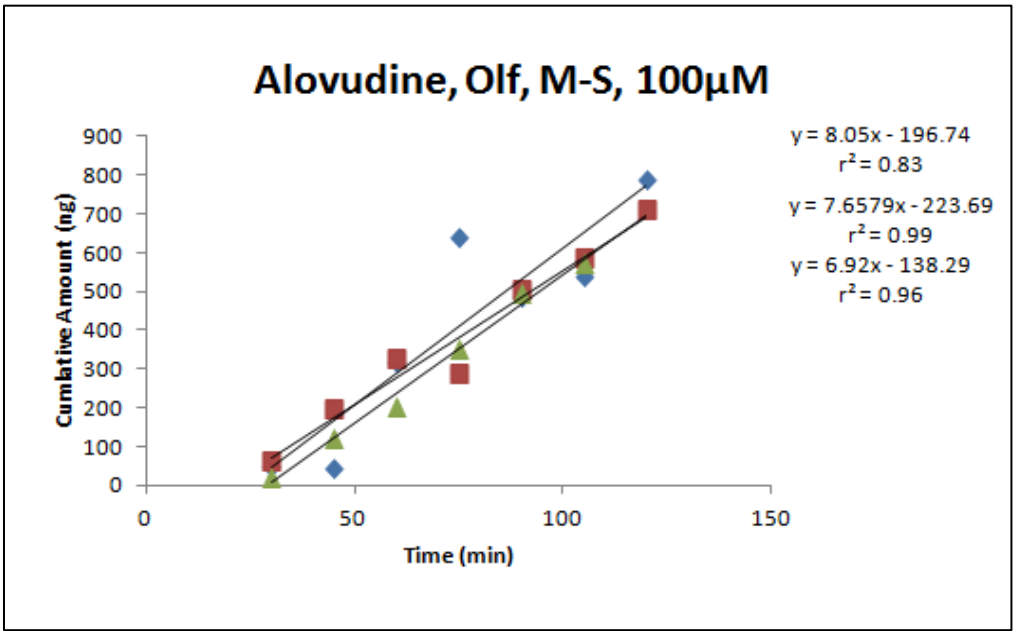
Alovudine, Olf, M-S, 100µM
Cumulative Amount (ng)
Time (min)
0
100
200
300
400
500
600
700
800
900
0
50
100
150
y = 8.05x - 196.74
r² = 0.83
y = 7.6579x - 223.69
r² = 0.99
y = 6.92x - 138.29
r² = 0.96

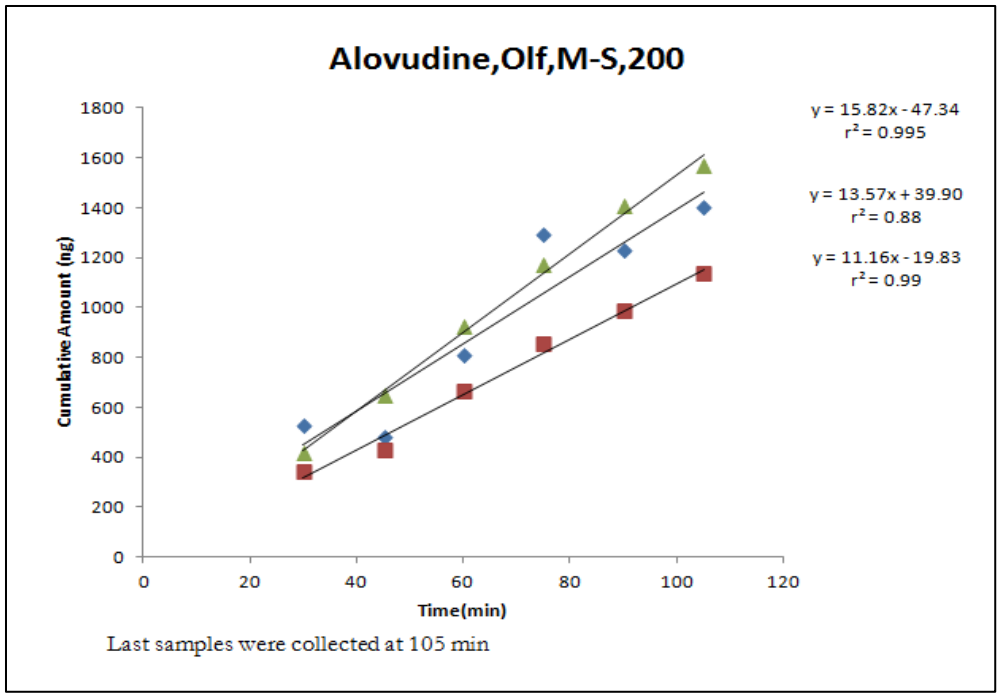


Last samples were collected at 105 min

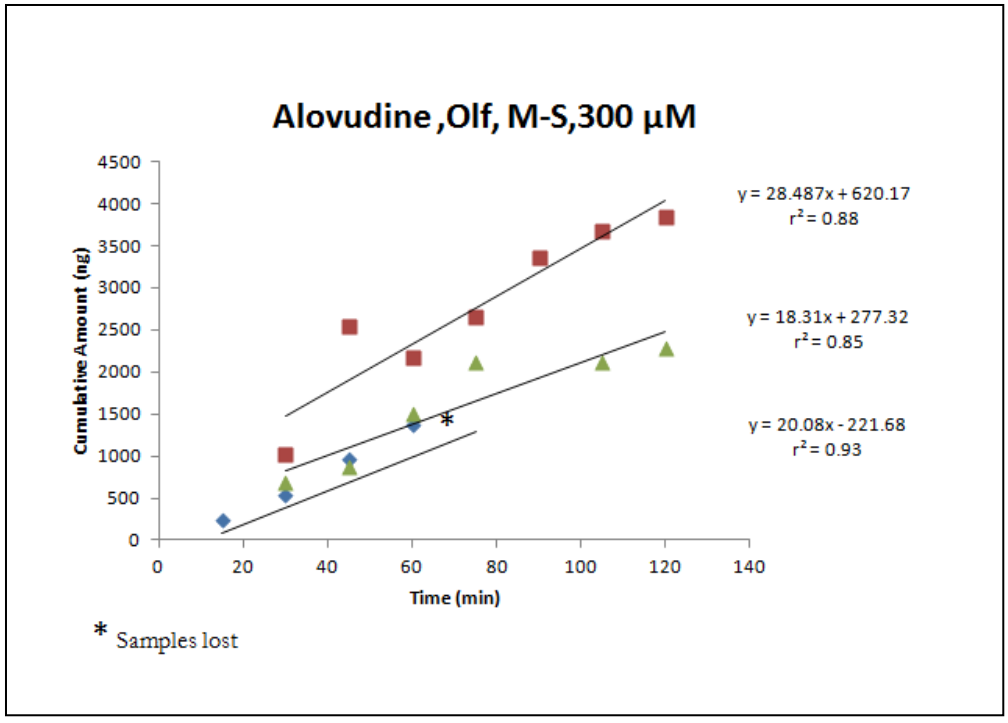


* Samples lost

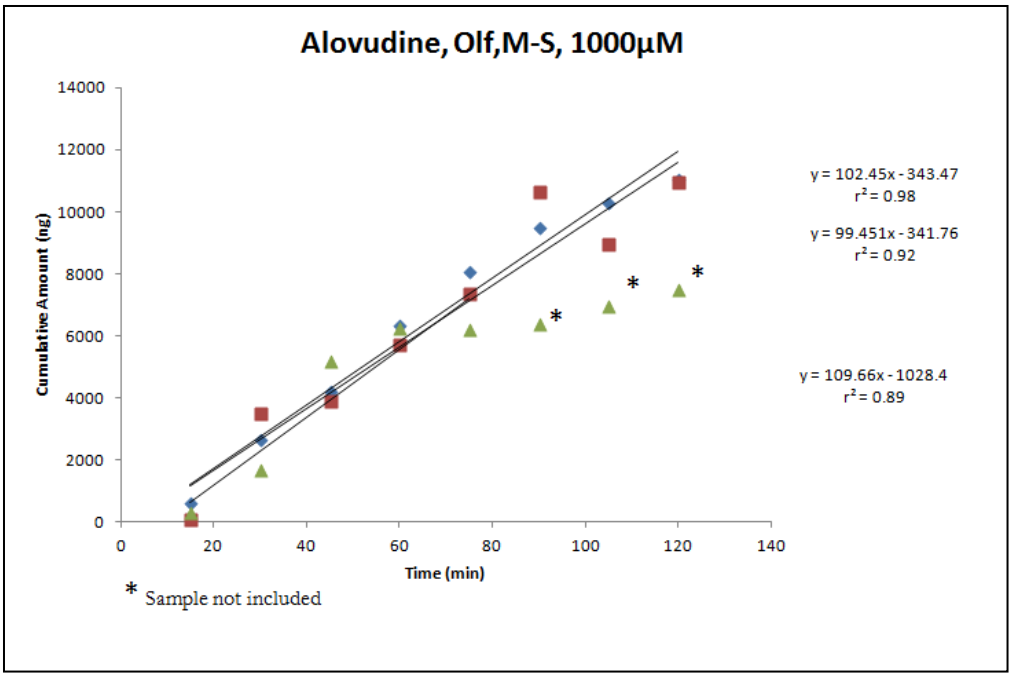
Alovudine, Olf,M-S, 1000µM
Cumulative Amount (ng)
Time (min)
y = 102.45x - 343.47
r² = 0.98
y = 99.451x - 341.76
r² = 0.92
y = 109.66x - 1028.4
r² = 0.89
* Sample not included

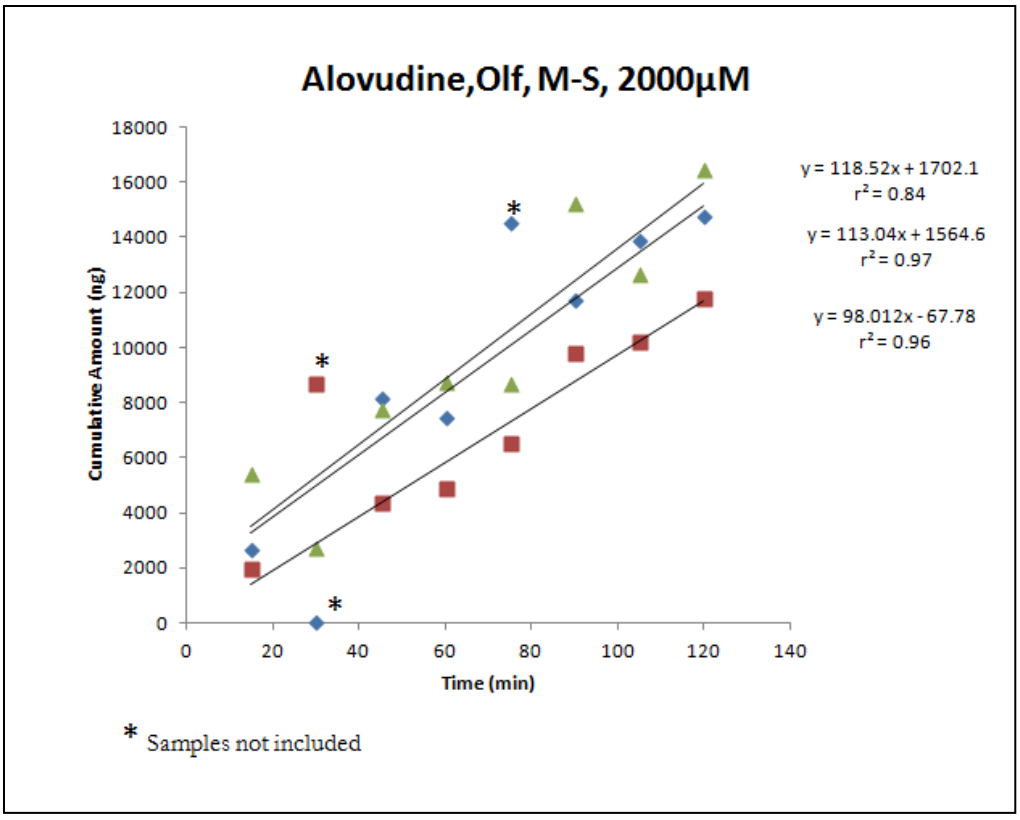
Alovudine,Olf, M-S, 2000µM
Cumulative Amount (ng)
Time (min)
y = 118.52x + 1702.1
r² = 0.84
y = 113.04x + 1564.6
r² = 0.97
y = 98.012x - 67.78
r² = 0.96
* Samples not included

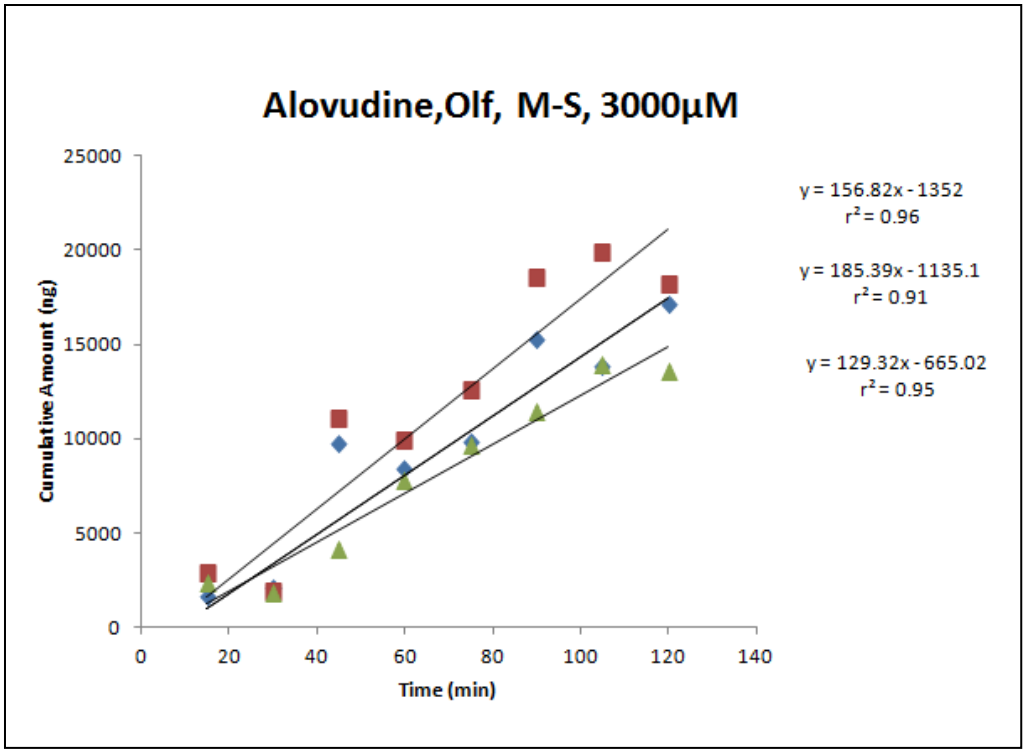
Alovudine,Olf, M-S, 3000µM
Cumulative Amount (ng)
Time (min)
y = 156.82x - 1352
r² = 0.96
y = 185.39x - 1135.1
r² = 0.91
y = 129.32x - 665.02
r² = 0.95

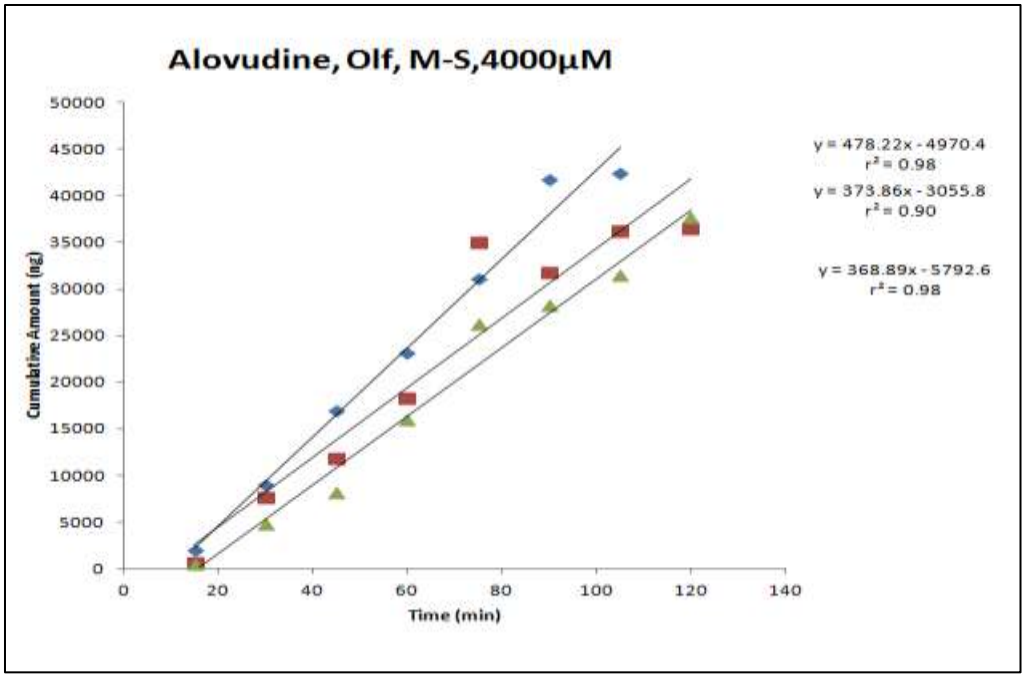
Alovudine, Olf, M-S,4000µM
Cumulative Amount (ng)
Time (min)
y = 478.22x - 4970.4
r² = 0.98
y = 373.86x - 3055.8
r² = 0.90
y = 368.89x - 5792.6
r² = 0.98

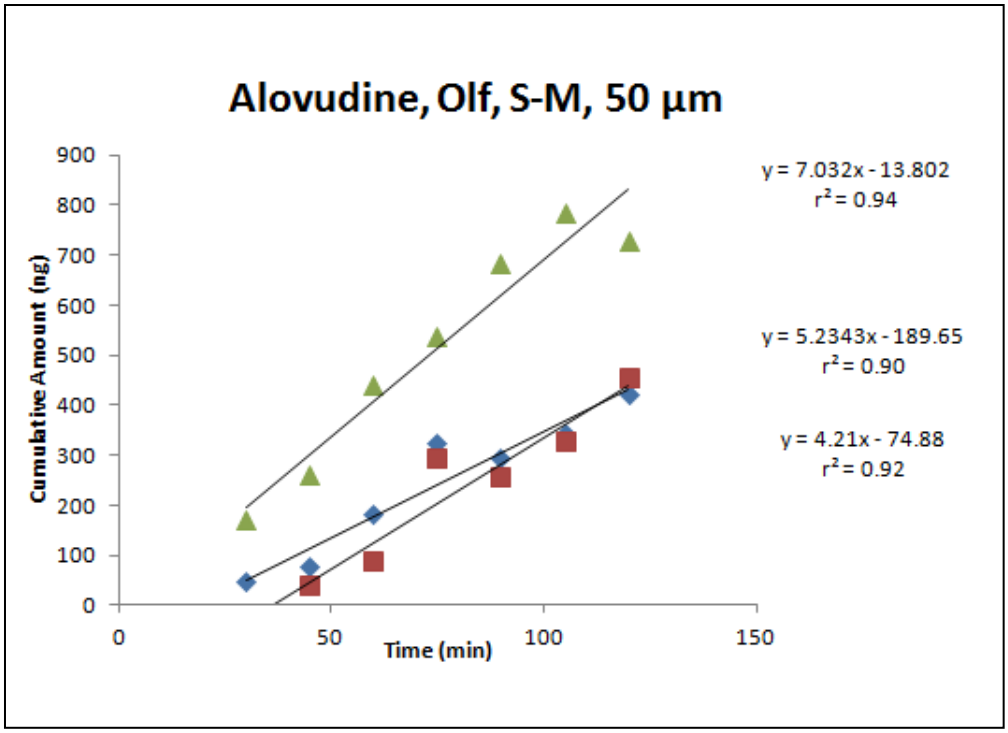


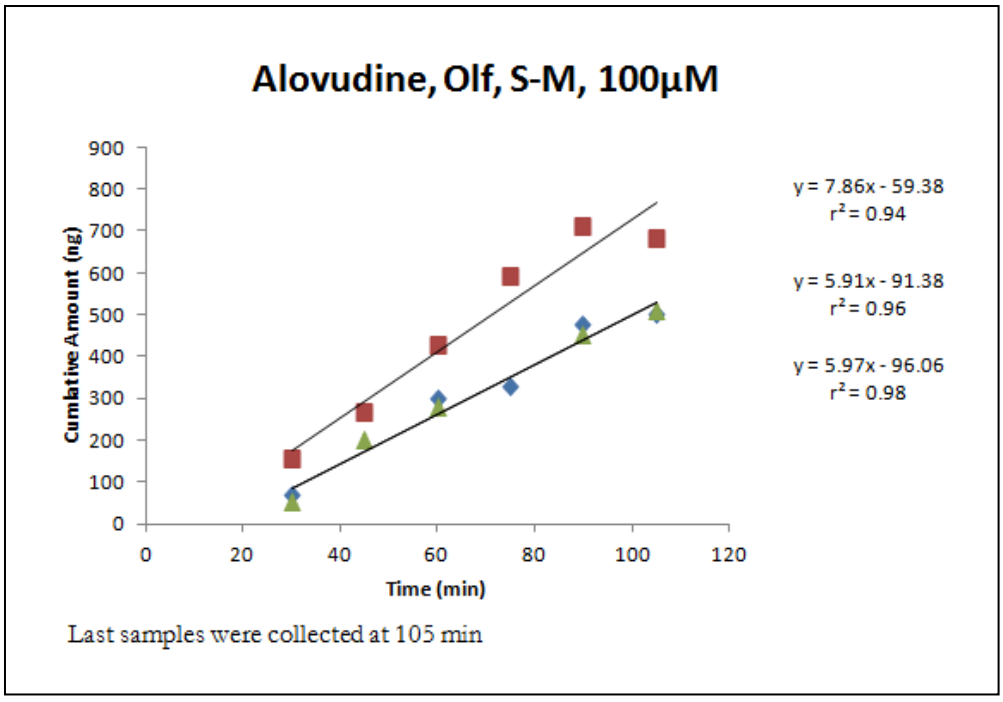


Last samples were collected at 105 min

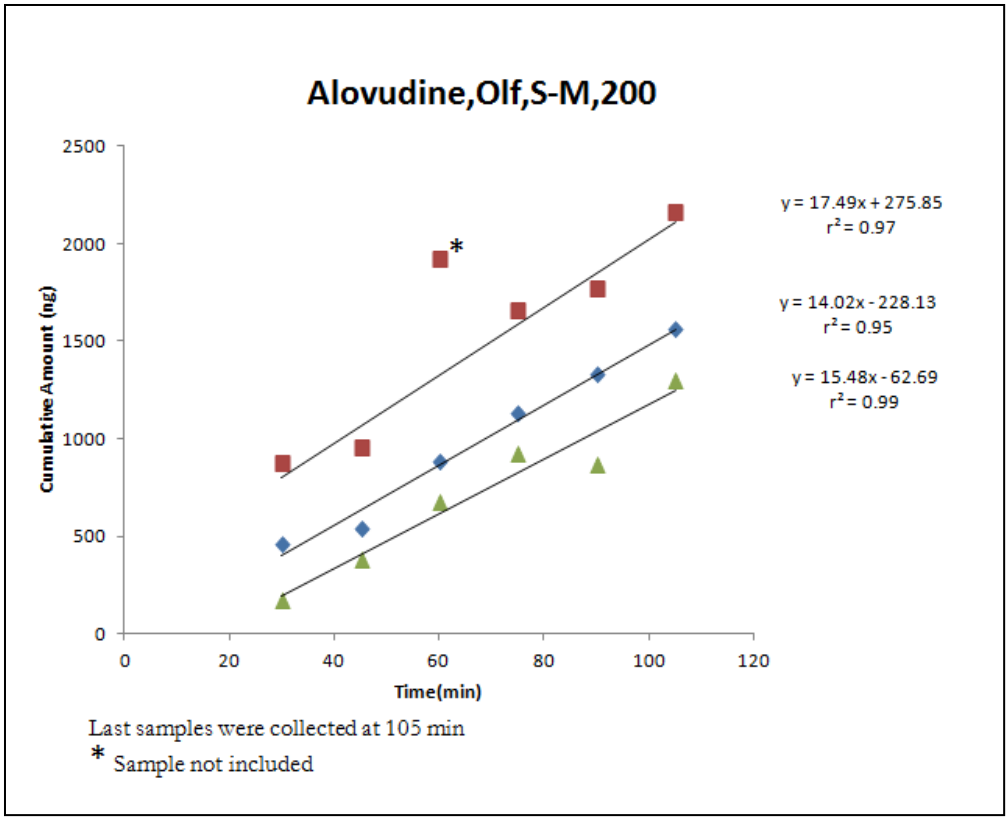
Alovudine,Olf,S-M,200
Cumulative Amount (ng)
Time(min)
y = 17.49x + 275.85
r² = 0.97
y = 14.02x - 228.13
r² = 0.95
y = 15.48x - 62.69
r² = 0.99
Last samples were collected at 105 min
* Sample not included

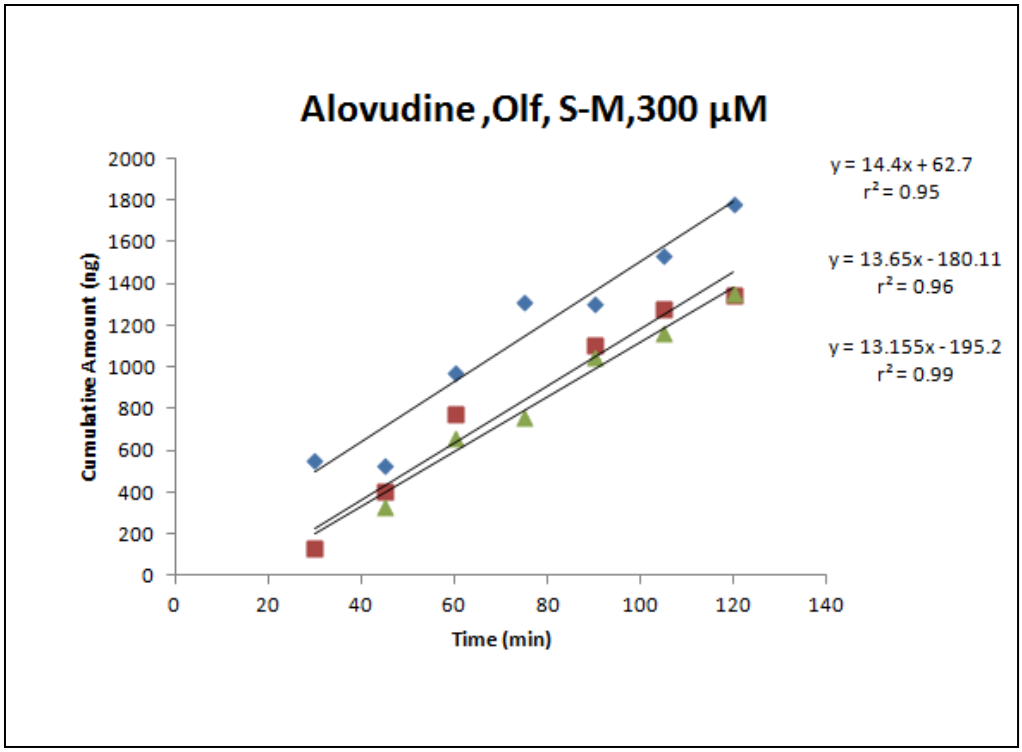
Alovudine ,Olf, S-M,300 µM
Cumulative Amount (ng)
Time (min)
y = 14.4x + 62.7
r² = 0.95
y = 13.65x - 180.11
r² = 0.96
y = 13.155x - 195.2
r² = 0.99

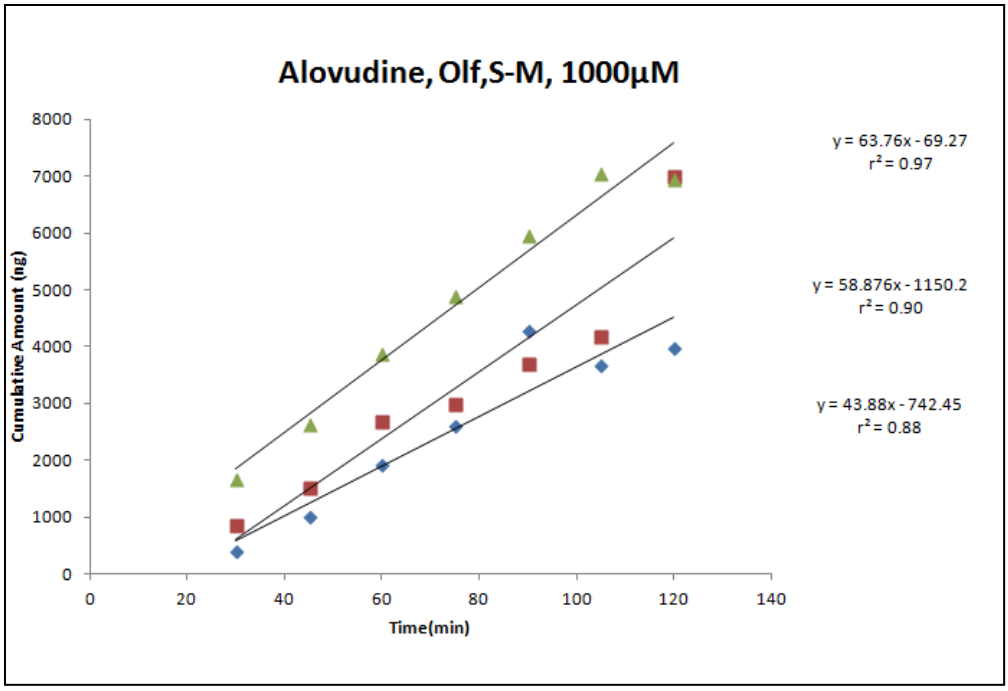
Alovudine, Olf,S-M, 1000µM
Cumulative Amount (ng)
Time(min)
y = 63.76x - 69.27
r² = 0.97
y = 58.876x - 1150.2
r² = 0.90
y = 43.88x - 742.45
r² = 0.88

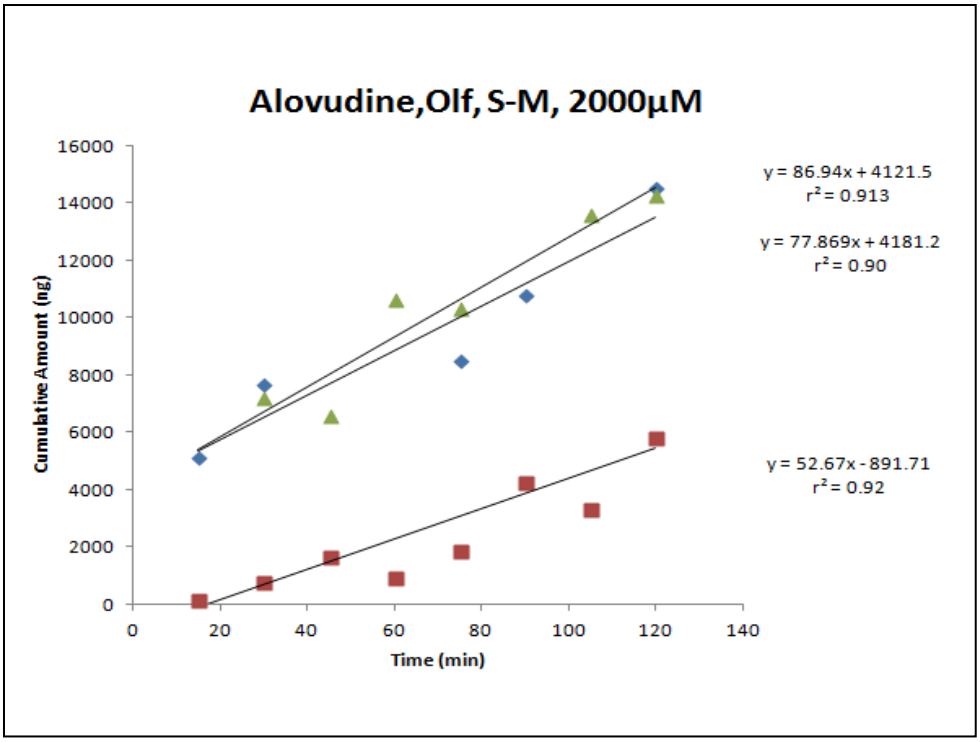
Alovudine,Olf, S-M, 2000µM
Cumulative Amount (ng)
Time (min)
y = 86.94x + 4121.5
r² = 0.913
y = 77.869x + 4181.2
r² = 0.90
y = 52.67x - 891.71
r² = 0.92

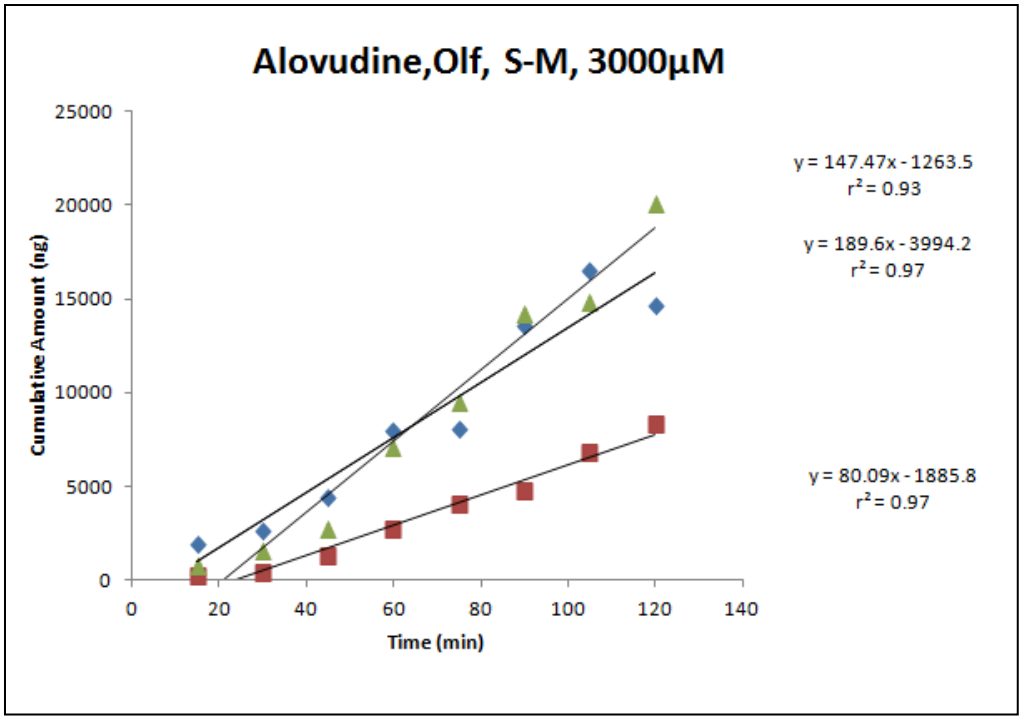
Alovudine,Olf, S-M, 3000µM
Cumulative Amount (ng)
Time (min)
y = 147.47x - 1263.5
r² = 0.93
y = 189.6x - 3994.2
r² = 0.97
y = 80.09x - 1885.8
r² = 0.97

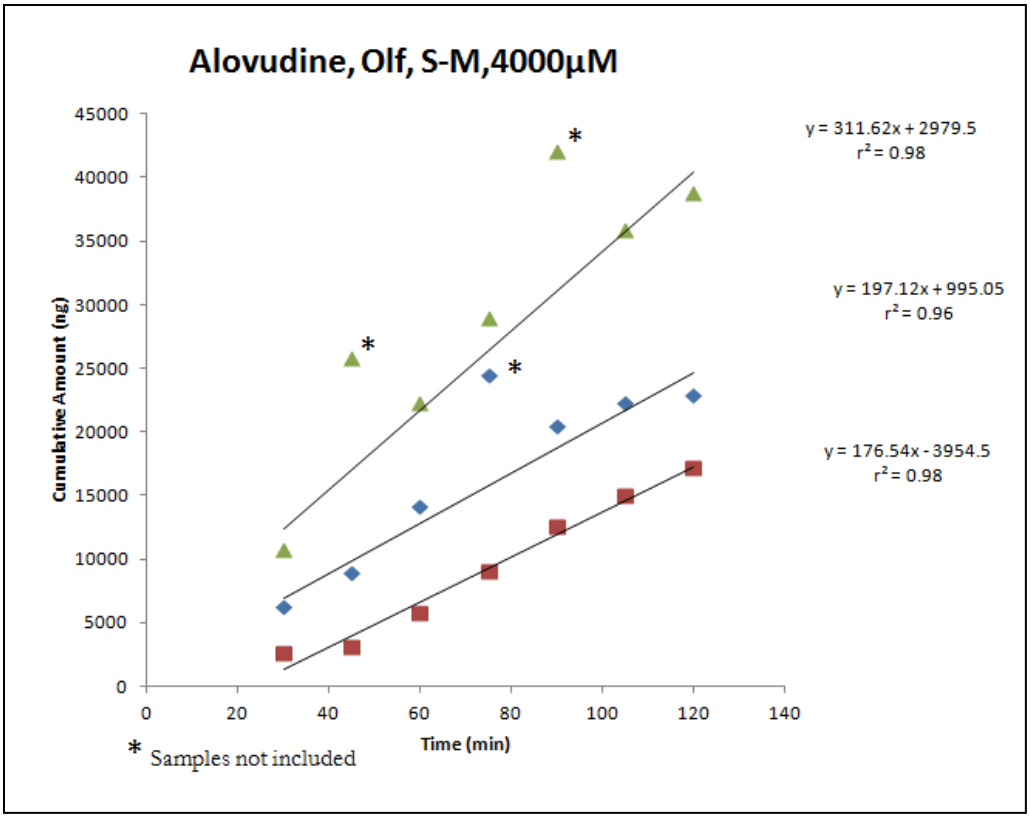
Alovudine, Olf, S-M,4000µM
Cumulative Amount (ng)
Time (min)
* Samples not included
y = 311.62x + 2979.5
r² = 0.98
y = 197.12x + 995.05
r² = 0.96
y = 176.54x - 3954.5
r² = 0.98

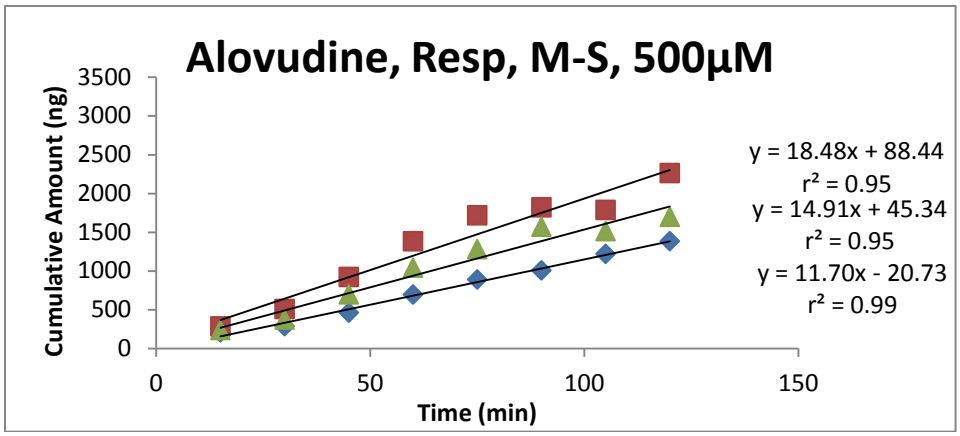
Alovudine, Resp, M-S, 500µM
Cumulative Amount (ng)
3500
3000
2500
2000
1500
1000
500
0
0
50
100
150
Time (min)
y = 18.48x + 88.44
r² = 0.95
y = 14.91x + 45.34
r² = 0.95
y = 11.70x - 20.73
r² = 0.99

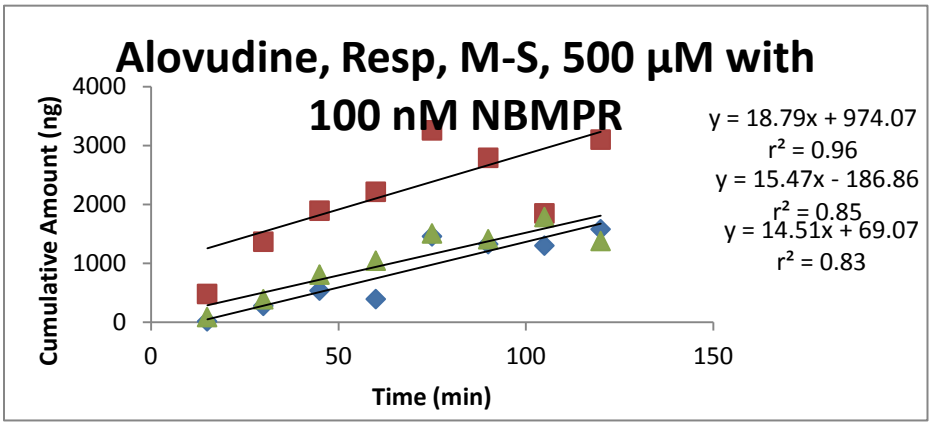
Alovudine, Resp, M-S, 500 µM with 100 nM NBMPR
Cumulative Amount (ng)
4000
3000
2000
1000
0
0
50
100
150
Time (min)
y = 18.79x + 974.07
r² = 0.96
y = 15.47x - 186.86
r² = 0.85
y = 14.51x + 69.07
r² = 0.83

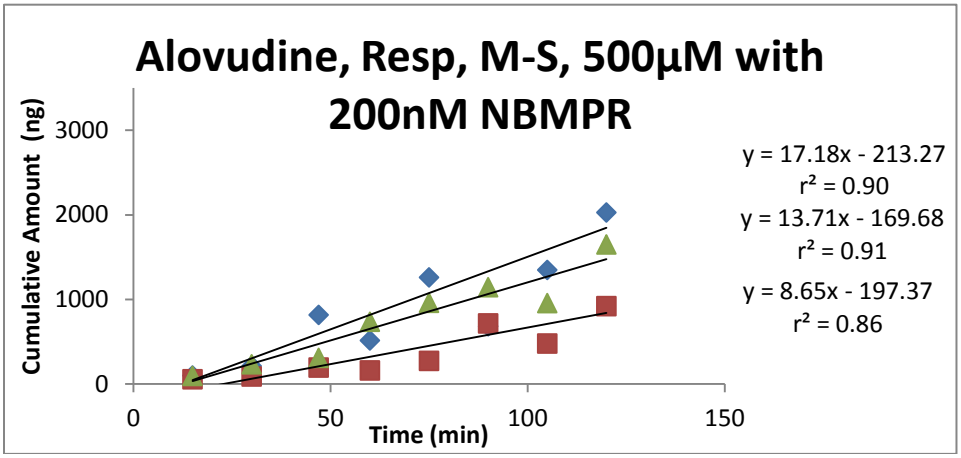
Alovudine, Resp, M-S, 500µM with 200nM NBMPR
Cumulative Amount (ng)
3000
2000
1000
0
0
50
100
150
Time (min)
y = 17.18x - 213.27
r² = 0.90
y = 13.71x - 169.68
r² = 0.91
y = 8.65x - 197.37
r² = 0.86

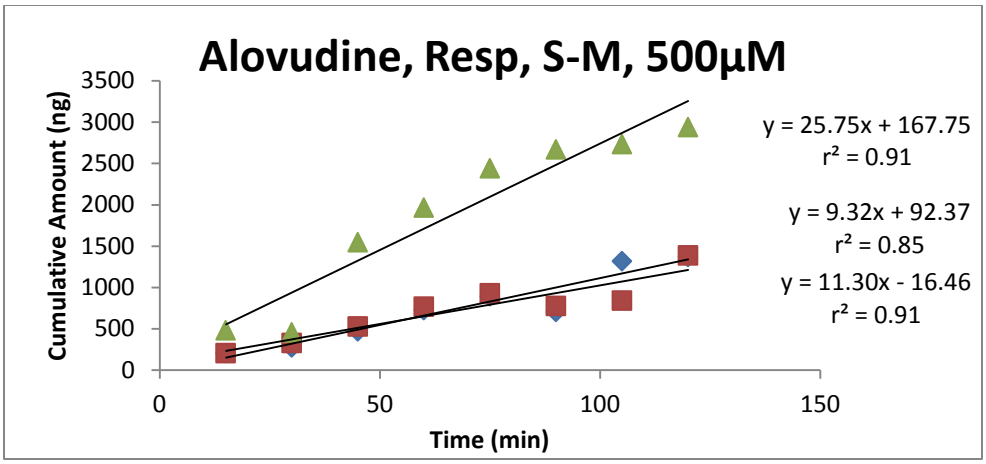
Alovudine, Resp, S-M, 500µM
Cumulative Amount (ng)
3500
3000
2500
2000
1500
1000
500
0
0
50
100
150
Time (min)
y = 25.75x + 167.75
r² = 0.91
y = 9.32x + 92.37
r² = 0.85
y = 11.30x - 16.46
r² = 0.91

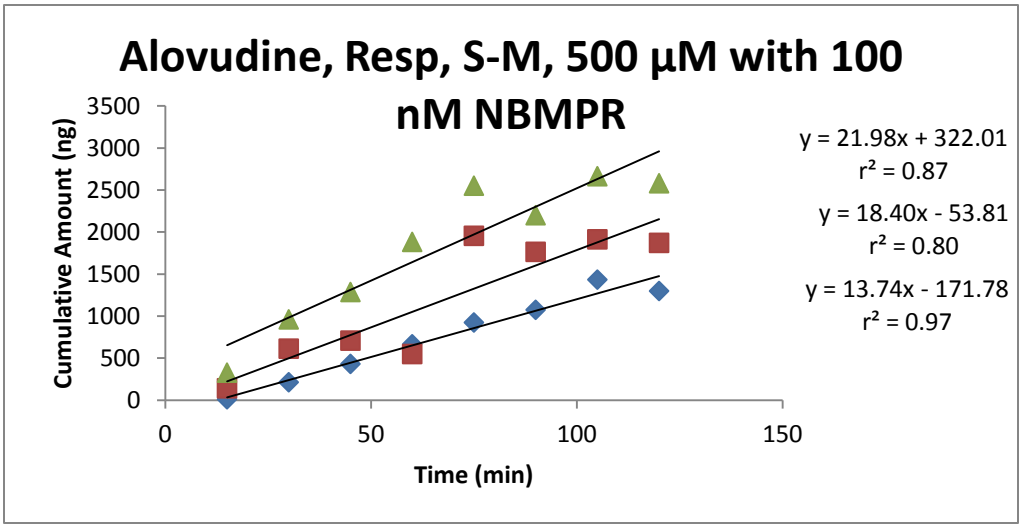
Alovudine, Resp, S-M, 500 µM with 100 nM NBMPR
Cumulative Amount (ng)
3500
3000
2500
2000
1500
1000
500
0
0
50
100
150
Time (min)
y = 21.98x + 322.01
r² = 0.87
y = 18.40x - 53.81
r² = 0.80
y = 13.74x - 171.78
r² = 0.97

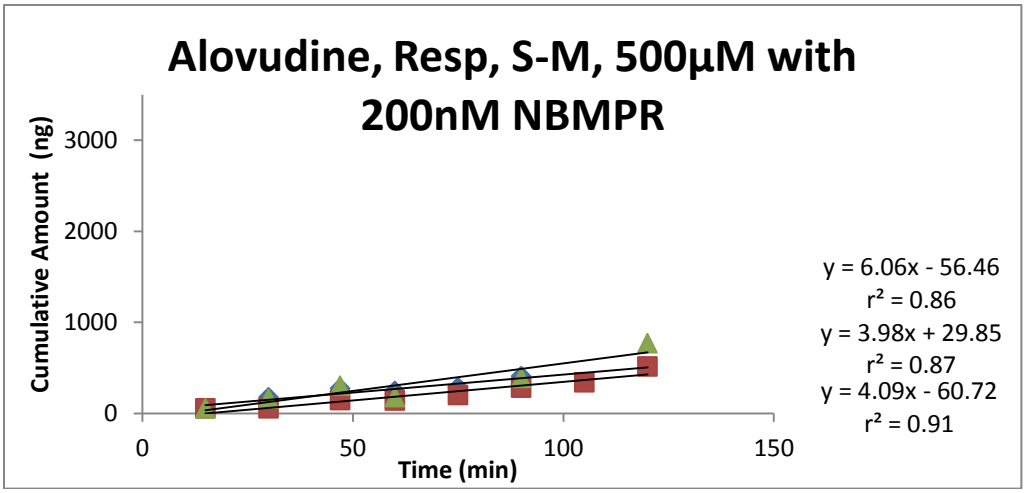
Alovudine, Resp, S-M, 500µM with 200nM NBMPR
Cumulative Amount (ng)
3000
2000
1000
0
0
50
100
150
Time (min)
y = 6.06x - 56.46
r² = 0.86
y = 3.98x + 29.85
r² = 0.87
y = 4.09x - 60.72
r² = 0.91

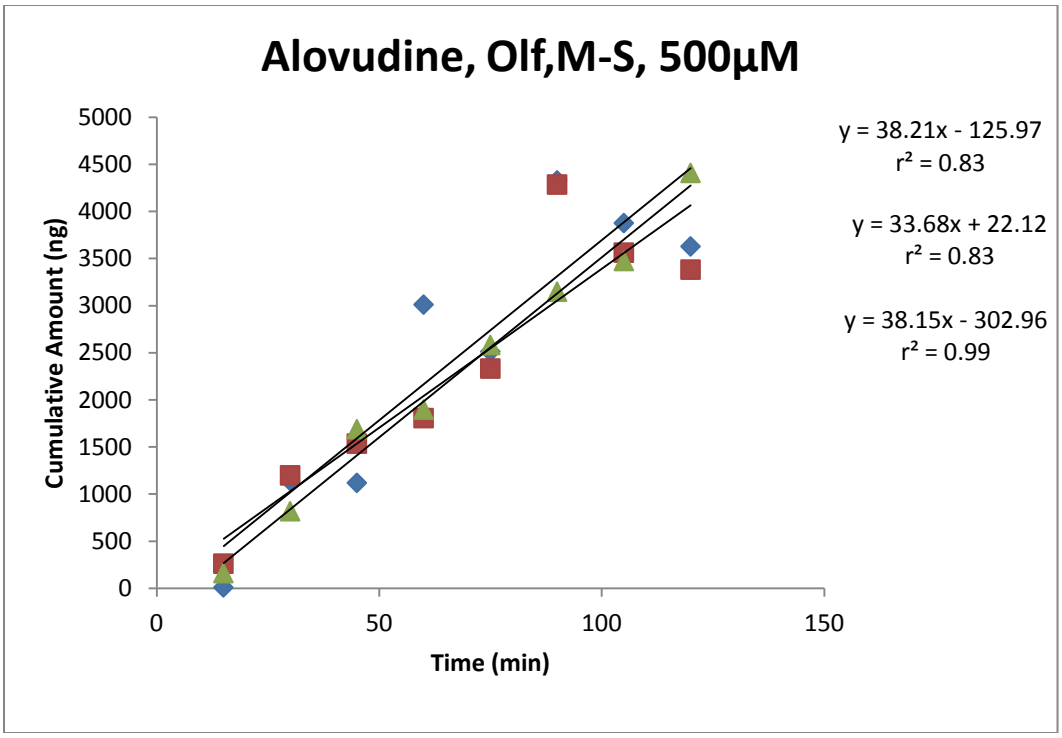
Alovudine, Olf,M-S, 500µM
Cumulative Amount (ng)
Time (min)
0
500
1000
1500
2000
2500
3000
3500
4000
4500
5000
0
50
100
150
y = 38.21x - 125.97
r² = 0.83
y = 33.68x + 22.12
r² = 0.83
y = 38.15x - 302.96
r² = 0.99

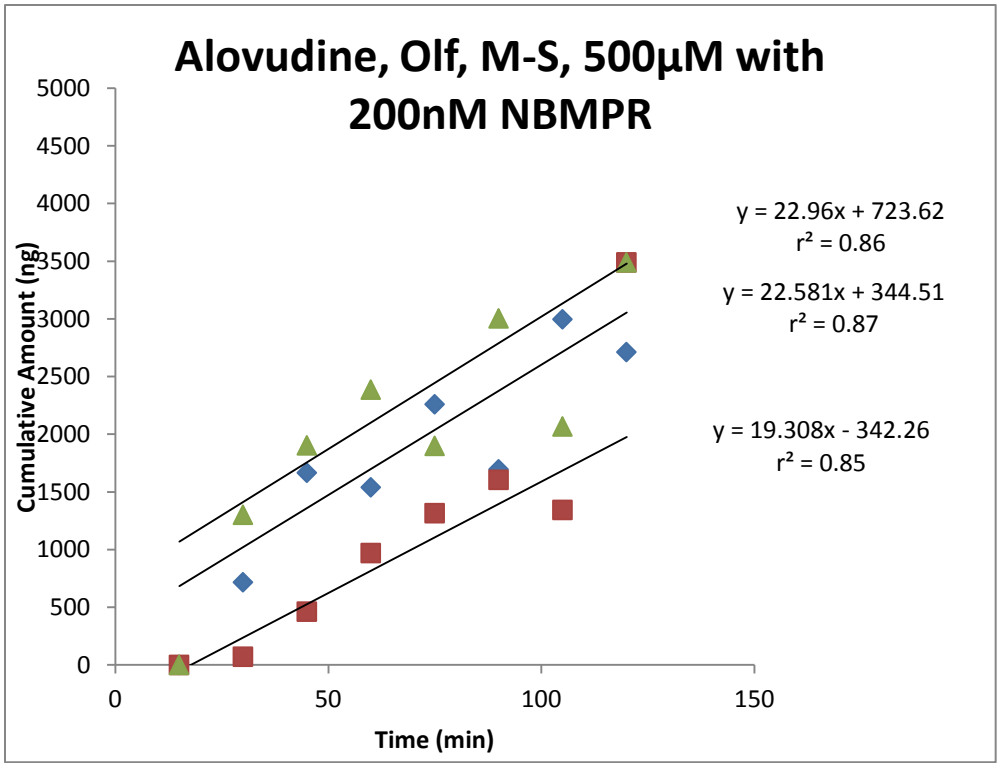
Alovudine, Olf, M-S, 500µM with 200nM NBMPR
Cumulative Amount (ng)
Time (min)
0
500
1000
1500
2000
2500
3000
3500
4000
4500
5000
0
50
100
150
y = 22.96x + 723.62
r² = 0.86
y = 22.581x + 344.51
r² = 0.87
y = 19.308x - 342.26
r² = 0.85

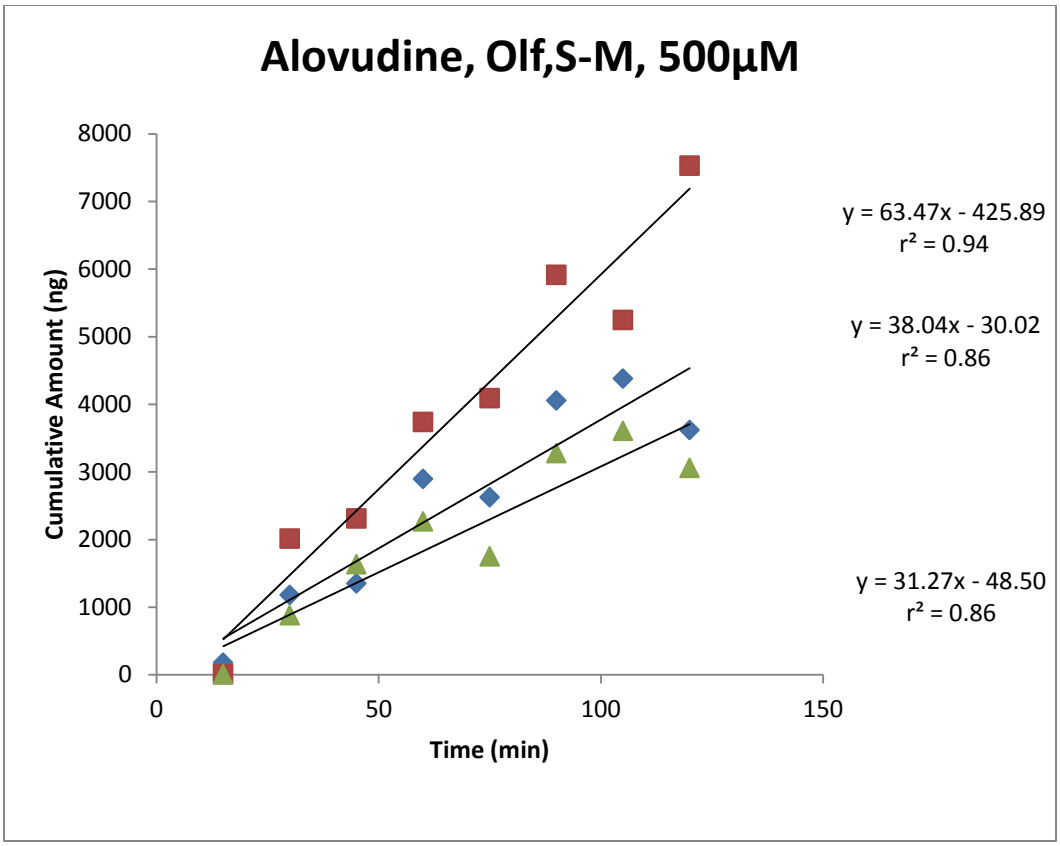
Alovudine, Olf,S-M, 500µM
Cumulative Amount (ng)
Time (min)
0
1000
2000
3000
4000
5000
6000
7000
8000
0
50
100
150
y = 63.47x - 425.89
r² = 0.94
y = 38.04x - 30.02
r² = 0.86
y = 31.27x - 48.50
r² = 0.86

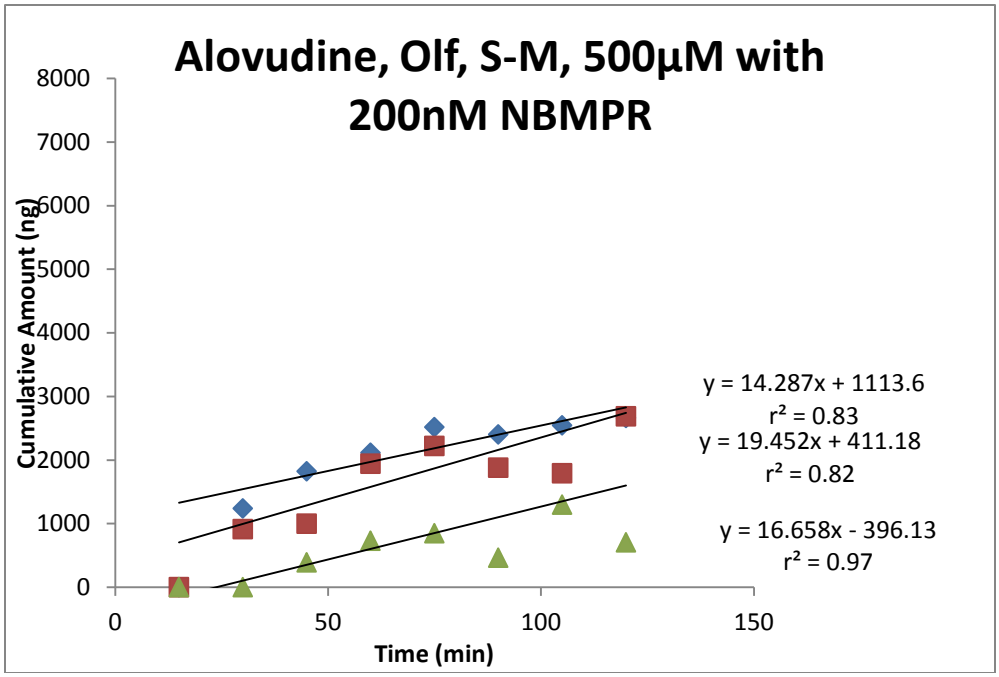
Alovudine, Olf, S-M, 500µM with 200nM NBMPR
Cumulative Amount (ng)
Time (min)
0
1000
2000
3000
4000
5000
6000
7000
8000
0
50
100
150
y = 14.287x + 1113.6
r² = 0.83
y = 19.452x + 411.18
r² = 0.82
y = 16.658x - 396.13
r² = 0.97

# REFERENCES

1. Dahl R, Mygind N. Anatomy, physiology and function of the nasal cavities in health and disease. Adv Drug Deliv Rev 1998; 29(1-2):3-12.

2. Pires A, Fortuna A, Alves G, Falcao A. Intranasal drug delivery: How, why and what for? J Pharm Pharm Sci 2009; 12(3):288-311.

3. Illum L. Nasal delivery. The use of animal models to predict performance in man. J Drug Target 1996; 3(6):427-42.

4. Gopinath P, Gopinath G, Kumar A. Target site of intranasally sprayed substances and their transport across the nasal mucosa: A new insight into the intranasal route of drug delivery. Curr Ther Res 1978; 23(5):596-607.

5. Illum L. Nasal drug delivery--possibilities, problems and solutions. J Control Release 2003; 87(1-3):187-98.

6. Illum L. Transport of drugs from the nasal cavity to the central nervous system. Eur J Pharm Sci 2000; 11(1):1-18.

7. Harkema JR, Carey SA, Wagner JG. The nose revisited: A brief review of the comparative structure, function, and toxicologic pathology of the nasal epithelium. Toxicol Pathol 2006; 34(3):252-69.

8. Jogani V, Jinturkar K, Vyas T, Misra A. Recent patents review on intranasal administration for CNS drug delivery. Recent Pat Drug Deliv Formul 2008; 2(1):25-40.

9. Costantino HR, Illum L, Brandt G, Johnson PH, Quay SC. Intranasal delivery: Physicochemical and therapeutic aspects. Int J Pharm 2007; 337(1-2):1-24.

10. Orange Book: Approved drug products with therapeutic equivalence evaluations [Internet]: U.S. Food and Drug Administration. Available from: http://www.accessdata.fda.gov/scripts/cder/ob/docs/querytn.cfm.

11. Drug.com:drug information online [Internet]; [cited 2013 July 17]. Available from: http://www.drugs.com/.

12. Kristensson K. Sorting signals and targeting of infectious agents through axons: An annotation to the 100 years' birth of the name "axon". Brain Res Bull 1996;41(6):327-33.

13. Thorne RG, Emory CR, Ala TA, Frey WH, 2nd. Quantitative analysis of the olfactory pathway for drug delivery to the brain. Brain Res 1995; 692(1-2):278-82.

14. Wang F, Jiang X, Lu W. Profiles of methotrexate in blood and CSF following intranasal and intravenous administration to rats. Int J Pharm 2003;263(1-2):1-7.

15. Shingaki T, Inoue D, Furubayashi T, Sakane T, Katsumi H, Yamamoto A, Yamashita S. Transnasal delivery of methotrexate to brain tumors in rats: A new strategy for brain tumor chemotherapy. Mol Pharm 2010;7(5):1561-8.

16. Chou KJ, Donovan MD. Distribution of antihistamines into the CSF following intranasal delivery. Biopharm Drug Dispos 1997; 18(4):335-46.

17. Jayachandra Babu R, Dayal PP, Pawar K, Singh M. Nose-to-brain transport of melatonin from polymer gel suspensions: A microdialysis study in rats. J Drug Target 2011; 19(9):731-40.

18. Stevens J, Ploeger BA, Van der Graaf PH, Danhof M, De Lange EC. Systemic and direct nose-to-brain transport pharmacokinetic model for remoxipride after intravenous and intranasal administration. Drug Metab Dispos 2011; 39(12):2275-82.

19. Jogani VV, Shah PJ, Mishra P, Mishra AK, Misra AR. Intranasal mucoadhesive microemulsion of tacrine to improve brain targeting. Alzheimer Dis Assoc Disord 2008; 22(2):116-24.

20. Sakane T, Yamashita S, Yata N, Sezaki H. Transnasal delivery of 5-fluorouracil to the brain in the rat. J Drug Target 1999; 7(3):233-40.

21. Born J, Lange T, Kern W, McGregor GP, Bickel U, Fehm HL. Sniffing neuropeptides: A transnasal approach to the human brain. Nat Neurosci 2002; 5(6):514-6.

22. Benedict C, Hallschmid M, Schultes B, Born J, Kern W. Intranasal insulin to improve memory function in humans. Neuroendocrinology 2007; 86(2):136-42.

23. Benedict C, Hallschmid M, Schmitz K, Schultes B, Ratter F, Fehm HL, Born J, Kern W. Intranasal insulin improves memory in humans: Superiority of insulin aspart. Neuropsychopharmacology 2007; 32(1):239-43.

24. Benedict C, Frey WH,2nd, Schioth HB, Schultes B, Born J, Hallschmid M. Intranasal insulin as a therapeutic option in the treatment of cognitive impairments. Exp Gerontol 2011; 46(2-3):112-5.

25. Hanson LR, Frey WH,2nd. Intranasal delivery bypasses the blood-brain barrier to target therapeutic agents to the central nervous system and treat neurodegenerative disease. BMC Neurosci 2008; 9 Suppl 3:S5,2202-9-S3-S5.

26. Pietrowsky R, Claassen L, Frercks H, Fehm HL, Born J. Time course of intranasally administered cholecystokinin-8 on central nervous effects. Neuropsychobiology 2001; 43(4):254-9.

27. Dhuria SV, Hanson LR, Frey WH, 2nd. Intranasal delivery to the central nervous system: Mechanisms and experimental considerations. J Pharm Sci 2010; 99(4):1654-73.

28. Thorne RG, Pronk GJ, Padmanabhan V, Frey WH,2nd. Delivery of insulin-like growth factor-I to the rat brain and spinal cord along olfactory and trigeminal pathways following intranasal administration. Neuroscience 2004;127(2):481-96.

29. Einer-Jensen N, Larsen L. Local transfer of diazepam, but not of cocaine, from the nasal cavities to the brain arterial blood in rats. Pharmacol Toxicol 2000;87(6):276-8.

30. Einer-Jensen N, Larsen L. Transfer of tritiated water, tyrosine, and propanol from the nasal cavity to cranial arterial blood in rats. Exp Brain Res 2000;130(2):216-20.

31. Skipor J, Grzegorzewski W, Einer-Jensen N, Wasowska B. Local vascular pathway for progesterone transfer to the brain after nasal administration in gilts. Reprod Biol 2003;3(2):143-59.

32. Thorne RG, Hanson LR, Ross TM, Tung D, Frey WH,2nd. Delivery of interferon-beta to the monkey nervous system following intranasal administration. Neuroscience 2008;152(3):785-97.

33. Dhuria SV, Hanson LR, Frey WH,2nd. Novel vasoconstrictor formulation to enhance intranasal targeting of neuropeptide therapeutics to the central nervous system. J Pharmacol Exp Ther 2009;328(1):312-20.

34. Pardridge WM. Drug transport in brain via the cerebrospinal fluid. Fluids Barriers CNS 2011;8(1):7,8118-8-7.

35. Agu R, Ugwoke M. In situ and ex vivo models for preclinical drug development studies. In: C. Ehrhardt, K. Kim, editors. Drug absorption studies: In sito, in vitro, in silico models. U.S.A: Spinger; 2008. 112-34.

36. Merkle HP, Ditzinger G, Lang SR, Peter H, Schmidt MC. In vitro cell models to study nasal mucosal permeability and metabolism. Adv Drug Deliv Rev 1998;29(1-2):51-79.

37. Reichl S, Becker K. Cultivation of RPMI 2650 cells as an in-vitro model for human transmucosal nasal drug absorption studies: Optimization of selected culture conditions. J Pharm Pharmacol 2012;64(11):1621-30.

38. Reardon PM. *In vitro* nasal models. In: Ronald T. Borchardt, Philip L. Smith, Glynn Wilson, editors. Models for assessing drug absorption and metabolism. USA: Springer; 1996. 309-23.

39. Schmidt MC, Simmen D, Hilbe M, Boderke P, Ditzinger G, Sandow J, Lang S, Rubas W, Merkle HP. Validation of excised bovine nasal mucosa as in vitro model to study drug transport and metabolic pathways in nasal epithelium. J Pharm Sci 2000;89(3):396-407.

40. Hirsh AJ, Stonebraker JR, van Heusden CA, Lazarowski ER, Boucher RC, Picher M. Adenosine deaminase 1 and concentrative nucleoside transporters 2 and 3 regulate adenosine on the apical surface of human airway epithelia: Implications for inflammatory lung diseases. Biochemistry 2007; 46(36):10373-83.

41. Zhang H, Schmidt M, Murry DJ, Donovan MD. Permeation and systemic absorption of R- and S-baclofen across the nasal mucosa. J Pharm Sci 2011;100(7):2717-23.

42. Chemuturi NV, Donovan MD. Role of organic cation transporters in dopamine uptake across olfactory and nasal respiratory tissues. Mol Pharm 2007; 4(6):936-42.

43. Lee KR, Maeng HJ, Chae JB, Chong S, Kim DD, Shim CK, Chung SJ. Lack of a primary physicochemical determinant in the direct transport of drugs to the brain after nasal administration in rats: Potential involvement of transporters in the pathway. Drug Metab Pharmacokinet 2010;25(5):430-41.

44. Graff CL, Pollack GM. Functional evidence for P-glycoprotein at the nose-brain barrier. Pharm Res 2005; 22(1):86-93.

45. Kandimalla KK, Donovan MD. Localization and differential activity of P-glycoprotein in the bovine olfactory and nasal respiratory mucosae. Pharm Res 2005; 22(7):1121-8.

46. Kandimalla KK, Donovan MD. Carrier mediated transport of chlorpheniramine and chlorcyclizine across bovine olfactory mucosa: Implications on nose-to-brain transport. J Pharm Sci 2005; 94(3):613-24.

47. Anderle P, Huang Y, Sadee W. Intestinal membrane transport of drugs and nutrients: Genomics of membrane transporters using expression microarrays. Eur J Pharm Sci 2004; 21(1):17-24.

48. Sun D, Lennernas H, Welage LS, Barnett JL, Landowski CP, Foster D, Fleisher D, Lee KD, Amidon GL. Comparison of human duodenum and caco-2 gene expression profiles for 12,000 gene sequences tags and correlation with permeability of 26 drugs. Pharm Res 2002; 19(10):1400-16.

49. Seithel A, Karlsson J, Hilgendorf C, Bjorquist A, Ungell AL. Variability in mRNA expression of ABC- and SLC-transporters in human intestinal cells: Comparison between human segments and caco-2 cells. Eur J Pharm Sci 2006; 28(4):291-9.

50. Gutmann H, Hruz P, Zimmermann C, Beglinger C, Drewe J. Distribution of breast cancer resistance protein (BCRP/ABCG2) mRNA expression along the human GI tract. Biochem Pharmacol 2005; 70(5):695-9.

51. Englund G, Rorsman F, Ronnblom A, Karlbom U, Lazorova L, Grasjo J, Kindmark A, Artursson P. Regional levels of drug transporters along the human intestinal tract: Co-expression of ABC and SLC transporters and comparison with caco-2 cells. Eur J Pharm Sci 2006; 29(3-4):269-77.

52. Kim HR, Park SW, Cho HJ, Chae KA, Sung JM, Kim JS, Landowski CP, Sun D, Abd El-Aty AM, Amidon GL, et al. Comparative gene expression profiles of intestinal transporters in mice, rats and humans. Pharmacol Res 2007; 56(3):224-36.

53. Genter MB, Krishan M, Augustine LM, Cherrington NJ. Drug transporter expression and localization in rat nasal respiratory and olfactory mucosa and olfactory bulb. Drug Metab Dispos 2010;38(10):1644-7.

54. Thiebaud N, Menetrier F, Belloir C, Minn AL, Neiers F, Artur Y, Le Bon AM, Heydel JM. Expression and differential localization of xenobiotic transporters in the rat olfactory neuro-epithelium. Neurosci Lett 2011; 505(2):180-5.

55. Monte JC, Nagle MA, Eraly SA, Nigam SK. Identification of a novel murine organic anion transporter family member, OAT6, expressed in olfactory mucosa. Biochem Biophys Res Commun 2004;323(2):429-36.

56. Molinas A, Sicard G, Jakob I. Functional evidence of multidrug resistance transporters (MDR) in rodent olfactory epithelium. PLoS One 2012;7(5):e36167.

57. Kudo H, Doi Y, Fujimoto S. Expressions of the multidrug resistance-related proteins in the rat olfactory epithelium: A possible role in the phase III xenobiotic metabolizing function. Neurosci Lett 2010 Jan 4;468(2):98-101.

58. You G, Morris ME. Overview of drug transporters families. In: G. You, M. E. Morris, editors. Drug transporters: Molecular characterization and role in drug. Hoboken, New Jersay: John Wiley & Sons, Inc.; 2007.1-10.

59. Holland IB. ABC transporters, mechanisms and biology: An overview. Essays Biochem 2011 Sep 7;50(1):1-17.

60. Nies AT, Rius M, Keppler D. Multidrug resistance proteins of the ABCC subfamily. In: G. You, M. E. Morris, editors. Drug transporters: Molecular characterization and role in drug disposition. John Wiley & Sons, Inc.; 2007. 263-318.

61. Sharom FJ. Multidrug resistance protein: P-glycoprotein. In: G. You, M. E. Morris, editors. Drug transporters: Molecular characterization and role in drug disposition. Hoboken, New Jersey: John Wiley & Sons, Inc.; 2007. 223-62.

62. Robey RW, Polgar O, Deeken J, To KKW, Bates SE. Breast cancer resistance protein. In: G. You, M. E. Morris, editors. Drug transporters: Molecular characterization and role in drug disposition. Hoboken,New Jerssey: John Wiley & Sons, Inc.; 2007. 319-58 .

63. Hediger MA, Romero MF, Peng JB, Rolfs A, Takanaga H, Bruford EA. The ABCs of solute carriers: Physiological, pathological and therapeutic implications of human membrane transport proteinsIntroduction. Pflugers Arch 2004 Feb;447(5):465-8.

64. Verrey F, Closs EI, Wagner CA, Palacin M, Endou H, Kanai Y. CATs and HATs: The SLC7 family of amino acid transporters. Pflugers Arch 2004 Feb;447(5):532-42.

65. Nunez-Parra A, Cortes-Campos C, Bacigalupo J, Garcia Mde L, Nualart F, Reyes JG. Expression and distribution of facilitative glucose (GLUTs) and monocarboxylate/H+ (MCTs) transporters in rat olfactory epithelia. Chem Senses 2011 Nov;36(9):771-80.

66. Sinicrop D, Cronin M, Liu ML. Gene expression profiling utilizing microarray technology and RT-PCR. In: M. Ferrari, M. Ozkan, M. Heller, editors. BioMEMS and biomedical nanotechnology. US: Springer; 2007.23-46.

67. Agu R, MacDonald C, Cowley E, Shao D, Renton K, Clarke DB, Massoud E. Differential expression of organic cation transporters in normal and polyps human nasal epithelium: Implications for in vitro drug delivery studies. Int J Pharm 2011 Mar 15;406(1-2):49-54.

68. Shao D, Massoud E, Anand U, Parikh A, Cowley E, Clarke D, Agu RU. Organic cation transporters in human nasal primary culture: Expression and functional activity. Ther Deliv 2013;4(4):439-51.

69. George M. The role of organic cation transporters in the nasal uptake and brain distribution of OC+ (organic cation) substrates. Iowa City,Iowa: University of Iowa; 2013. unpublished.

70. Ferriera AExpression and activity of an L-type amino acid transporter in bovine nasal mucosa. Unpublished data.

71. Kudo H, Doi Y, Fujimoto S. Expressions of the multidrug resistance-related proteins in the rat olfactory epithelium: A possible role in the phase III xenobiotic metabolizing function. Neurosci Lett 2010;468(2):98-101.

72. Xia L, Zhou M, Wang J. Nucleoside transporters: CNTs and ENTs. In: G. You, M. Morris, editors. Drug transporters:Molecular characterization and role in drug disposition. 1st ed. USA: John Wiley & Sons, Inc; 2007. 171-200.

73. Rose JB, Coe IR. Physiology of nucleoside transporters: Back to the future. . . Physiology (Bethesda) 2008; 23:41-8.

74. King AE, Ackley MA, Cass CE, Young JD, Baldwin SA. Nucleoside transporters: From scavengers to novel therapeutic targets. Trends Pharmacol Sci 2006 Aug;27(8):416-25.

75. Parkinson FE, Damaraju VL, Graham K, Yao SY, Baldwin SA, Cass CE, Young JD. Molecular biology of nucleoside transporters and their distributions and functions in the brain. Curr Top Med Chem 2011;11(8):948-72.

76. Damaraju VL, Damaraju S, Young JD, Baldwin SA, Mackey J, Sawyer MB, Cass CE. Nucleoside anticancer drugs: The role of nucleoside transporters in resistance to cancer chemotherapy. Oncogene 2003;22(47):7524-36.

77. Damaraju VL, Elwi AN, Hunter C, Carpenter P, Santos C, Barron GM, Sun X, Baldwin SA, Young JD, Mackey JR, et al. Localization of broadly selective equilibrative and concentrative nucleoside transporters, hENT1 and hCNT3, in human kidney. Am J Physiol Renal Physiol 2007;293(1):F200-11.

78. Young JD, Yao SY, Sun L, Cass CE, Baldwin SA. Human equilibrative nucleoside transporter (ENT) family of nucleoside and nucleobase transporter proteins. Xenobiotica 2008;38(7-8):995-1021.

79. Gray JH, Owen RP, Giacomini KM. The concentrative nucleoside transporter family, SLC28. Pflugers Arch 2004;447(5):728-34.

80. Pastor-Anglada M, Errasti-Murugarren E, Aymerich I, Casado FJ. Concentrative nucleoside transporters (CNTs) in epithelia: From absorption to cell signaling. J Physiol Biochem 2007 Mar;63(1):97-110.

81. Molina-Arcas M, Casado FJ, Pastor-Anglada M. Nucleoside transporter proteins. Curr Vasc Pharmacol 2009;7(4):426-34.

82. Varatharajan L, Thomas SA. The transport of anti-HIV drugs across blood-CNS interfaces: Summary of current knowledge and recommendations for further research. Antiviral Res 2009 May;82(2):A99-109.

83. Seki T, Sato N, Hasegawa T, Kawaguchi T, Juni K. Nasal absorption of zidovudine and its transport to cerebrospinal fluid in rats. Biol Pharm Bull 1994 Aug;17(8):1135-7.

84. Kovacs Z, Juhasz G, Palkovits M, Dobolyi A, Kekesi KA. Area, age and gender dependence of the nucleoside system in the brain: A review of current literature. Curr Top Med Chem 2011;11(8):1012-33.

85. Lu H, Chen C, Klaassen C. Tissue distribution of concentrative and equilibrative nucleoside transporters in male and female rats and mice. Drug Metab Dispos 2004 Dec;32(12):1455-61.

86. Abcam protcols book [Internet]: Abcam; c2012 [cited 2013 June/7]. Available from: http://docs.abcam.com/pdf/misc/abcam-protocols-book-2010.pdf.

87. Smith PK, Krohn RI, Hermanson GT, Mallia AK, Gartner FH, Provenzano MD, Fujimoto EK, Goeke NM, Olson BJ, Klenk DC. Measurement of protein using bicinchoninic acid. Anal Biochem 1985;150(1):76-85.

88. Jamur MC, Oliver C. Overview of antibodies for immunochemistry. In: Maria Celia Jamur, Constance Oliver, editors. Immunocytochemical methods and protocols. 3rd ed. New York, NY: Humana Press; 2010. 3-9.

89. Wanner A, Salathe M, O'Riordan TG. Mucociliary clearance in the airways. Am J Respir Crit Care Med 1996;154(6 Pt 1):1868-902.

90. Morse DM, Smullen JL, Davis CW. Differential effects of UTP, ATP, and adenosine on ciliary activity of human nasal epithelial cells. Am J Physiol Cell Physiol 2001 Jun;280(6):C1485-97.

91. Rusconi S. Alovudine medivir. Curr Opin Investig Drugs 2003 Feb;4(2):219-23.

92. Alovudine - Compound Summary (CID 33039) [Internet]: NCBI. [cited 2013 June/7] Available from: http://pubchem.ncbi.nlm.nih.gov/summary/summary.cgi?cid=33039&loc=ec_rcs.

93. Kong XB, Zhu QY, Vidal PM, Watanabe KA, Polsky B, Armstrong D, Ostrander M, Lang SA,Jr, Muchmore E, Chou TC. Comparisons of anti-human immunodeficiency virus activities, cellular transport, and plasma and intracellular pharmacokinetics of 3'-fluoro-3'-deoxythymidine and 3'-azido-3'-deoxythymidine. Antimicrob Agents Chemother 1992;36(4):808-18.

94. Kim EY, Vrang L, Oberg B, Merigan TC. Anti-HIV type 1 activity of 3'-fluoro-3'-deoxythymidine for several different multidrug-resistant mutants. AIDS Res Hum Retroviruses 2001;17(5):401-7.

95. Katlama C, Ghosn J, Tubiana R, Wirden M, Valantin MA, Harmenberg J, Mardh G, Oberg B, Calvez V. MIV-310 reduces HIV viral load in patients failing multiple antiretroviral therapy: Results from a 4-week phase II study. AIDS 2004 ;18(9):1299-304.

96. Ghosn J, Quinson AM, Sabo N, Cotte L, Piketty C, Dorleacq N, Bravo ML, Mayers D, Harmenberg J, Mardh G, ValdezH, KatlamaC. Antiviral activity of low-dose alovudine in antiretroviral-experienced patients: Results from a 4-week randomized, double-blind, placebo-controlled dose-ranging trial. HIV Med 2007;8(3):142-7.

97. Barwick T, Bencherif B, Mountz JM, Avril N. Molecular PET and PET/CT imaging of tumour cell proliferation using F-18 fluoro-L-thymidine: A comprehensive evaluation. Nucl Med Commun 2009; 30(12):908-17.

98. Paproski RJ, Ng AM, Yao SY, Graham K, Young JD, Cass CE. The role of human nucleoside transporters in uptake of 3'-deoxy-3'-fluorothymidine. Mol Pharmacol 2008;74(5):1372-80.

99. Mirza A, Rathore MH. Human immunodeficiency virus and the central nervous system. Semin Pediatr Neurol 2012;19(3):119-23.

100. Stahle L, Guzenda E, Ljungdahl-Stahle E. Pharmacokinetics and extracellular distribution to blood, brain, and muscle of alovudine (3'-fluorothymidine) and zidovudine in the rat studied by microdialysis. J Acquir Immune Defic Syndr 1993;6(5):435-9.

101. Stahle L, Borg N. Transport of alovudine (3'-fluorothymidine) into the brain and the cerebrospinal fluid of the rat, studied by microdialysis. Life Sci 2000;66(19):1805-16.

102. Ponto LLB, Huang J, Walash S, Mundt C, Acevedo MR, Sunderland J, Donovan M. Use of PET imaging to measure nucleoside transporter-mediated distribution from the nasal mucosa. AAPS annual conference; Oct 15, 2012; Poster.

103. Ponto LLB, Walash S, Huang J, Mundt C, Sunderland J, Donovan M. Pharmacoimaging of drug disposition after intranasal administration. AAPS annual meeting; Oct 25, 2011; Poster.

104. Specialty Vertical Ussing/Diffusion Chamber Systems [Internet]: Harvard Bioscience Company [cited 2013 Jul/20]. Available from:https://www.harvardapparatus.com/webapp/wcs/stores/servlet/product_11051_10001_35615_-1_HAI_ProductDetail___.

105. Habel R, Budras KD. Chapter 3:Head. In: K. D. Budras, R. E. Habel, A. Wünsche, S. Buda , editors. Bovine anatomy:An illustrated text. Hannover,Germany: GmbH & Co. KG; 2003. 30-49.

106. Stahle L, Mian A, Borg N. Use of multivariate characterization, design and analysis in assay optimization. J Pharm Biomed Anal 1995;13(4-5):369-76.

107. Fleisher D. Biological transport phenomena in the gastrointestinal tract. In: G. L. Amidon, E. M. Topp , P. Lee I, editors. Transport processes in pharmaceutical systems. Informa Healthcare; 1999.147-84.

108. Flynn GL, Yalkowsky SH, Roseman TJ. Mass transport phenomena and models: Theoretical concepts. J Pharm Sci 1974;63(4):479-510.

109. Yang Z, Huang Y, Gan G, Sawchuk RJ. Microdialysis evaluation of the brain distribution of stavudine following intranasal and intravenous administration to rats. J Pharm Sci 2005;94(7):1577-88.

110. Ved PM, Kim K. Poly(ethylene oxide/propylene oxide) copolymer thermo-reversible gelling system for the enhancement of intranasal zidovudine delivery to the brain. Int J Pharm 2011;411(1-2):1-9.

111. Strachan T, Read AP. PCR, DNA sequencing and in vitro mutagenesis. In: T. Strachan, A. P. Read, editors. Human molecular genetics. 2nd ed. New York: Wiley-Liss; 1999. Available from: http://www.ncbi.nlm.nih.gov/books/NBK7571/.